INFLUENCE OF DELTA MORPHODYNAMICS ON COASTAL RESPONSE TO CLIMATE CHANGE

Marco Daniel Melo Ferraz

A thesis submitted in fulfilment

of the requirements for the degree

of Doctor of Philosophy

Ph.D.

Faculty of Science

University of Sydney

2014

to Cristina
for changing my world.

Statement of originality

I declare that the research results presented in this thesis are my own original work, except where due reference is made in the text, and has not been submitted to any other institution for the award of a degree.

Signature: 

Abstract

This study examined the proposition that deltas are sedimentary structures of importance to the control of depositional processes responsible for the morphologic evolution of adjacent coastlines. More specifically, deltaic sensitivity to external forcing factors including climate change and sea-level variations, is demonstrated in this study to influence morphologic evolution of adjacent coastlines while regulating sediment dispersal patterns. This influence is also shown to depend on the morphologic complexity of the coastline and the relation between the existing sedimentary structures.

The study combined field data and modelling techniques to examine the dependence of adjacent coastal behaviour on a deltaic structure assessing the contribution of each forcing factor on sediment mass balance and morphologic evolution. This dependence was explored using as a natural laboratory, the Caparica coastal cell located on the Portuguese west coast, south of Lisbon, which was studied using two different approaches: coastal evolution since sea-level stabilization (<7ky BP) and risk based forecast modelling for coastline position.

The results demonstrate that coastline position as well as the development and/or erosion of sedimentary structures (e.g. climbing dunes and prograded barriers) is mainly dependent on sediment supply conditions governed by deltaic behaviour along the proximal adjacent-coast. Here, the influence of deltaic processes is characterized by highly dynamic sediment exchanges that subordinate effects of climate change and sea-level variations on coastal evolution for frequently observed conditions and conservative predictions that consider average values of climatic variations. These factors only become relevant when extreme conditions, characterized by significant sea-level and climate variations, are considered resulting from low-probability higher magnitude risk in forecasts that account for uncertainty in factors driving morphological response.

In contrast, the morphology of the distal adjacent-coast is not governed by sediment exchanges with the delta and may be better aligned than the proximal coastline with the delta.

For the Caparica cell, the strong distal alignment is governed by refraction of the swell-wave field over the delta lobe bathymetry. The proximal coastline is out of alignment with the delta because sediment exchanges between it and the delta overwhelm morphodynamic effects involving the wave field. These relationships make the distal-adjacent-coast more responsive than the proximal coast to sea level rise in model forecasts.

Table of Contents

List of Figures

List of Tables

List of Acronyms

ARI – Average Return Intervals

DEM - Digital Elevation Model

DSAS - Digital Shoreline Analysis System

FCT - Portuguese Science and Technology Foundation

FNMOC - Fleet Numerical Meteorology and Oceanography Centre

GIS – Geographic Information Systems

GPR - Ground-Penetrating Radar

HWL - High Water Line

IH –Hydrographical Institute (Portugal)

IPCC - Intergovernmental Panel on Climate Change

LGM - Last Glacial Maximum

MWC - Mean Wave Conditions

MWD - Mean Wave Direction

NAO - North Atlantic Oscillation

OSL - Optical Stimulated Luminescence

PBSE - Parabolic Bay Shape Equation

PBSM - Parabolic Bay Shape Model

PDF - Probability Density Functions

PWC - Peak wave conditions

STM- Shoreface Translation Model

TIN - Triangulated Irregular Network

TPC - Tagus Paleo-Channel

USGS - United States Geological Survey

WRS - Wave Ravinement Surface

RTK-GPS - Real Time kinematics Global Positioning System

List of Notations

α	angle (degrees)
β	wave obliquity angle (degrees)
σ	standard deviation
ρ	water density (km/m^3)
d	distance (m)
D	mean grainsize (mm)
D_A	depth band shoreface area (m)
dl	maximum water depth for motion initiation by extreme wave condition (m)
di	maximum water depth for nearshore erosion by mean wave condition (m)
f_p	peak frequency (Hz)
g	acceleration of gravity (m/s^2)
h	height (m)
H_{sig}/H_s	significant wave height (m)
ky	kiloyears
P	wave power or wave energy flux (kW)
P_A	shoreface area (m^2)
R_β	length of the control line (m)
R_n	radius calculated for a point (degrees)
(R_n,ϑ_n)	given point position
T_m/T_s	mean wave period (s)
T_p	peak wave period (s)
W_C	cell width (m)

Acknowledgments

Scientific work is a demanding task generally enhanced by the magnitude of the proposed objectives and the experienced difficulties related to it. The development of a research project combining distinct institutions in two remotely separated countries created significant difficulties of several orders where the lack of funds for research development was the most relevant. The work presented on this thesis was possible due to the assistance of a significant number of people and institutions that encouraged me to continue the work throughout the years and to whom I give a word of appreciation:

First I would like to thank Professor Peter Cowell that trusted in this project since its beginning, for his guidance, motivation and especially his friendship. This thesis would not be possible without him.

To Dr. Luís Rebêlo, my supervisor from LNEG, for his support, motivation and friendship through all the years that we have worked together allowing me to develop as a scientist and a person.

To Dr. Ana Vila-Concejo, my co-supervisor from the University of Sydney, for her guidance and mentoring capacity through the project.

To Dr. Derek Wyman, postgraduate adviser at the School of Geosciences of the University of Sydney, for all the support through all these years.

To Michael Kinsela, my colleague at the University of Sydney, for all the help, the countless afternoons of scientific discussions, share of ideas and his friendship.

To Pedro Brito and Susana Costas, my colleagues at LNEG, for all the given support during the several years of research and the constant share of office space.

To Marc Daley, Sallete Figueiredo, Kellie Adlam, Daniel Harris and Angela Wenping Jiang, my colleagues at the University of Sydney, for all the support during this thesis allowing a constant discussion of ideas through the years.

To José Hipólito Monteiro, Pedro Terrinha, Fátima Abrantes and Henrique Duarte from LNEG for the help in the marine geology setting and the participation in projects relevant for this thesis.

To Teresa Cunha and the Geology and Mapping Unit of LNEG for the geological maps provided.

To Judite Fernandes, from the Hidrogeology Unit of LNEG, for the data about water wells in the study area.

To João Mil-Homens, from TU Delft, for the wave data provided.

To Rui Taborda, from the University of Lisbon, for the wave data provided and the important inputs to this work.

To Stephen Barry, from the University of Sydney, for the support in the simulation process for the Delta Shoreface Translation Model final version.

To Carlos Antunes, from the University of Lisbon for the tide data for the study area.

To César Andrade and Maria da Conceição Freitas for the support in the enrolment of this PhD.

To WW - Consultores de Hidráulica e Obras Marítimas, S.A. for the wave data.

To DHI – Water Environment Health for the wave modelling software.

To Landmark SeisWorks for the seismic interpretation software.

To Tecnosol FGE for the bore hole data on the study area.

To Micore Project (Morphological Impacts and Coastal Risks Induced by Extreme Storm Events) for the hindcast wave data.

To the project DCCEE 2010/02213 NCCARF ARGP – "Approach to Risk Assessment on Australian Coasts" for the support for tuition fees.

To the project SCARPS – "Reconstruction of the shoreline position along the Portuguese coast over the last 6000 years - Analysis of the architecture and stratigraphy of sand barriers" (PTDC/CTE-GIX/101466/2008) - Portuguese Science and Technology Foundation (FCT) for the GPR and dating results.

To the Portuguese Science and Technology Foundation (FCT) that funded the PhD research scholarship (SFRH/BD/39802/2007) allowing the occurrence of this project.

To the School of Geosciences of the University of Sydney for the provided logistical support.

To the Marine Geology Unit of LNEG for all the support and funding during this work.

A special recognition to my family and friends that supported constant and long absences always with encouraging words. To my parents Fernando and Maria José for being so special, my grandmother Alda, my sister Carla and my niece Cátia for their concern and to Henrique and Celestina for their constant support. To David, Nuno and João Pedro for their irreversible friendship.

Finally to my wife Cristina that turned the world small and made everything possible, this thesis is for her, and to my baby daughter Mafalda for keeping the good mood all the time allowing Dad to finish the thesis.

CHAPTER 1

Introduction

Photo: Sand dune at Fonte-da-Telha beach

1.1 Premise and aims

Deltas and adjacent coastal sediment bodies have long been known to be dynamic systems with coupled through a shared sediment budget and mutual morphodynamic adjustments (Komar, 1973; Wright, 1978; Jimenez *et al*., 1997; Cowell *et al*., 2003a,b). Their evolution is the result of morphodynamic processes that occur in response to changes in external conditions through mutual adjustment between topographic behaviour and fluid dynamics that involves sediment transport (Wright & Thom, 1977). The non-linear development and the stochastic behaviour make the evolution of coastal morphologies difficult to predict on a long-term basis (decades to millennia), a problem referred in this study as large-scale coastal behaviour (LSCB) (Cowell and Thom, 1994; Cowell et al., 2003a,b).

A practical imperative now exists to apply knowledge on LSCB as a basis to forecast future coastal behaviour that might result from project climate change. According to IPCC (2007) a significant proportion of the world population inhabits coastal areas creating pressure for development that has not been matched by knowledge to resolve problems of coastal vulnerability (Short, 1999). Coastal environments, that include deltas, barriers, lagoons, dunes, beaches, sea-cliffs and others, are subject to LSCB involving internal adjustments in response to variations in external forcing factors that affect the local sediment budget, associated with the alongshore and cross-shore transport: a fundamental factor being variation in sea-level position through time (Cowell et al., 2003a). Sea level changes govern creation of accommodation space available for deposition: positive and negative accommodation changes being associated respectively with rising a falling sea level (Roy et al., 1994).

Other external factors affecting the sediment budget include deltaic sediment supply, losses to estuaries, and changes in nearshore wave climate, including dominant direction (Goodwin et al., 2006). These factors may be affected by anthropic impacts directly on the sediment dynamics causing significant interferences on coastal behaviour leading to unexpected evolution. To understand the evolution of such complex systems, low order coastal behaviour

studies are needed to comprehend mean-trend coastal evolution to inform efficient management solutions, with such studies may involve morphologic parts of the coast that are not usually considered (Cowell et al., 2003a). The practical objective also calls for quantified estimates of coastal evolution in response to climatic changes in secular variations (Carter & Woodroffe, 1994). This focuses on sediment exchanges (Cowell, 2002) associated with morphologic evolutionary trends. The 'coastal tract concept' was developed by Cowell et al. (2003a) to organise analysis for these types of problems, through distinguishing a hierarchy of morphodynamic forms and processes to define coastal systems across a wide range of scales (Stive et al., 2009).

During the 20th century and the beginning of the 21st century, enhanced coastline vulnerability caused by increase of human population in coastal areas has probably been compounded by effects of global sea-level rise that has contributed to coastal inundations, erosion and coastline retreat, often with permanent land loss (Church *et al*., 2008). Predictions from the Intergovernmental Panel on Climate Change (IPCC) indicate a significant and certain future sea-level rise, intensification of storm conditions and increase of human population near the coastal areas (Nicholls et al., 2007). Negative impacts with significant proportions are expected as comprehensive coastal management procedures are critical to maintain the usage of these areas.

The complexity of geohistorical and historically recent coastal change raises questions about how these changes factor into processes and predictions of future coastal behaviour under conditions projected with anthropogenic global warming (Church *et al*., 2008). The objective of this study therefore was to examine how background coastal evolution can affect or mask the possible responses to projected sea level rise in environments with locally compounding effects of coupled morphological systems that have driven continual coastal evolution during throughout the preceding geohistorical period (*i.e*., throughout decades to millennia).

This objective requires an understanding of morphologic changes in coastline over time longer spatial and temporal scales that take into account large-scale processes and shoreface dynamics (Cowell, et al., 1999). In the context of LSCB (Cowell and Thom, 1994), this study investigates the impacts of the different external forcing factors on sediment-exchange processes and specific morphologies. For the investigative analysis of this sediment exchange, quantitative procedures were developed that permit inclusion of constraints imposed by local substrate geology. Obtained variables were stochastically applied using process related sediment-budget modelling with the objective of exploring likely coastal behaviour on a long-term basis, reflecting the range of conditions that a specific coastal cell is exposed to through time.

The broad aims of this study were twofold. The first was to examine the relative significance of internal, coupled morphological adjustments versus external forcing factors in governing the morphologic behaviour of coastlines. The second was to address the same question in relation to future coastal behaviour forecast for conditions of sea level rise projected with global warming.

Specifically this study addresses two questions arising from these broad aims:

1. Are coastal morphologic variations more sensitive to sediment supply conditions than to sea level rise on the historical time scale?
2. Excluding deltaic sediment supply to the adjacent coast, do other factors associated with long term evolution of deltaic structure influence adjacent coastline behaviour?

The Costa da Caparica coastal cell, which includes the Tagus River delta and estuary, provided a natural laboratory to explore principles relevant to the aims implicit in these research questions. The study investigated deltaic influence on a wave dominated coast connecting the shoreface behaviour with the delta morphology and its sediment supply capacity to develop and erode sedimentary features in the adjacent coastline.

1.2 Wave dominated coasts and deltaic influence

Wave dominated coasts as described by Roy et al., (1994) are sedimentary accumulations that experience significant physical reworking during the sediment transport processes culminating in a depositional phase. Waves and wave-induced currents are the main engine for the evolution of this type of coast that generally experiences a direct increase in erosion rates due to sea-level rise (Stive et al., 2009). However, winds, tidal currents and river discharges also act as transporting agents in coastal areas that may conceal wave action in specific periods. Coastal sand barriers are the basic depositional element for wave-dominated coasts (Roy et al., 1994) as their development depends on the local geological inheritance resulting in different types of barrier structure depending on the available accommodation and sediment volume (Swift & Thorne, 1991).

When a specific coastal cell occurs near a fluvial system and this has a sediment deposition rate that subordinates the marine sediment reworking capacity, deltaic systems develop (Wright, 1978; Sutter, 1994). The development of deltas is strongly dependent on several environmental factors including tides, waves, nearshore currents and substrate morphology (geologic inheritance) that delineate its morphologic configuration and sedimentary sequences. Once developed, deltas regulate sedimentary exchanges between the river basin (e.g. estuaries) and the oceanic basin often contributing to the development of sedimentary morphologies in the adjacent coastline as prograded barriers (Roy et al., 1994; Leatherman, 1983). The sensitivity of deltas to accommodation space (Emery & Myers, 1996) determined either by sea-level or sediment supply variations cause significant changes in the shoreface geometry of the adjacent coastline affecting its morphologic evolution (Cowell *et al*., 2003a).

1.3 Modelling coastal environments

Geologic processes and their effects on coastal environments can be studied based on process-response models that predict coastal behaviour under certain conditions (Fox, 1978). The traditional approach demands a geostatistical analysis of morphologic changes over historical time scales and involving sediment supply characterization at regional scales. This has proved to be problematic in addressing low order coastal behaviour problems due to persistent uncertainty in quantifying sediment transport processes (Cowell et al., 2003a; Kinsela, 2007). Low order coastal change involves morphologic evolution and coastal topography at a geological time scale (10^3 years) and a wide geographical scale (10^2 to 10^3 meters) (Cowell et al., 1995; Cowell et al., 2003a). The use of numerical models based on morphologic aggregation of variables allows simplified quantification of morphological change in which models can be calibrated using geological data to run Monte Carlo simulations to produce validated forecasts or to evaluate uncertainty when assessing hypothesised coastal change (Cowell et al., 2006). This study used several aggregated models, but principally the Shoreface Translation Model (STM) (Cowell et al., 1995), to evaluated hypothesised coastal behaviour in the Costa da Caparica coastal cell. This STM based on the sediment budget approach where the quantification of coastal change is based on a balance between hypothesised gains, losses and redistribution of sediments in the presence of gains and losses in accommodation due to sea level change. The STM is computationally simple enough to apply stochastic simulation techniques where input are represented by probably distribution functions defined based on available geostatistical data or heuristics (Cowell et al., 2006; Kinsela, 2007). Generated outputs come as probability forecasts that allows uncertainty to be managed through risk based analysis. Model application is guided by a formal methodology, the 'coastal-tract template' (Cowell et al., 2003a), that allows partitioning of coastal-change constituents on the basis of scale. This approach thus allows the isolation of low-order coastal behaviour from

more superficial changes that can be considered as noise over the long term (decades to millennia).

1.4 The Caparica coastal cell

The field area selected as a natural laboratory to address the aims of this thesis is located on the Portuguese Atlantic west-coast, immediately south of Lisbon. The juxtaposition of the embayed barrier coastline in the south to the adjacent delta complex immediately to the north, and evidence of a complex, ongoing history of morphological evolution affords an opportunity to examine the role of the delta in governing behaviour of the adjacent coast.

Situated between Trafaria and Espichel Cape, the Caparica coastal cell comprises a prograded barrier complex (Cowell et al., 2003a,b) with a drumstick configuration (Davis and Hayes, 1984) with the backbeach zone attached to mainland with no lagoon where the north end is wider than the south one due to recent coastline progradation (fig. 1.1). In this area, beaches are wide, dissipative (Short, 1979; Wright and Short, 1984; Sunamura, 1988; Lippmann and Holman, 1990; Short, 1999) and with a well-developed dune system. Towards the south, the prograded barrier gives way to a transgressive barrier with mainland narrow reflective beaches (Short, 1979; Wright and Short, 1984; Sunamura, 1988; Lippmann and Holman, 1990; Short, 1999). Average grainsize values gradually increase from north to the south probably due to wave power influence (Teixeira, 1990).

The barrier system is truncated by the presence of a coastal lagoon (Albufeira) in the middle of the cell. This lagoon with a 3.5 km maximum width and a 625 m maximum length (Freitas e Ferreira, 2004) is separated from the ocean with a barrier, where an inlet is artificially opened once a year. It is also common that during storms, overwash events occur.

The inland limit of the barrier system is a sea-cliff (Caparica cliff) that can be more than 100 meters height in some areas, interpreted by Azevedo (1983) as fluvial sediments deposited during Pliocene, essentially composed by unconsolidated detritic and carbonate geological

material (Teixeira, 1990). According to Cabral et al. (1984) the development of the cliff morphology is related to movements in a local set of geological faults that developed between the upper Pliocene to lower Quaternary.

Along a significant portion of this cliff it is possible to observe cliff-top dunes (fig. 1.1) as well as a Late Pleistocene (Costas et al., 2012), extensive dune field on the leeward side of the cliff. The thickness of these deposits varies between 30 and 60 meters (Azevedo, 1983; Pais et al., 2006; Costas et al., 2010) and its geometry demonstrates that its development was in the seaward-landward direction (Costas et al., 2012) as its development is related with the presence of climbing dune structures in positive sediment supply conditions (Tsoar, 1983; Ferraz et al., 2011).

North of the coastal segment, the Tagus delta is a prominent sedimentary structure that enters the Atlantic Ocean near Lisbon in a passive continental margin with a narrow shelf (<30km) (Vis et al., 2008) that limits the size of the basin forming the Tagus estuary. The morphological structure comprises a well-developed ebb-tide delta and a small flood tide delta where the overall morphology is a function of the interaction between tide effects and wave energy. Although this is a mesotidal environment, both ebb and flood tide deltas are not structurally similar (Fisher and Simpson, 1979) due to ebb-tide dominance in the estuary mouth. In spite of its sheltered position, wave effects are relevant in the development and evolution of the delta (mixed energy – wave dominated according to Hayes, 1979), and also play a minor role within the estuary (Fortunato et al., 1999). The delta is the main sand sediment source for the adjacent coastline. The offshore limit of this composed coastal system is the continental shelf boundary, between the 130 meters and 180 meters bathymetry, with a 30 kilometres width in the north part, near the Tagus delta, and a 5 kilometres width in the south part, next to Espichel headland (Freire, 1999). Two canyons cross the continental shelf to cut the platform of the cell: the Lisbon canyon and the Cascais canyon. The proximity of the studied segment to Lisbon canyon makes it a potential sediment sink in specific conditions.

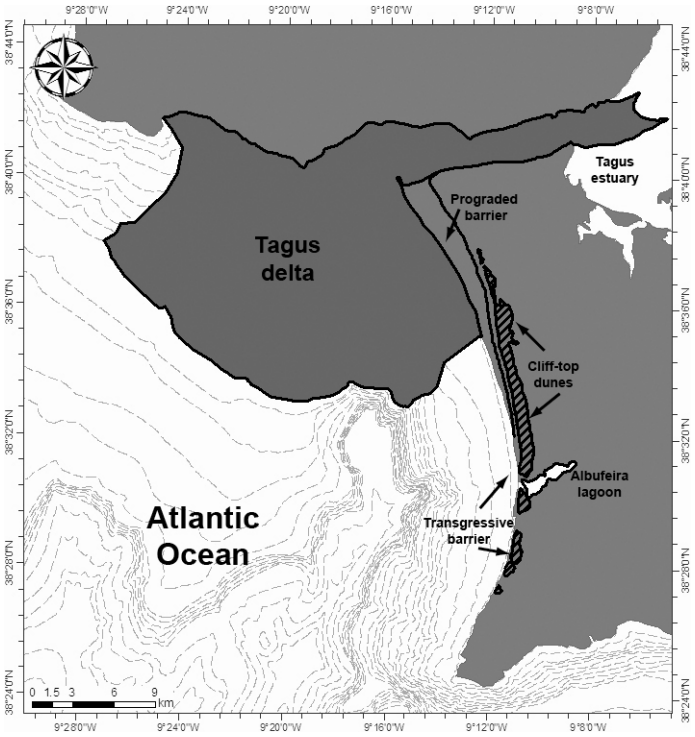

Figure 1.1 – Main morphological features of the studied segment

1.5 Thesis outline

This thesis comprises four chapters, not including this general introduction and the conclusions, with each chapter dealing with separate but related aspects of the evidence used to address the aims and overall research questions outlined above (Sec. 1.1). However, a line of thought is maintained throughout the thesis as chapters are intrinsically related allowing progressive development of the evidence. Because the chapters are self contained, inevitable repetitions occur particularly in the introduction and regional setting.

Chapter 2 addresses the deltaic influence on sediment exchanges in the determination of local sediment budget based on the evolution of morphological structures. The geometric definition of each sedimentary structure was investigated based on the data obtained from different methods and datasets as boreholes, offshore seismic interpretation, ground-penetrating radar (GPR) data, dating procedures as well as Geographic Information Systems (GIS) and wave modelling analysis. This permitted obtaining a well defined morphologic framework with a clear identification of the main sedimentary processes and dynamics.

Chapter 3 relates the existence of cliff-top dunes to the long-term coastal evolution and chronology of the studied cell. The study of physical processes capable of developing a climbing dune structure on top of a prograded barrier was based on physical principles developed by others using GIS modelling to define size and geometry parameters. The characterization of sediment dynamics was based on the relation between the geometric findings, GPR sub-surface imagery and chronological information. The identification of the progradation/recession mechanisms allowed a quantitative determination of coastline behaviour and related processes.

Chapter 4 focuses on changes in wave climate induced by the delta and resulting effects on stability of the adjacent coastline. The study of wave refraction/diffraction over the delta allowed the development of a new approach to embayed beach stability based on changes in

the conjunction of three processes: wave direction, substrate bathymetry and sea-level. This approach allowed the identification of past planforms as well as forecast future coastline instability problems and consequent vulnerability.

Chapter 5 addresses the influence of deltaic morphology on response of the adjacent coast to effects of climate change, principally sea level rise. This chapter compiles the process based information from the previous chapters in order to apply the coastal tract template on local morphology to provide for geological calibration of the Shoreface Translation Model.

CHAPTER 2

Deltaic influence on the adjacent coast: predominance over sea level rise as the cause of coastal erosion

Photo: Low tide at Costa da Caparica

2.1 Introduction

Deltas are important depositional systems defined as coastal sediment accumulations extending both above and below sea-level (Sutter, 1994). The development of these accumulations is often related to local tidal dynamics near an inlet or a river mouth (tidal deltas) in variable sea-level conditions. Deltaic structures are important elements controlling the littoral sediment-budget dynamics that influence coastal processes on the adjacent coastlines (Hicks and Hume, 1996). This influence is exerted directly though the supply of sediment: in some places deltas can be responsible of 30 to 60% of the sediment deposited in barrier systems (Hayes, 1980).

The proposition in this study, however, is that deltas can also have and indirect influence through protection of the adjacent coastline to direct wave action (sheltering and refraction) influencing littoral drift. This proposition is in counterpoint to the wave-related *delta-margin erosion* documented by Wright et al. (1980). Under stable sea-level conditions, even with a negative sediment supply (i.e, when a deltaic source becomes an estuarine sink, due to sea level rise or harbour dredging), deltaic development may be predominantly influenced by wave conditions indicating an adjacent wave-dominated sedimentary coast (Roy and Boyd, 1997) comprising accumulations of deltaic sediment.

In such complex sedimentary systems evaluation of low-order coastal behaviour to understand chronic erosion problems for effective management solutions can be applied. Analysis of low-order coastal behaviour (Cowell et al., 2003a) is required to quantify how a coastline reacts to secular variations in environmental conditions (Carter & Woodroffe, 1997). The quantification involves deriving estimates sediment exchanges that define the local sediment budget (Cowell, 2002) associated with evolution of local morpho-sedimentary structures. Morphodynamically, the sediment budget corresponding to

morphologic changes are mutual counterparts: *i.e*, estimates of one can be derived measurements or inferences about the other.

The objective of this Chapter is to reconstruct and quantify evolution of a delta-barrier complex in terms of sediment exchanges inferred from geological interpretations of the internal adjustments between the morphologies of the delta and adjacent coast of the Setúbal peninsula on the Portuguese west coast (Fig. 2.1) where a combination of morphologic structures, environmental conditions, and existing data provide a natural laboratory to examine the deltaic effects on an adjacent coast. The aim was to investigate the principle that deltas can control proximal coastal evolution regulating sediment supply processes. It was also investigated the deltaic sensitivity to external variations and if its morphologic reshaping can condition sediment dispersal patterns near the coast.

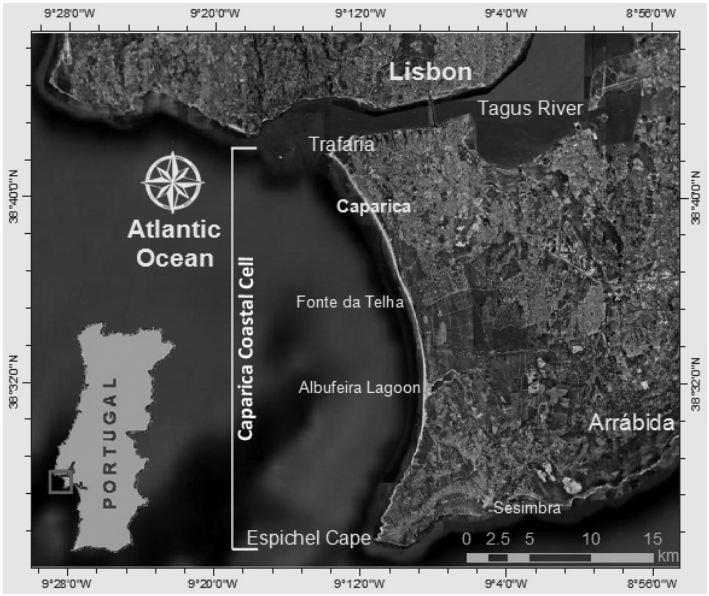

Figure 2.1 – Setúbal peninsula, Portuguese west coast.

2.2 Regional Setting

The study area is located in the Portuguese Atlantic west coast, immediately south of Lisbon, in a setting partially sheltered from the ocean wave climate by the prominent headland to the north of the coastal cell (Fig. 2.1). The cell forms the coast of Setúbal peninsula and comprises a set of morphological features (Fig. 2.2) indicative of distinctive modes of barrier evolution that vary with along the coast with proximity from the Tagus River delta. The barrier along the northern part the cell is part of, and therefore directly affected by, the delta (Fig 2.2). The southern portion of the cell is not part of the delta, but the question remains of the degree to which remote effects of the delta have influenced the evolution of this southern segment.

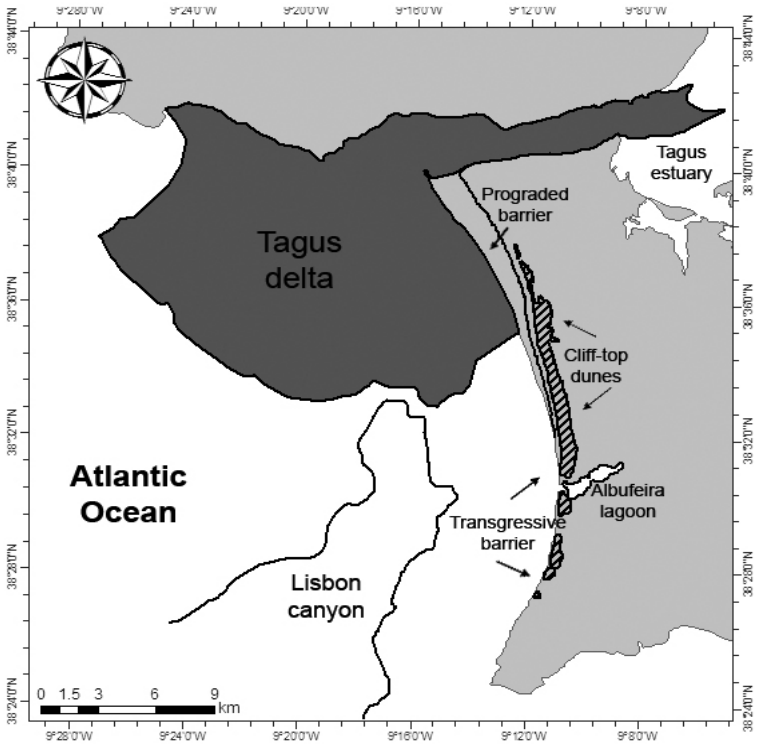

Figure 2.2 – Main morphological features of the studied segment.

Tides are semi-diurnal with mean spring tide amplitudes of 2.6 meters and 1.2 meters neap tides in a high mesotidal regime according to Hayes (1979) classification (Freire, 1993). The main wave direction is from the NW (77.3%) followed by the W direction (20%), while SW conditions are not common (<3%). Mean wave conditions include significant wave height of 1-2m (49%) and period of 5-7s (44%) while for peak wave conditions the period is 9-13s (60%) (Costa et al., 2001)

The Tagus delta is a prominent structure that enters the Atlantic Ocean near Lisbon in a passive continental margin with a narrow shelf (<30km) (Vis et al., 2008) significantly limiting the size of the the Tagus estuary basin. The delta comprises a well-developed ebb-tide delta and a small flood tide delta reflecting the interaction between tide effects and wave energy. Although a mesotidal environment, both ebb and flood tide deltas are not structurally similar (Fisher and Simpson, 1979) due to ebb-tide dominance in the estuary mouth. In spite of its sheltered position, wave effects have been significant in the development and evolution of the delta (mixed energy – wave dominated according to Hayes, 1979), but have played only a minor role within the central basin (Fortunato et al., 1999).

A prograded barrier complex (Roy et al., 1994) forms a strandplain immediately south of the river mouth but landward of the ramp-margin shoals of the delta. This strandplain has a classical drumstick configuration (Davis and Hayes, 1984) with the backbeach zone attached to mainland with no lagoon where the proximal northern end is wider than the southern end due to differences in progradation distances (Fig. 2.2). Corresponding to this alongshore variation in strandplain width, beaches are wide are wider in the northern proximal area, with dissipative surf zones (Short, 1979; Wright and Short, 1984; Sunamura, 1988; Lippmann and Holman, 1990; Short, 1999) and a well-developed dune system. Alongshore to south, the distal prograded barrier gives way to a much narrower transgressive mainland beach with characteristically reflective beach states (Short, 1979; Wright and Short, 1984; Sunamura, 1988; Lippmann and Holman, 1990; Short, 1999).

The barrier system is truncated by the presence of a coastal lagoon (Albufeira) in the middle of the coastal cell (Fig. 2.1). This lagoon has a 3.5 km maximum width and its axial length is 625 m (Freitas and Ferreira, 2004), separated from the ocean by a barrier beach, across which an inlet is artificially opened once a year. Overwash events commonly occur during storms.

The inland limit of the barrier system is a Mio-Pleistocene sea-cliff (Caparica cliff) that runs the full length of the cell, extending more than 100 meters above sea level in places (Azevedo, 1983). This cliff is composed essentially of detritic and carbonate geological formations (Teixeira, 1990). According to Cabral et al. (1984) the development of the cliff morphology is related to movements in a local set of geological faults that occurred between the upper Pliocene and the lower Quaternary. Because the base of the cliff is buried by barrier sediments along most of the cell, and by backbarrier sediments in the northern segment of the cell, the cliff is a paleo feature.

Along a significant portion of this cliff it is possible to observe cliff-top dunes as well as an older, extensive dune field further landward on the leeward side of the cliff. The thickness of these deposits varies between 30 and 60 meters (Azevedo, 1983; Pais et al., 2006; Costas et al., 2010) and their sediments are classified, according to Folk and Ward (1957) parameters, as fluvial sands (Azevedo, 1983). This infers that the possible origin of these sediments was the Tagus River prior to drainage network reorganization. Optical Stimulated Luminescence (OSL) (Costas et al., 2012) and ^{14}C paleosoils dating (Pais, et al., 2006) place dune deposit activity occurring until late Holocene (1190$\pm$90 ky BP to 0.98$\pm$0.05 ky BP). The development of these cliff top dunes relates to the presence of climbing dune structures in positive sediment supply conditions (Tsoar, 1983; Ferraz et al., 2011)

The offshore limit of this system is the continental shelf boundary, between the 130 meters and 180 meters bathymetry, with a 30 kilometres width in the north part, near the Tagus delta, and a 5

kilometres width in the south part (Fig. 2.1), next to Espichel headland (Freire, 1999). Two canyons cut the shelf platform: the Lisbon Canyon and the Cascais Canyon. The Lisbon Canyon extends in the shoreface, making it a potential sediment sink under some conditions.

Human activities in the Lisbon area and Tagus River started before Roman occupation (Pimenta et al., 2005) and became more intense through time. Vis et al., (2010) identified four distinct depositional phases in the river catchment, approximately between 2300 and 670 cal BP, that were more related to increasing human activity (deforestation and erosion) than climate change. During the Portuguese age of discoveries, Lisbon became a major harbour with ships constantly sailing on the river (Nabais, 2009). Harbour activity and development however increased significantly in the 20th century (Freire, 1993) with the use of larger ships and the need of bigger dockyards. Progressive intensification in anthropogenic impacts such as dredging and harbour-mole construction in the Tagus estuary, during the development of Lisbon as a major port, changed sediment availability (Ferraz et al., 2011) leading to the assumption that this could be one of the causes for the observed erosion of the proximal coastline south of the estuary.

2.3 Methods

2.3.1 Geological coastal evolution

The quantification procedure was applied to the main sedimentary structures whose changes can be representative on long-term coastal behaviour.

The Tagus delta

The depositional history of the Tagus deltaic was interpreted from seismic data obtained on two separate oceanographic survey cruises offshore of Lisbon, LX98 and TESA, using a boomer sound source for seismic profiling. A total of 23 2D seismic lines were used to interpret morphology, depositional thickness and the position of the basal shoreface-ravinement surface to characterise the architecture of the deltaic deposit. From this set of seismic lines, four specific lines were chosen due to its location relative to the delta and barrier complex (fig. 2.3). Data were interpreted using Landmark SeisWorks® software and integrated in GIS for proper geographical location.

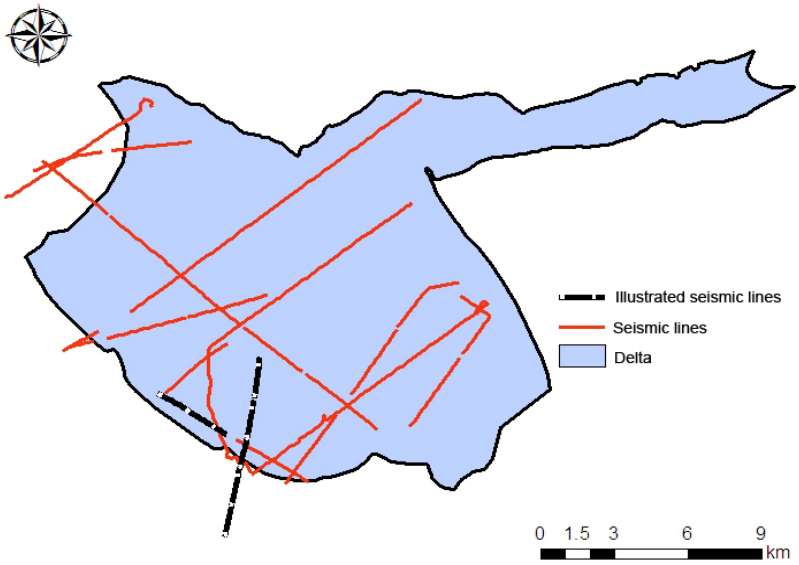

Figure 2.3 – Seismic lines over deltaic structure (SW-NE profile composed of three lines)

Prograded and transgressive barrier system

The prograded barrier volume was quantified using borehole data from local geotechnical surveys in the Caparica area (Fig. 2.4) (see appendix I). This information made possible to evaluate the thickness of recent deposits of the prograded barrier as well as constraining the boundary position of the Miocene substrate. Since there were no data from the south part of the cell, the transgressive barrier thickness was inferred from the prograded barrier borehole information.

Figure 2.4 – Location of the geotechnical bore holes.

The Albufeira lagoon flood-tide delta was quantified as part of the barrier system. This analysis was performed in GIS with bathymetric data of the area (Freitas, 1995) where the sediment thickness was established from the geometric relation between the positive barrier topography, the negative flood-tide delta bathymetry and the overall lagoon depth.

Cliff-top and climbing dunes complex

Analysis of cliff-top dune dimensions was performed using topographic data from local Digital Elevation Models (DEM) imported into GIS. The DEMs were used to estimate volume of cliff-top dune deposits based on the average thickness calculated for each deposit based on Ground-Penetrating Radar results obtained by Costas et al., (2010) and Costas et al., (2012). Groundtruthing of topography was performed using a GIS/GPS integrated system.

Climbing dune geometry was modelled based on physical principles developed by Tsoar (1983). According to Tsoar's (1983) wind tunnel experiments, when wind encounters a vertical cliff its velocity begins to drop and direction reverses with the formation of an eddy. If the sediment supply is constant or the cliff is inclined, with slopes less than 55 degrees, the size of the reverse-flow eddy decreases and sediment begins to deposit at the base of the cliff (Fig. 2.5). Sediment tends to accumulate forming a climbing dune. The wind-tunnel experiments also indicated that the region in which dunes accumulated in front of the cliff was limited to a maximum distance (d) from the cliff that varied with cliff height (h): $2.0 \leq d/h \leq 3.5$ (Tsoar, 1983; Ferraz et al., 2011).

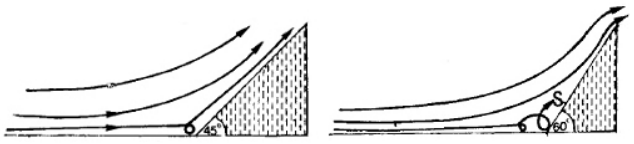

Figure 2.5 - Wind flow over cliffs with different slopes. Examples of 45º (left) and 60 º (right) (adapted from Tsoar, 1983).

The geometry and volume of the climbing dunes, as well as their base positions, were inferred from Tsoar's empirical relations applied to DEM representation of the Caparica cliff configuration in the areas where cliff-top dunes could be observed.

Quantification of sediment sinks

Sediment sinks were identified using composed geological and bathymetry data from LNEG (Portuguese Geological Survey) database. GIS analysis was performed to quantify available sediment accommodation volumes.

Wave climate modelling

Wave data analysis was based on two different data sets: Sines buoy data from the Fleet Numerical Meteorology and Oceanography Center (FNMOC) for a period between September 2003 and January 2009; and data from a 57 year hindcast (1953-2009) from the Micore project (Morphological impacts and coastal risks induced by extreme storm events) (Dodet et al., 2010). The available data were compared to validate the 57 year hindcast results with the 5 year effective measurements.

The DHI software Mike 21 spectral wave model (SW) was used to estimate inshore the wave conditions in the study area for the main wave directions (NW – 330º, W – 270º, SW – 250º). Mean and peak wave conditions parameters from the wave data were used with the bathymetry of the area to characterise nearshore wave directions. The selected domain of the model is larger than the study area, using a significant part of the Portuguese coast to avoid boundary reflections that can affect results.

Each one of the main directions was modelled using the most frequent values of significant wave height, period and direction for mean and peak wave conditions. Output results relate wave direction and wave power due to its relevancy to nearshore sediment transport.

2.3.2 Historical shoreline mapping and volumetric estimates

Recent evolution was characterised using a georeferenced historical map (1882) and aerial photographs (1958, 1967, 1980, 1989, 1999 and 2007) of the area that were compared through GIS analysis. Accuracy of the data is strongly dependent on image quality for the case of the aerial photographs where pixel size varies between 0.16m and 0.5m. Historical maps precision is difficult to determine. However, the capacity of the image to constrain proportions during the georeferencing process is a good indicator of accuracy.

Coastline position on aerial photographs was established through standard mapping methods (Morton and Speed, 1998; Pajak and Leatherman, 2002) using relevant morphologic indicators (beach berm, dune toe and sea-walls). If these indicators were not visible due to low image quality the high water line (HWL) was used (Leatherman, 2003). To minimize effects of fluctuating coastal change perturbations (short-term changes in morphology) only three periods were considered for sediment balance purposes: 1882, 1958 and 2007.

The Digital Shoreline Analysis System (DSAS) (Thieler et al., 2009) was used to compute the statistics of shoreline migration through time using vector data. The time series of historically mapped shoreline positions were referenced against static baseline (cliff base) using transects spaced at 500 m intervals, from which erosion and accretion was calculated as the areas between successive shorelines. Volume calculations for the overall evolution (1882-2007) were performed comparing DEM surfaces, using the 1882 altimetry data and the most recent bathymetric datasets.

2.4 Results

2.4.1 Geological evolution – the long-term approach

Interpretation of the geological evolution was based on the coastal tract concept (Cowell et al., 2003a,b) were dynamically interacting morphological elements work as sediment sharing systems over a common substrate.

The Tagus delta

The Tagus delta development can be expected to have been determined by sand supply and the influenced of local tide and wave conditions. Previous studies (Hidroprojecto, 2001) show constant morphologic changes in the delta through time, some of it influenced by anthropogenic actions.

Seismic longitudinal profiles results show an aggradational structure with overlapping topsets and well developed clinoforms that become narrower towards the bottomsets (Fig. 2.6). This upward translation is typical of positive accommodation and sediment supply conditions (Emery and Myers, 1996). The lower limit of the deltaic structure is identifiable by the presence of a wave ravinement surface (WRS) located between depths of 130m and 110m. The onset of transgressive system tract development was estimate to have occurred at 20,000yr BP from relative positions of the WRS with global (Fleming et al., 1998) and local (Dias et al., 2000) eustatic sea-level curves.

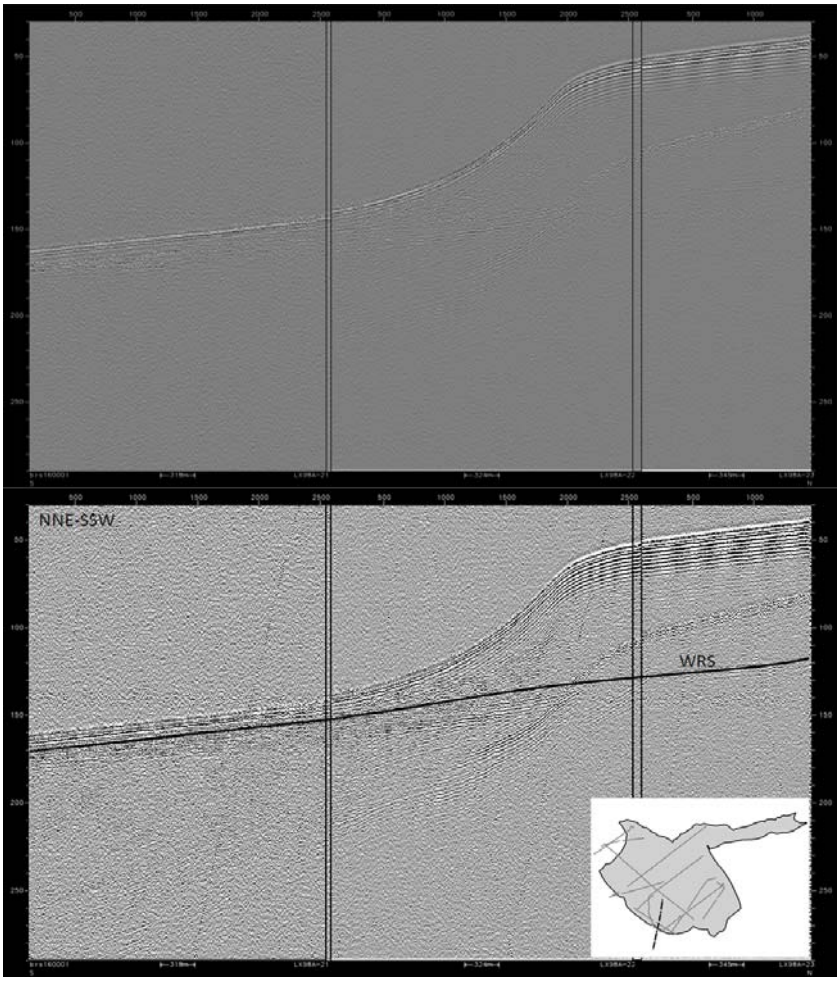

Figure 2.6 - Seismic longitudinal profile of the Tagus delta (depth in ms) composed by three seismic lines.

Below the WRS, transverse profiles allowed the identification of a lowstand system tract represented by a Tagus paleo-channel (TPC) resultant from multiple stages of channel cut and fill (Fig. 2.7), typical of inlet tidal deltas (Oertel et al., 1991). It is assumed that the TPC maximum incision was developed during the last glacial maximum (LGM) period over a Miocene to Pleistocene substrate. The sediment filling has an indeterminate age while the WRS is related to the fast sea-level rise occurred between 20,000 and 7,000 cal BP. Over the WRS it is possible to observe a thin layer that comprises the transgressive system tract. Immediately above the WRS, pro-delta deposits started developing 7,000 years ago, when sea-

level stabilized in the area (Vis et al., 2008). At the top, the high stand system tract caps the transgressive sequence with a recent deposit and a smooth surface.

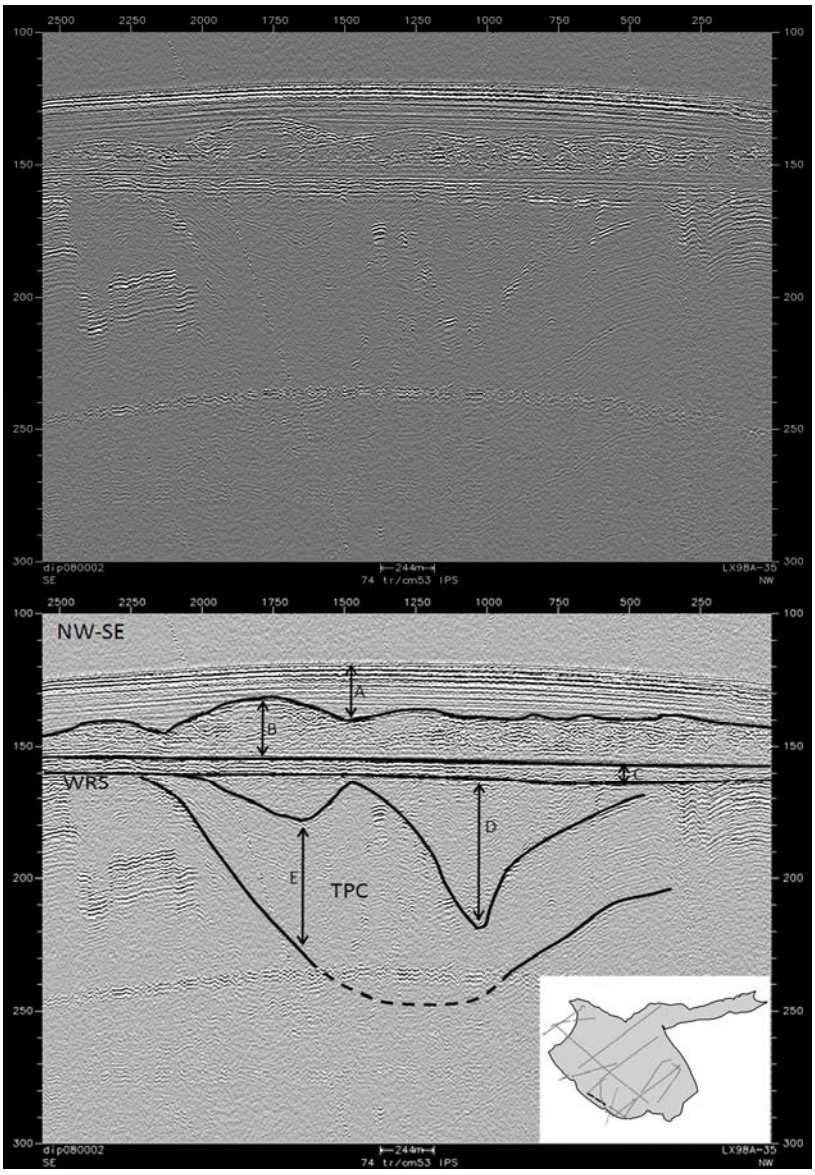

Figure 2.7 - Seismic transverse profile of the Tagus delta. (A – High stand system tract deposits; B – Pro-delta deposits; C – Transgressive system tract deposits; D and E – Channel filling deposits) (depth in ms).

The WRS position was adopted as the base for GIS analysis and calculations of deltaic volume which totals $3.9988x10^{9}m^{3}$ with an overall area of $1.9779x10^{8}m^{2}$.

Prograded and transgressive barrier system

Borehole data from three different geotechnical campaigns resulted in 11 bore holes that were used to define the internal structure of the prograded barrier system. Bore logs (see Appendix I) indicate two major geologic layers: An Holocene medium to fine sand layer with a thickness between 7.6m and 13m on top of a sub-horizontal Miocene substrate with a small northwards slope of 0.1 degrees, composed by compacted sand and/or clay often with marine shell fragments (Fig. 2.8). The erosive action of the ocean on the Miocene layers developed a superficial notch where Holocene sediments became stranded during relative sea-level rise. After sea-level stabilization (~7000 cal BP) (Vis, 2008) development of prograded barrier is evident implying positive sediment supply conditions.

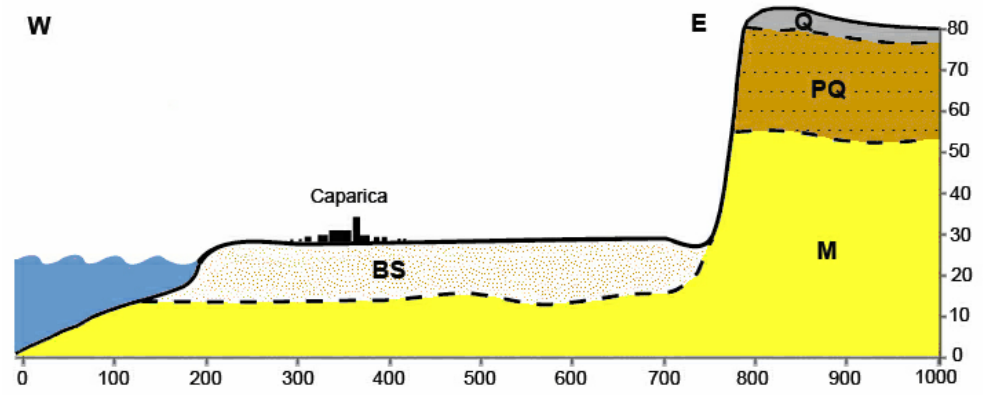

Figure 2.8 – Interpretative illustration of the local geological setting (BS – Barrier System; M – Miocene; PQ – Plio-Quaternary; Q – Quaternary. Axis in meters).

Insufficient information about the transgressive barrier system in the south part of the segment forced an interpolation exercise where an internal geometry similar to the prograded barrier was assumed.

Quantitative calculations based on the reconstructed barrier geometry yielded a total area of $9.4647x10^6m^2$ for the overall prograded and transgressive barrier system corresponding to a volume of $1.3419Ex10^8m^3$.

The rough description of the geological setting in bore logs did not allow the observation of finer structures that may occur within the barrier system.

The Albufeira lagoon flood tide delta was also quantified as part of the barrier system as its development provides a proxy for dimensions of backbarrier deposits associated with the barrier rollover mechanism under transgressive conditions (Cowell et al., 2006). For this purpose, the barrier geometry was estimated from the flood-tide delta bathymetry, from which a volume of $2.5718x10^5m^3$ for an $8.5725x10^4m^2$ area was obtained.

Cliff-top and climbing dunes complex

GIS analysis of the Caparica cliff showed that the most common slopes are between 20 and 40 degrees and only one occurrence is greater than 55 degrees (60°). The presence of landslide deposits comprising Mio-Pleistocene material at the base of the cliff contributed to the reduced angles.

Lower angle slopes assist the development of climbing dunes under prevailing-wind conditions. Assuming a paleo-wind regime similar to the predominant direction at present, conditions would have been favorable for the development of climbing dunes. At present, data from the Lavradio meteorological station, located 15km East of the Caparica area, indicates predominant winds from the

westerly quadrant occurring 35.1% of the time with relatively constant average annual speeds of 3.9 m/s (CostaPolis, 2005), which exceeds the threshold shear velocity for the dune sand.

GIS analysis also indicates that the cliff heights, where cliff-top dunes are present, vary between 5 and 80 m with an average value of 49 m. Applying the principles of Tsoar (1983) $2.0 \leq d/h \leq 3.5$, the deposition distance from the cliff varies between 10 and 280 m (Table 2.1). Quantitative calculations of the modeled climbing dunes were based on the obtained average distances for each d/h ratio resulting in estimated volumes of $1.5198 \times 10^7 m^3$ and $6.0332 \times 10^6 m^3$ for *d/h* ratios of 3.5 and 2.0 respectively.

Table 2.1 - Deposition distance (*d*) based on the cliff height (*h*) and the *d/h* ratio. It is also represented the slope value (α) of the climbing dune for each case.

d/h		**3.5**			**2.0**	
	Min.	Avg.	Max.	Min.	Avg.	Max.
h(m)	80	49	5	80	49	5
d(m)	280	171	18	160	97	10
α(º)		16			27	
Vol.(m^3)		15,197,740			6,033,201	

Separate quantification of the cliff-top dunes indicates that these deposits occupy an area of $10{,}005{,}3001.0005 \times 10^7 m^2$ with a corresponding volume of $1.2913 \times 10^8 m^3$.

Comparison of the modeled climbing dunes with the present-day coastline position indicates that, in order to accommodate these deposits, the coastline must have experienced significant changes throughout most of the cell. Given that the northern segment of the cell lies within the Tagus delta margin, whereas the southern portion lies beyond discernible morphology of the delta margin, it is

possible to divide the coastal cell in two sub cells with the division being on Fonte da Telha beach (Fig. 2.2). The sub cell south of Fonte da Telha does not have physical horizontal space at present to accommodate a climbing dune (Fig. 2.9) due to the narrow beaches at the base of the sea-cliff. The insufficient physical space suggests that coastline has migrated inland since the dune complex developed, resulting in the destruction of the climbing dune component.

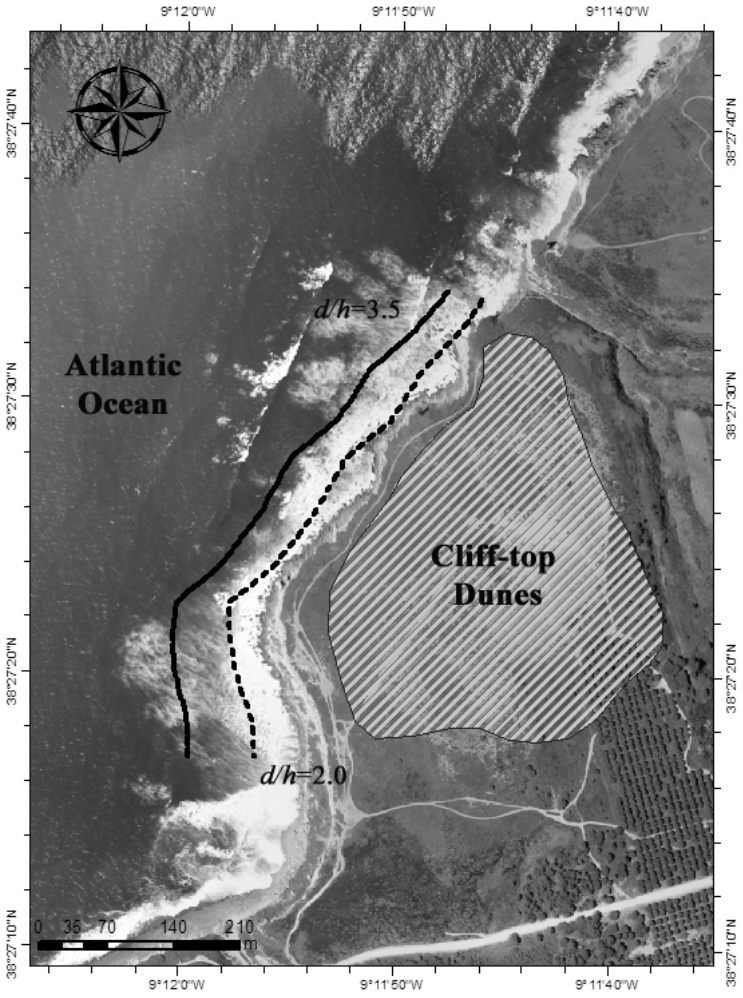

Figure 2.9 - Southern area. Solid and dashed lines represent the different deposition distances and consequent position of the climbing dune base (*d/h*=3.5 – solid line; *d/h*=2.0 – dashed line).

North of Fonte da Telha, where the barrier becomes wider (Sec. 2.2), the coastline position has sufficient horizontal space for the development of a climbing dune. However, the absence of the deposit today implies an erosive event where the coastline migrated inland eroding the sand ramp material and redistributing it leaving the cliff-top dunes isolated as evidence that a sand ramp formerly existed (Fig. 2.10). This sediment redistribution could be one of the engines related with the prograded barrier development.

From these results it is possible to infer two distinct coastline migration events after the development of the climbing dunes:

(1) Coastline retrogradation related with erosion of the climbing dune structure leaving the cliff-top dunes as testimony;

(2) Coastline progradation (only in the segment north of Fonte da Telha) allowing the development of a prograded barrier.

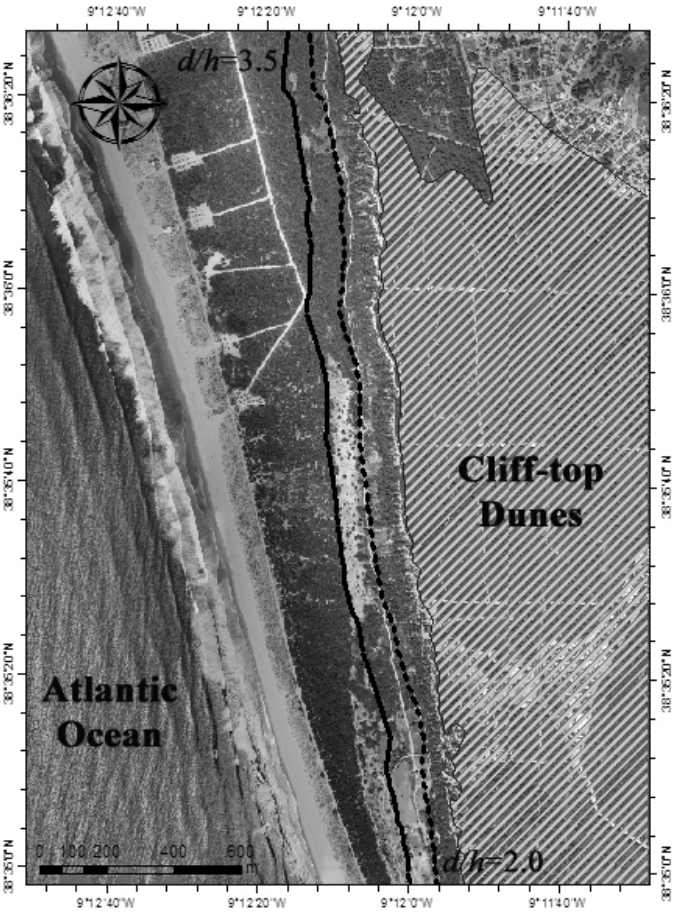

Figure 2.10 - Northern area. Solid and dashed lines represent the different deposition distances and consequent position of the climbing dune base (*d/h*=3.5 – solid line; *d/h*=2.0 – dashed line)

These remnant cliff top dunes provide evidence from which estimates of former shoreline shoreline positions, now effaced through erosion, can be estimated. These dunes, when dated, therefore provide evidence to assist in reconstruction of the depositional history and for the estimation of paleo-erosion volumes.

Quantification of sediment sinks

Since the evolution of this coastal cell is dominated by erosive events, it is important to identify availability of accommodation space available for the eroded sediment. Three distinct areas were identified has possible sediment sinks: The Tagus estuary (deltaic channel and estuary entrance), the Lisbon canyon and an enclosed area between Jurassic rocky outcrops offshore Espichel headland (Fig. 2.11). The importance and the activity of each sink is significantly dependent on local wave conditions.

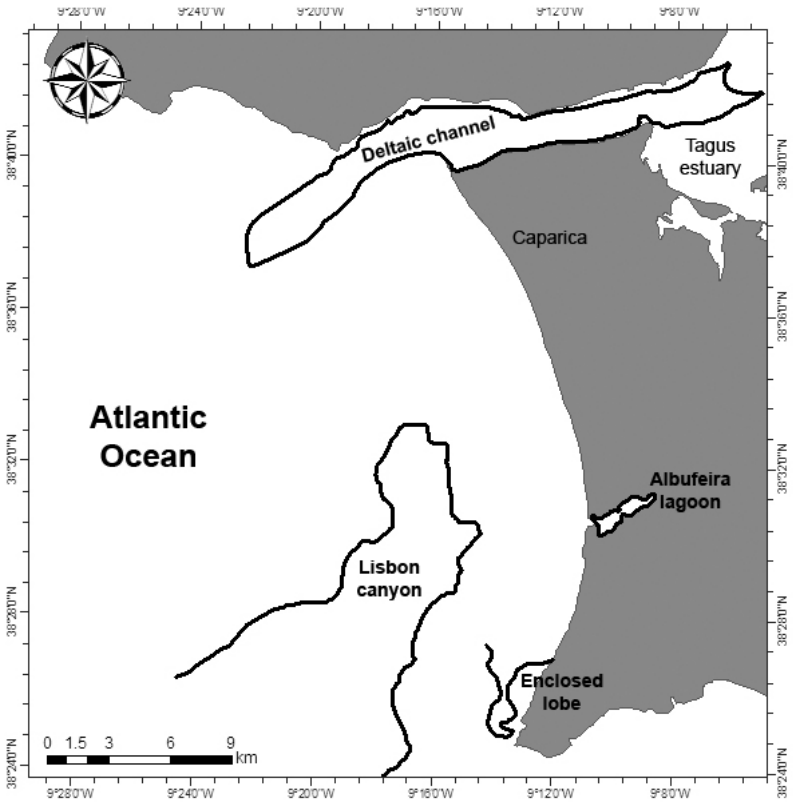

Figure 2.11 - Local sediment sinks

The Tagus estuary and deltaic channel potentially provide the main sediment sinks of the area. Their location near the delta-barrier complex probably influences the erosion of the north part of the segment in specific wave conditions. An analysis to the bathymetry and measurements relative to mean sea-level allowed to quantify an overall accommodation volume of $5.4570x10^{8}m^{3}$ in an area of $4.5400x10^{7}m^{2}$ for this sink.

A comparison between the present bathymetry with that of 1882 shows no significant changes in the delta for this period, with bathymetric differences ranging between 2 and 10m. However, in the northernmost part of the cell it is possible to observe a significant loss involving more than 15 meters surface lowering in places, representing a volume of $2.2330x10^{7}m^{3}$ for an area of $3.1160x10^{6}m^{2}$. This loss is related to dredging executed to allow large cereal transport vessels to reach this area of the harbour.

Although the Lisbon canyon is potentially the biggest sink of the area, sediment bypassing from the shelf to the canyon is unlikely to be common at present. An analysis to the local sediment map (IH, 2005) shows a clear separation (4.3 to 1.1km) between the sandy sediment areas and the head of the canyon where muddy sediments are dominant. Nevertheless, the possibility cannot be ruled out that in some conditions it still can work as a sediment sink.

The analysis of the local bathymetry as well as the sediment map (IH, 2005) revealed a lobe on an enclosed area between rocky outcrops in the south part of the coastal cell, immediately to the north and offshore from Cape Espichel (Fig. 2.12). The comparison between the present bathymetric data with that for 1882 and 1939 shows that in this specific area bathymetry varies considerably through time (Fig. 2.13).

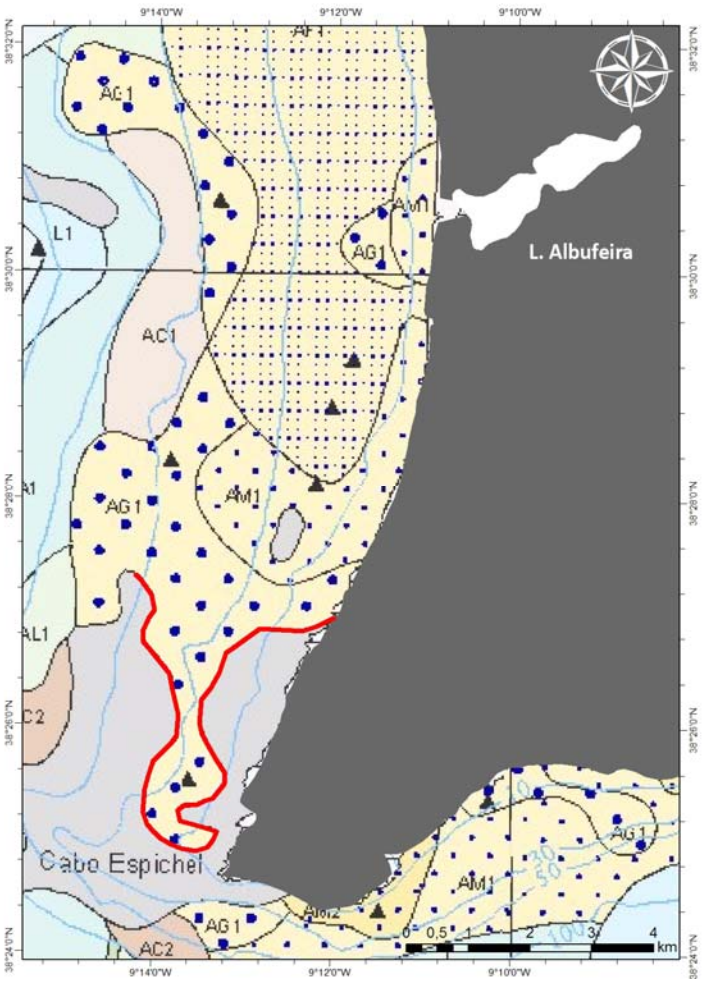

Figure 2.12 - Enclosed lobe between rocky outcrops (red outline). Sediment distribution map as background (IH, 2005).

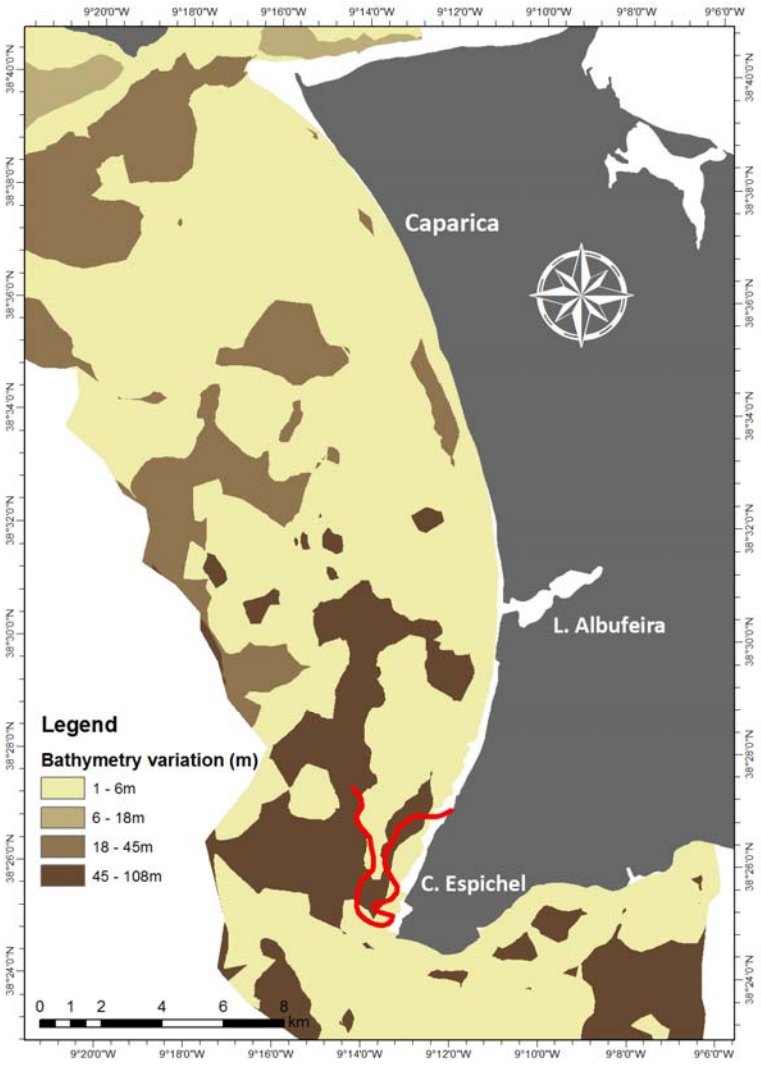

Figure 2.13 – Surface comparison between the present bathymetry and the 1882 data (trend validated by 1939 data). Darker colours reflect the areas with larger variation in sediment thickness.

Based on its area, the lobe is capable of accommodating considerable amounts of sediment (6 to 15 million cubic meters), if local bathymetry changes of few meters (1.2 to 3 meters respectively) are assumed. It also seems reasonable to infer that sediment bypass may occur between this segment and the segment located immediately south, in certain conditions, contributing for the development of perched beach deposits in between Jurassic cliffs of the south coast of Sesimbra (Fig. 2.14).

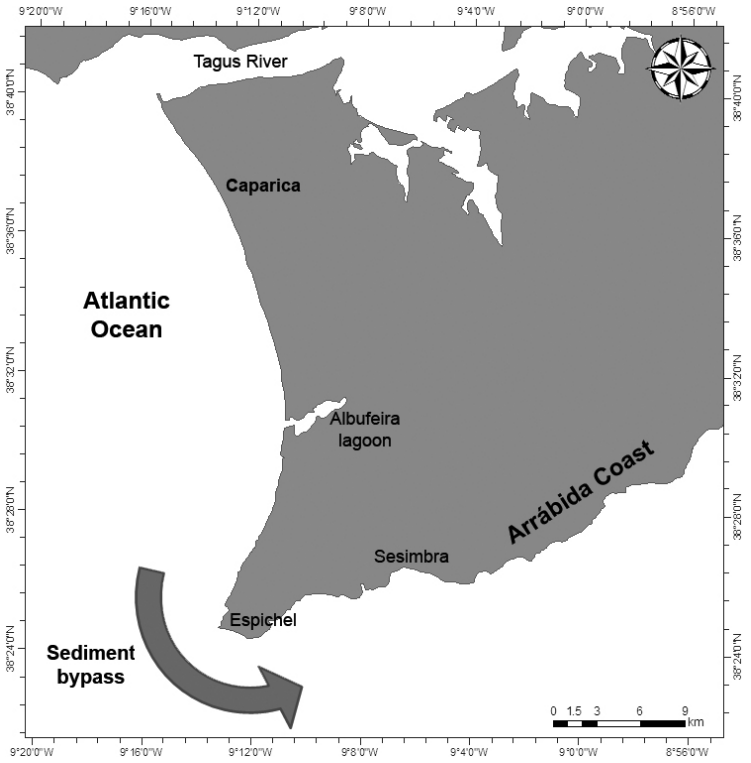

Figure 2.14 - Sediment bypass between the west coast and the south coast (Sesimbra and Arrábida).

Despite its small size, the Albufeira lagoon is an important sediment sink particularly for the south part of the segment. Its inlet, artificially opened once a year, draws sediment into the lagoon creating a protrusion in the coastline and a slight retreat in the adjacent flanks. The overwash events, more common during winter storms, also contribute for the sediment retention and the possible ongoing

growth: the depth of lagoon indicates that considerable accommodation potential remains of the flood tide delta. Any sea level rise further increases accommodation capacity of the lagoon as a sink. Volumetric quantification based on the bathymetry shows that the lagoon can accommodate $7.1845 \times 10^6 m^3$ in an area of $1.2439 \times 10^6 m^2$.

2.4.2 Wave climate modelling

Since the Caparica coastal cell is a wave-dominated coast exposed to an open ocean regional wave climate (Roy et al., 1994), locally generated currents and wind waves were not considered. Wave model results show that, for both mean and peak wave conditions, results are similar regarding the main wave directions (NW, W and SW) (Fig. 2.15). The main differences are related with wave diffraction caused by the northern headland (Roca headland) and the delta bathymetry that causes two different sand-circulation cells, divided by a divergence point that migrates depending on the main wave direction.

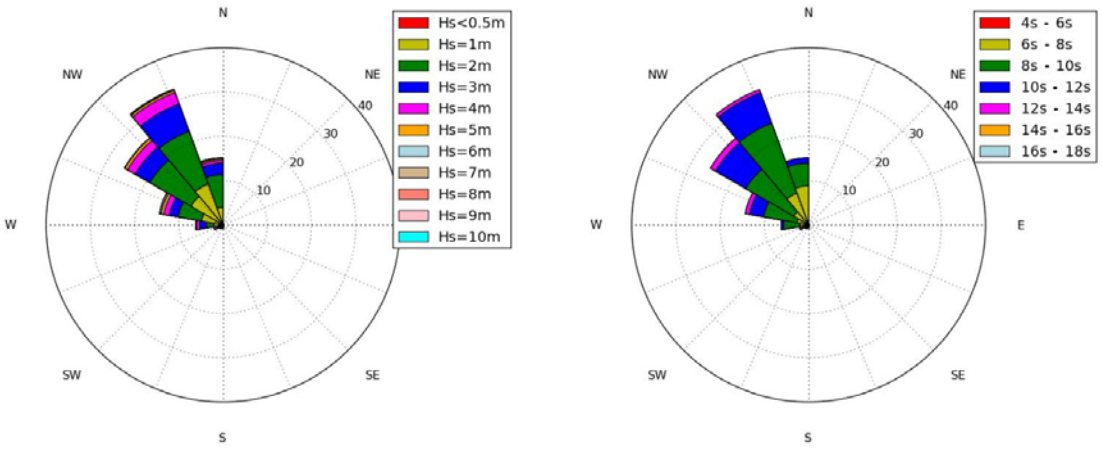

Figure 2.15 – Wave direction in relation with T_m and H_{sig}

In NW swell conditions (330º), the most common with 77% of the occurrences (Costa, et al., 2001), nearshore wave propagation separates into two cells as a result of the wave refraction mainly caused by the deltaic structure. In the north part, south to north wave driven transport predominates while in the southern area the opposite occurs (Fig. 2.16). The surfzone sand transport directions indicated by these refraction patterns suggest that

(a) sediment eroded from the north part of the prograded barrier is mainly deposited inside the estuary, while

(b) in the southern area the sediment is distributed to the available sinks (lobe offshore Espichel headland, Albufeira lagoon and the Lisbon canyon) if the conditions allow.

The refraction results indicate NW wave conditions are the most favourable to supply the prograded barrier with deltaic sediment.

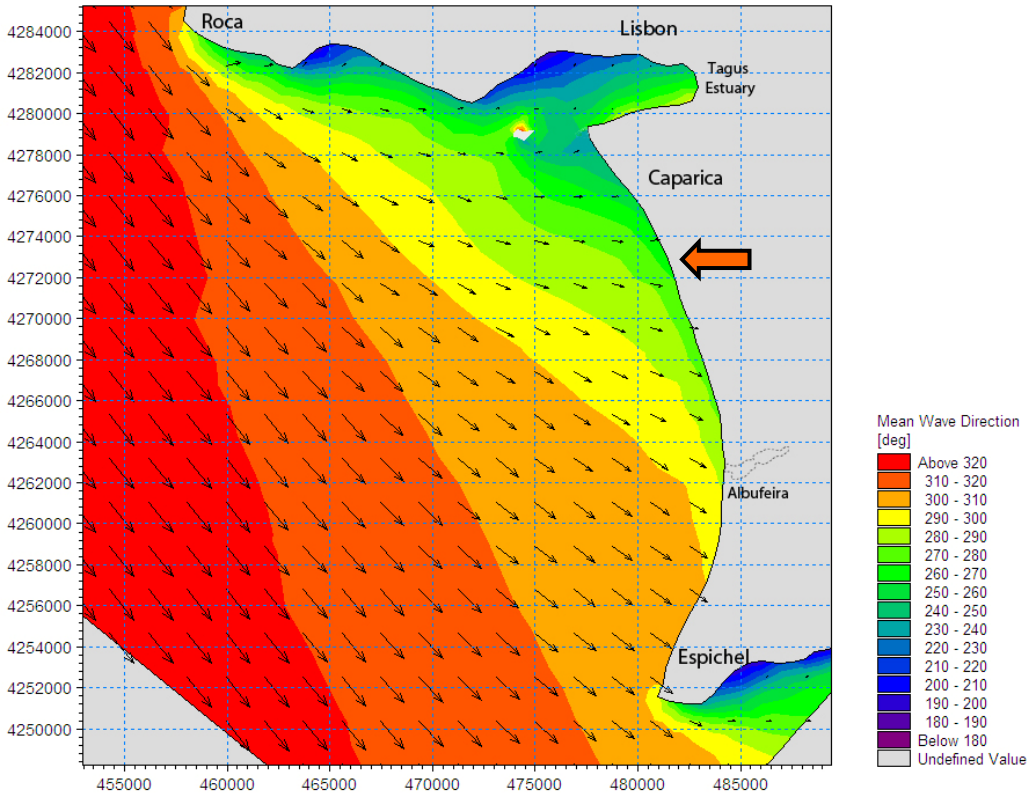

Figure 2.16 - Model results for NW direction (330°) in peak wave conditions (large arrow indicates the wave divergence point)

In the case of the W swell (270º), the second most common with 20% of the occurrences (Costa, et al., 2001), nearshore wave propagation is once more divided in two cells as a result of the wave refraction caused by the delta. In the north part of the cell, south to north wave driven transport is dominant while in the southern part the transport is the opposite. Between both areas, a small segment of shoreline exists where waves propagate parallel to the coastline diminishing the alongshore wave driven transport (Fig. 2.17). Sediment sinks and sources work in the same conditions as with the NW swell. However, in the central part of the cell, due to the parallel swell, cross-shore transport predominates and sediment

is conserved in most of the area. The only exception is the Albufeira Lagoon that works as a sediment sink for shoreface sediment.

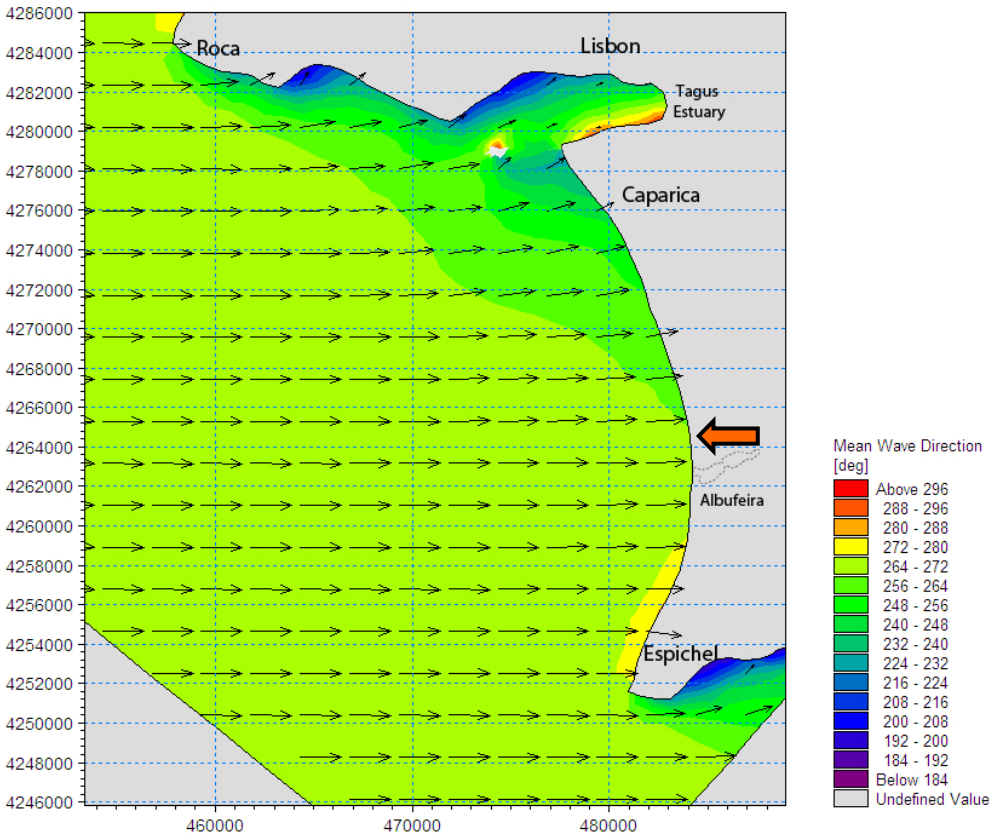

Figure 2.17 - Model results for W direction (270°) in mean wave conditions (large arrow indicates the wave divergence point)

For SW swell (250º), which is less common with 2.4% of the occurrences (Costa, et al., 2001), nearshore wave propagation occurs from SW to NE in the entire segment (Fig. 2.18) without any divergence point. Tagus estuary works as the main sediment sink under these conditions while the delta does not contribute sediment to the barrier complex. Albufeira lagoon can also be pointed as a sink for the southern end sediment.

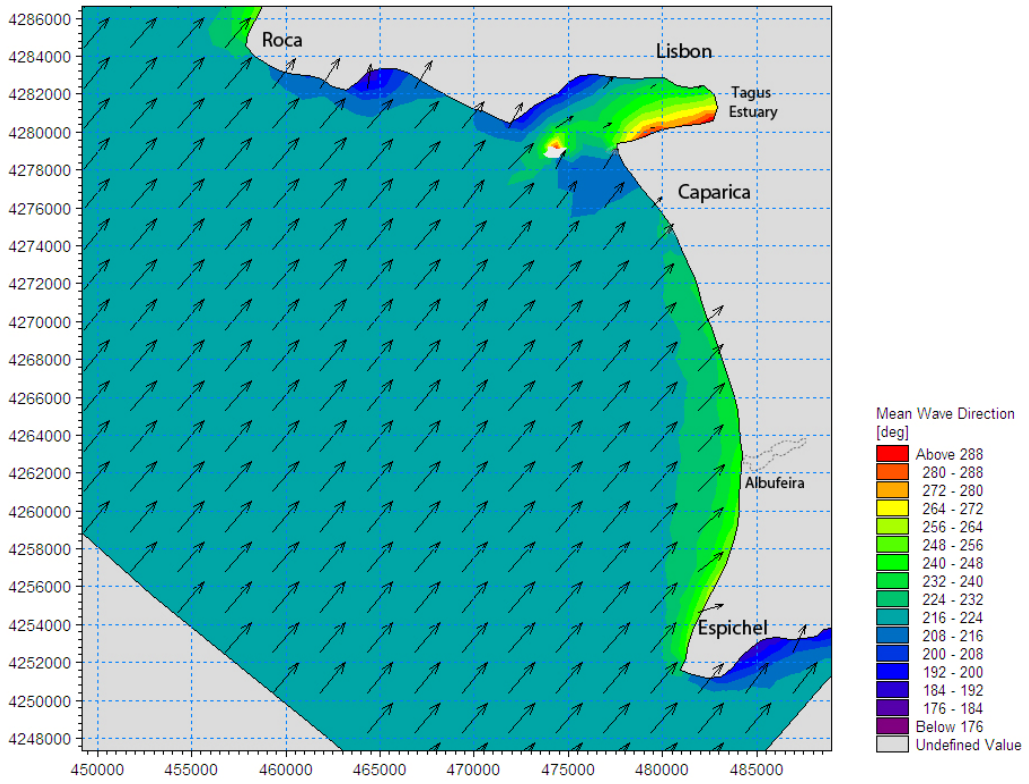

Figure 2.18 - Model results for SW direction (250°) in mean wave conditions

Overall therefore, since NW swell is predominantly followed by W swell (Costa, et al., 2001), it is likely that peak and mean wave conditions for both swell directions shape result in two sub cells of divergent alongshore transport in the surf zone. These results suggest that Tagus delta works as the main sediment source and the Tagus estuary as the main sediment sink. In the south part of the segment the Albufeira lagoon, despite its small size, works as sediment sink in most of the situations.

2.4.3 Recent coastline evolution – Erosion

Despite different authors having already studied the recent evolution of the Caparica coastal cell, no previous analysis has been undertaken to eliminate local and periodic fluctuations (<50m) that can affect the characterization of large scale coastal behaviour. The recent dynamics of the area shows an erosive tendency, almost exclusively in the north part, where a significant land loss and shoreline retreat of a cuspate spit has occurred (Fig. 2.19).

Figure 2.19 - Coastline position (1882, 1958 and 2007) and erosion area between 1882 and 2007 (in red).

The period is characterized by intensive erosive episodes interspersed by small accretion phases in which artificial nourishment was performed to maintain coastline position. Comparative results based on GIS analysis using DSAS (Thieler et al., 2009) (Table 2.2) show an average shoreline retreat of 406m between 1882 and 2007 with a gradient of 3.2m/yr and $6.3161 \times 10^6 m^2$ of area lost. Between 1958 and 2007 the average retreat was 79m (1.6m/yr retreat gradient) with a corresponding area loss of

$8.3134x10^5m^2$. This shows that the most significant coastline retreat occurred between 1882 and 1958 with 327m corresponding to a 4.3m/yr retreat gradient and a $5.4847x10^6m^2$ loss. Results from topographic comparison between 1882 and 2007 show an overall erosive volume of $4.6428x10^7m^3$.

Table 2.2 – Quantitative erosion based on DSAS and GIS analysis.

Period	Average retreat (m)	Retreat rate (m/yr)	Area (m^2)	Volume (m^3)
1882-1958	327	4.3	5,484,736	n/a
1958-2007	79	1.6	831,342	n/a
1882-2007	406	3.2	6,316,078	46,428,110

The magnitude of the erosive processes is significantly larger for the 1882-1958 period. However, despite being a longer period (76 years) relative to the 1958-2007 period (49 years), the difference in erosion magnitudes indicate an exponential decrease of available sediment in the barrier complex. As the sediment availability diminishes the erosion rates follow, and the negative exponential trend is consistent with the tendency for a dynamic equilibrium to be established. The construction of permanent coastal protection structures in the 1960's may also be responsible for a decrease in erosion rates.

Sediment losses in the south part of the deltaic structure are mainly caused by the presence of a flood-tide channel (Hidroprojecto, 2001) transporting sediment from the delta and the barrier into the estuary. The erosion of three small islands near Bugio (visible in the 1882 map) and the landward migration of the sand spit at the northern end of the barrier are all indicative of an overall erosion erosive tendency (Fig. 2.20).

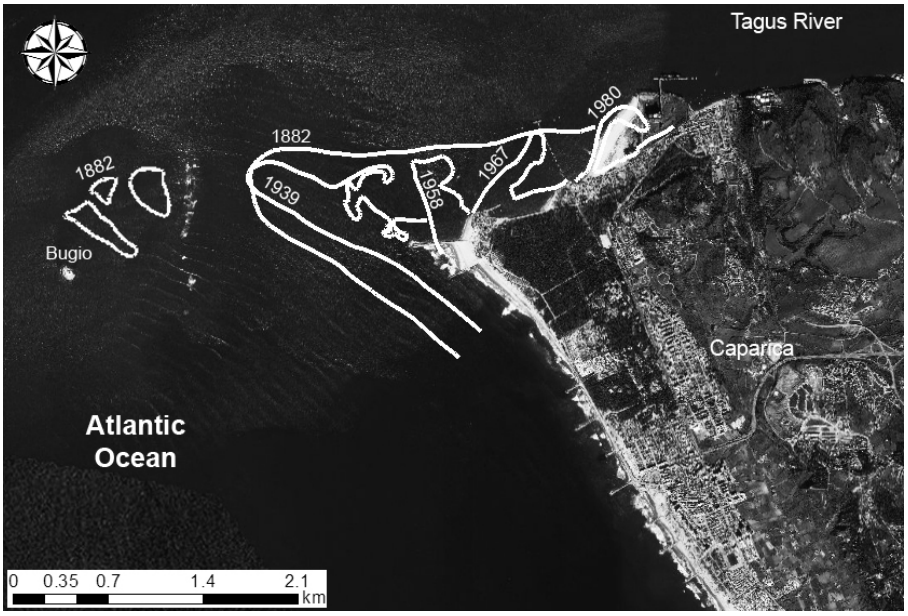

Figure 2.20 - Illustration of sands pit erosion and migration towards the estuary through different periods (2007 aerial photo in the background).

2.5 Discussion

The thickness of the transgressive system tract seen on seismic data is an obvious signature of the fast sea-level rise that occurred in this area between 20,000 and 7,000 years. After relative sea-level stabilised (~7000 cal BP) (Vis et al., 2008) available sediment either from the river and the continental shelf contributed to the development of the delta and adjacent morphological features. These features are typical of those developing under stable sea-level conditions, as prograded barriers and spits (Roy et al., 1994). This depositional history indicates the importance of the delta in controlling sediment storage and dispersal in which the morphological development of the overall coastal cell is dependent.

Since no chronological information is available for the prograded barrier it can be inferred that the development of the barrier is coeval to the delta. However, knowing that the cliff-top and climbing dunes complex was still intact and growing up to 1000 years ago constrains the time frame (Costas et al., 2012; Ferraz et al., 2011). Coastline configuration was different at this stage especially in the south part where its position was well offshore of its present location, inferred from the necessary existence of sand ramps with the cliff-climbing dunes at that time. A subsequent major erosive event caused the complete erosion of the climbing dune structure inferring a significant coastline retrogradation to the base of the cliff. The eroded sediments must have been displaced to sinks, which the results suggest include the Lisbon Canyon and sediment bypass to Sesimbra and Arrábida in the southern part of the cell. The mechanisms of this erosive phase are not well understood as there are no distinguishable sedimentary signatures to it. However, sea-level variation or changes in storm demand are possible causes.

The erosion phase was followed by a coastline progradation in the north part of the cell due to a positive sediment supply developing a prograded barrier system with a beach and dune complex. In the southern

area coastline position was preserved due to insufficient sediment supply and/or the continued action of the sediment sinks. This prevented progradation from conserving a relict transgressive barrier, to be replaced by a mainland type beach in a semi-equilibrium stage, examined further in Chapter 4. From this point in time the cell is likely to have been divided into two distinct cells with different morphologies and evolutionary characteristics.

As tidal currents on the shelf do not have sediment transport capacity (Monteiro and Moita, 1968) waves dominate the sediment transport through the NW and W predominant swells. The intense wave refraction caused by the delta defines the littoral drift pattern and consequent sediment distribution in the area (Fig. 2.21). Deltaic sediment is redistributed towards south, supplying the shelf and the barrier complex. Possible losses to the canyon may occur during this process. For a sediment budget definition it is also important to consider the contribution of the sediment eroded from the climbing dunes complex within the prograded barrier.

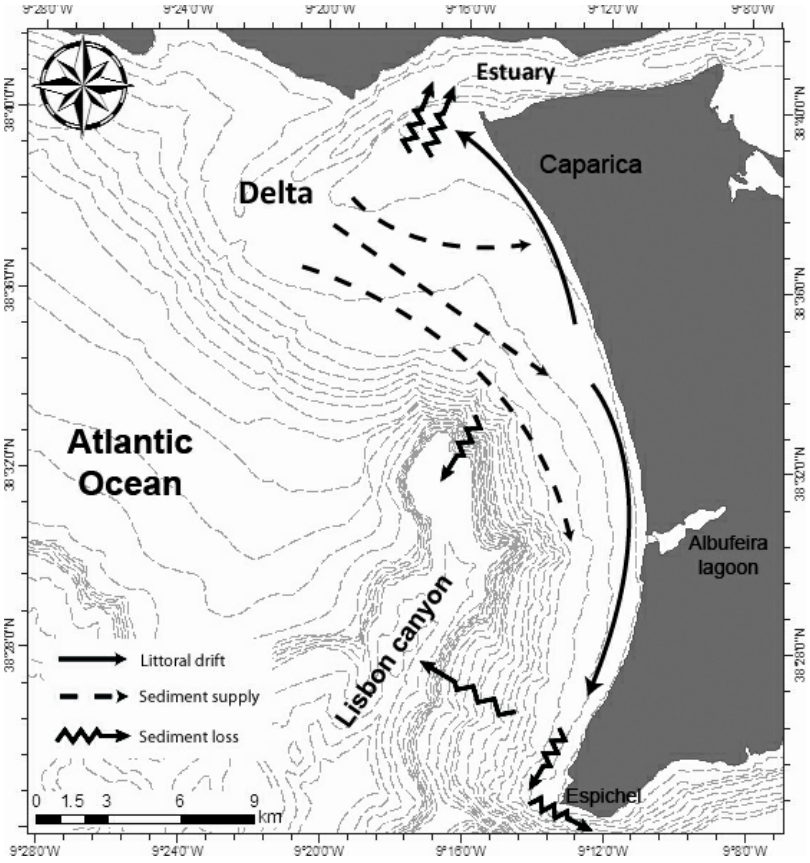

Figure 2.21 - Summary of sediment dispersal inferred from synthesis of the results.

Sediment transport calculations based on the previous assumptions indicate that a minimum positive supply of 99,991m^3/yr from the delta to the coastline was needed to maintain a progradation tendency in local morphology, either with climbing dunes development or barrier accretion. Comparison between the results obtained for longshore sediment-transport rates at various coastal sites (Komar, 1976) indicates a considerable magnitude on local sediment transport.

In the more recent evolution a significant erosive tendency is evident, causing a substantial coastline retrogradation over the last 125 years. Wave refraction patterns cause a permanent SW-NE longshore transport in the northern sub cell. This enhances the erosion transporting sediment into the estuary. The

consequent retrogradation resulted in a sediment loss that exceeded 46 million cubic meters (see 2.4.1) corresponding to a 372,000m^3/yr maximum transport rate.

The increased rate of longshore sediment-transport (by 268,009m^3/yr) and the switch in behaviour from progradation to trend erosion indicates a variation in sediment availability. During the period when deltaic sediment was supplied into the cell at a rate capable of overcoming the losses to the sinks, accretion and coastline progradation was dominant. However, once sediment supply decreased to a rate not capable of equalising the losses to the sinks, erosion and consequent retrogradation control the coastal evolution.

Other possible scenarios exist that can contribute toward explanation of the cell evolution. These include sea-level variations or changes in gross sediment supply. Vis et al., (2010) identified significant changes in the Lower Tagus Valley during the late Holocene involving different exogenous controls on fluvial activity. These controls include sediment availability to the coastal cell; sea-level variations (6500–5500 cal. BP), probable climate change (5500–1000 cal. BP) and human impact on sediment sources (1000–0 cal. BP). Together with this, the interpretation drawn from the results of this chapter is consistent with the progressive intensification in anthropogenic impacts, such as dredging and harbour-mole construction, in the Tagus estuary during development of Lisbon as a major port.

2.6 Conclusion

The results confirm the well-established principle that deltas are depositional environments that can control coastal evolution through the control of sediment supply. Although it is well established that deltaic sensitivity to sea-level and sediment supply variations can cause significant changes in the deltaic morphology influencing sediment dispersal patterns, the results presented here suggest that sea-level can be ruled out as the main factor driving coastal evolution over the past few thousand years, including during the medieval and modern historical periods. In particular, chronological information based on local cliff-top and climbing dunes shows that the prograded barrier development is not coeval with the delta evolution after relative sea-level stabilized in the area (~7000 cal BP). From this conclusion, and from volumetric results of potential sinks and sources, it can be further concluded that variations in sediment supply from the delta are mainly responsible for significant coastline migrations observed in the geohistorical and historical data. Significantly, the analyses suggest that the deltaic sediment supply can go negative when anthropogenic action causes the estuary to sequester coastal sand.

These implications of sink-source zone volume comparisons are also consistent with inferred wave-driven sedimentary exchanges between the deltaic environment and the adjacent coast. The intense wave refraction induced by the delta itself defines a complex littoral drift that controls the sediment dispersal along the cell, causing transport divergence that results in formation of two discrete sub cells: a northern sub cell with a recent prograded barrier strongly dependent on the deltaic environment sediment availability; and a southern sub cell comprising a retrogradational mainland beach.

For the northern sub cell, proximity of the Tagus estuary has enhanced the erosion of the strandplain during the historical period as wave refraction causes a south to north littoral drift, north of the

divergence point, advecting sand toward and into the estuary. In the sourthern sub cell, on the other hand, a semi-equilibrated shoreline is indicated at the base of a cliff. It can be concluded from the existence of the littoral transport divergence mid-way along the cell that the southern sub cell is no longer strongly coupled to the delta through littoral supply. This decoupling is consistent with a subtle inflexion in the shoreline planform roughly coinciding with the littoral-transport divergence point (Fig. 2.17). However, it is unlikely that a complete decoupling exists because the shorelines along the northern and southern sub cells remain reasonably aligned, although their planform equilibrium tendencies may differ (see Chapter 4).

Comparison of the long-term approach results with the short-term rates shows a significant increase of sediment transport magnitude through time from which a systematic variation in sediment availability may be concluded. The decrease of sediment supply from the delta to the coast enhanced the local erosion problems and consequent coastline retrogradation. The comparison between the results reported in this chapter and from other studies in the lower Tagus valley is consistent with the progressive intensification in anthropogenic impacts due to the intense usage of the estuary for navigation and building purposes. The deforestation of the catchment area, alteration of river margins through the construction of new and bigger harbour moles as well as sea-walls and groin fields in the adjacent coastline are some of the examples. These impacts probably have a significant responsibility in recent coastline migration as enhancing sediment transport.

CHAPTER 3

Cliff-top dune evidence in characterisation of coastline evolution and sediment transport

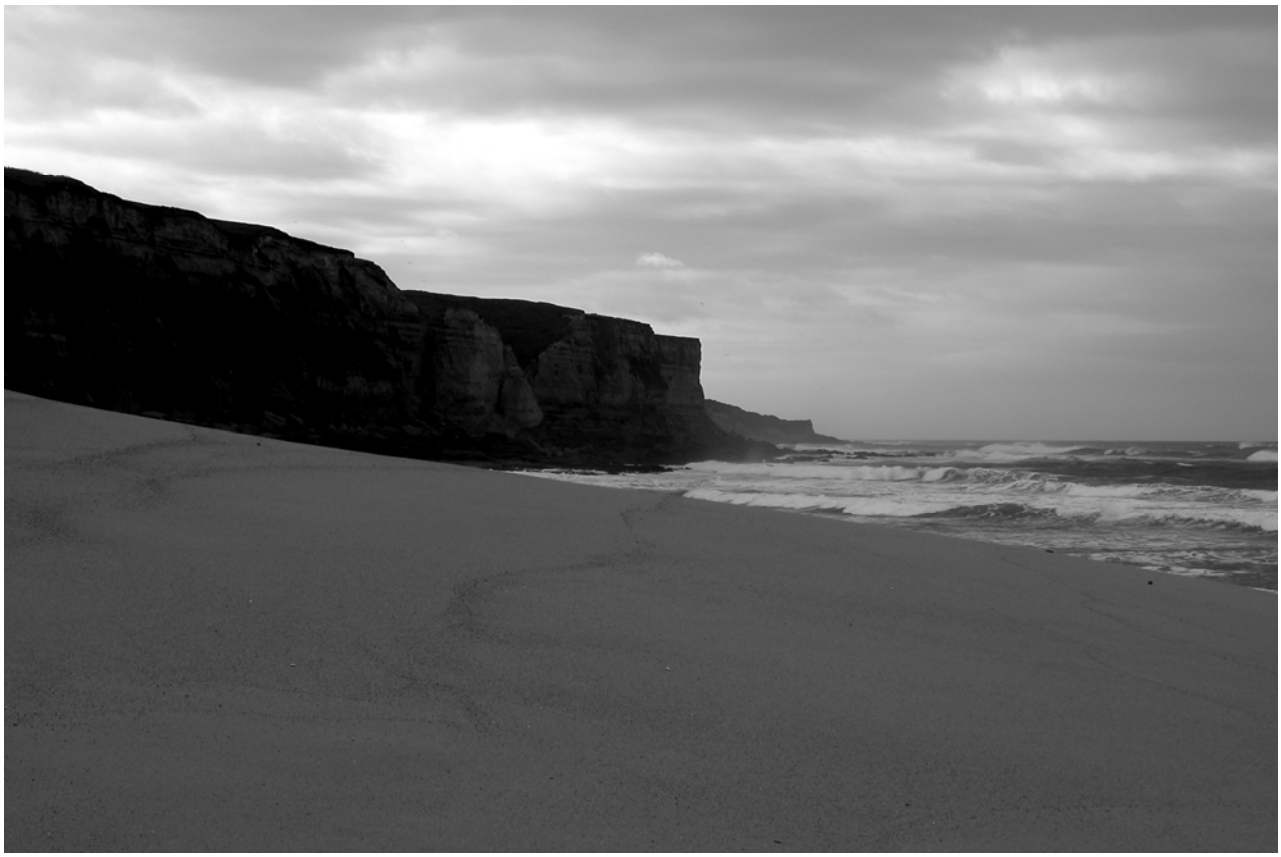

Photo: Sea-cliff near Espichel

3.1 Introduction

Coastline position is dependent on sediment gains and losses on the alongshore and cross-shore directions (local sediment budget) as well as in sea-level position (Cowell et al., 2003a). The balance between accommodation space, caused by sea-level variations, and sediment availability controls the rate of coastline progradation and retrogradation (Roy et al., 1994; Cowell et al., 2003b) as well as the development of local coastal morphology. However, in stable sea-level conditions the role of sediment budget becomes predominant in coastal evolution (Roy et al., 1994).

Sand barriers are basic depositional elements for wave dominated coasts (Roy et al., 1994) that comprise different morphological and stratal architectures. When conditions are favourable for coastline progradation, development occurs of strandplains, or prograded barriers, comprising a horizontally accreting series of beach and foredune ridges (Komar, 1976; Fisher & Simpson, 1979; Roy et al., 1994, Cowell & Thom, 1994). Under specific conditions of sediment supply, wind and wave climates, transgressive dune systems can develop surficially on these barriers (Hesp & Thom, 1990). Once the transgressive dune complexes become detached inland from the adjacent coastal sand source, cliff-top dunes may develop. This inland separation of the cliff-top dunes from its source involves the erosion of the sand ramp portion of a climbing dune (Tsoar, 1983; Ferraz et al., 2011) that originally formed the transport pathway between the sediment source and the cliff-top deposits. This erosion, usually associated with sea-level variations and changes in wind patterns (Jennings, 1967; Pye & Bowman, 1984; Short, 1988; Roy & Boyd, 1996), can be mainly due to changes in sediment supply conditions and coastline position (Ferraz et al., 2011).

The objective of this chapter is to explore in greater detail the evidence on cliff top dunes used in the preceding chapter to reconstruct the long-term coastal evolution of the Caparica coastal cell. Chapter 3 therefore documents results from analyses used to estimate past dune morphologies and their effaced

geometry through application of physical principles and other evidence drawn from results on coastline evolution presented in the preceding chapter.

More specifically, the aim of this chapter is to assess whether

(1) sufficient space exists landward on the of the beach along the existing coast to accommodate the minimum dimensions of climbing dunes that must have existed to allow development of the now isolated cliff-top dunes;

(2) the climbing dunes were emplaced during the later phase (Holocene) of the postgladial marine transgression or whether they are the product of post stillstand evolution of this deltaic coast as it adjusted to a re-equilibration of the delta sediment body under conditions in which generation of new accommodation had ceased.

The direct evidence of the sand ramps has been effaced by subsequent erosion, so the first of these aims needs to be addressed through application of general principles on climbing dunes. The second aim needs to address evidence that also necessarily gives insight into conditions leading to initiation of climbing dunes as well as conditions the result in destruction of their sand ramps.

3.2 Background principles

3.2.1 Phases in the evolution of a climbing and cliff-top dune complex

In this chapter it is assumed that the cliff top dunes of Setúbal peninsula, located on the Portuguese west coast (Fig. 3.1), develop according to Jennings (1967) and Roy & Boyd (1996) models (Fig. 3.2) where sand blown landward from the beach encounters an obstacle (sea-cliff) building a climbing dune (sand ramp) against the seaward face of the coastal cliff which is subsequently eroded due to sea-level effects leaving the isolated cliff-top dunes as a testimony of a transgressive dune system. However, the specific conditions about the development of climbing dunes are not well known.

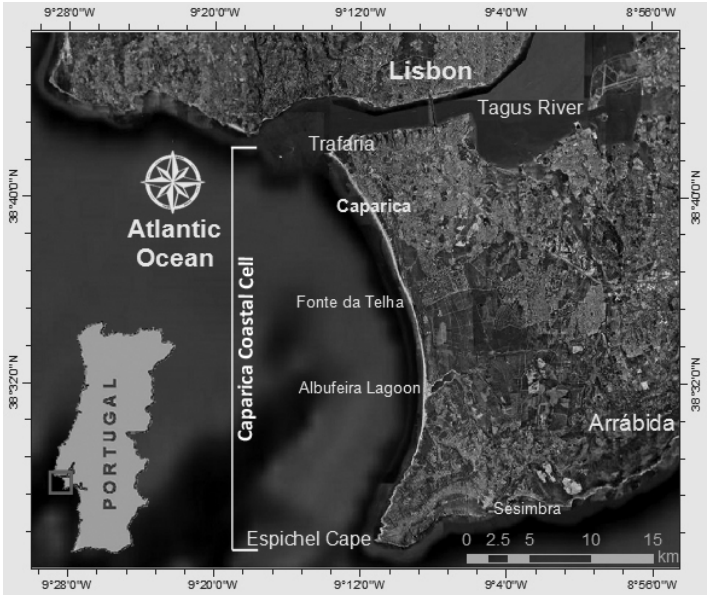

Figure 3.1 - Setúbal peninsula, Portuguese west coast.

Figure 3.2 - Schematic diagram of cliff-top dunes development (Adapted from Jennings, 1967).

Tsoar et al. (1996) defined conditions for which natural sand deposition occurs on slopes with inclinations between 0º and the maximum angle of repose, 33º in most sand sized materials for threshold shear velocities between 0,27m/s and 0,51 m/s, depending on the sediment characteristics (Liu et al., 2006). The presence of topographic obstacles creates perturbations in the wind flow generating variations in shear stress (Hunt et al., 1988) with deposition in principle favoured in regions where shear stress gradients are negative, or where boundary layer separation.

According to Tsoar's (1983) wind tunnel experiments, when wind encounters a vertical cliff its velocity begins to drop and the direction reverses with the formation of an eddy. If the sediment supply is constant or the cliff is inclined, with slopes less than 55 degrees, the size of the reverse flow eddy decreases and sediment begins to deposit at the base of the cliff (Fig. 3.3). Sediment tends to accumulate forming a climbing dune (sand ramp). Wind-tunnel experiments also indicated that the region where dunes tend to accumulate in front of the cliff is limited to a maximum distance, d, from the cliff that varies with the cliff height, h (Tsoar, 1983):

$$2.0 \leq d/h \leq 3.5 \qquad (3.1)$$

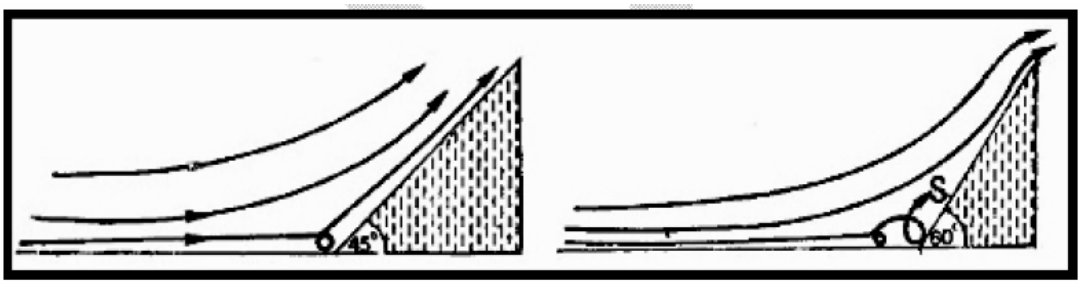

Figure 3.3 - Wind flow over cliffs with different slopes. Examples of 45º (left) and 60 º (right) (adapted from Tsoar, 1983).

The efficiency of the climbing dune as a sand transport pathway to the top of the cliff strongly depends on the sediment supply, Q_s, and on the cliff height: if the cliff height increases beyond a critical threshold or the sediment availability diminishes, the supply to the top of the cliff ceases (Haslett et al., 2000). Coasts with higher sediment supply (Q_s >10m^3/m/y, Short, 1987), higher wind energy and dissipative beaches, potentially have larger dune-fields (Hesp & Short, 1999) and fetch area for aeolian transport. Although climbing dunes not common, they can be observed on positive sediment supply environments (Fig. 3.4).

Figure 3.4 - Climbing dune complex on Boavista Island – Cape Verde (on the left); Climbing dune and cliff-top dune complex in Western Australia (photo on right by A. Short).

3.2.2 Local sea-level variations and progradation phases in late Holocene

According to Vis et al. (2008), samples from the lower Tagus valley indicate that present sea-level was permanently achieved at 7000 cal BP, when the valley was transgressed by tidal and marine environments sealing the local transgressive system tract. However, more recent progradation and retrogradation events occurred in proximate coastal areas (Goy et al., 1996; Haslet et al., 2000; Goy et al., 2003) providing possible evidence for changes in local sea-level and/or sediment supply conditions. According to Goy et al., (2003) six different prograding units identifiable on the south coast of the Iberian Peninsula are a result of the North Atlantic Oscillation (NAO) and sunspot oscillations that caused minor changes of local relative sea-level. The same variations were recognised by Guerra et al., (2000) who related fluctuations in mean sea-level on the Portuguese coast, measured using instrumental records of tide gauges between 1882 and 1991, to a significant inverse correlation with the NAO index. The higher sea level anomalies are favourable to dune instability and dune development (Pye & Bowman, 1984; Pye & Tsoar, 2009) and may cause changes in local sediment supply if the shoreface sequesters sand under these conditions (Cowell et al., 1999). It has been shown that coastline progradation and retrogradation can occur either in rising, stable or falling sea-level conditions depending on sand supply to beaches and dunes (Hesp & Short, 1999; Cowell et al., 2003b).

3.2.3 Geomorphologic setting

The Caparica coastal cell in which cliff top dunes were investigated lies between Trafaria and Espichel Cape (Fig. 3.1). The geomorphology is described in Chapter 2 (Sec. 2.2). Average grainsize values gradually increase from north to the south probably due to wave power influence (Teixeira, 1990).

3.3 Methods

3.3.1 Dune system modelling and quantification

In order to understand the morphologic development of the cliff-top dunes the analysis was performed using different sets of topographic data that was imported into GIS where Digital Elevation Models (DEM's) were built based on height and slope variations. The volume of cliff-top dune deposits was based on the average thickness previously calculated for each deposit. In order to validate the position of the dune geometry and the geologic setting of the area, groundtruthing was performed using a GIS/GPS integrated system.

Climbing dune structures were modelled based on physical principles developed by Tsoar (1983) where dunes accumulated in front of the cliff was limited to a maximum distance given by Equation 1 (Tsoar, 1983; Ferraz et al., 2011). A digital elevation model (DEM) using a Triangulated Irregular Network (TIN) was prepared along the Caparica cell where cliff-top dunes could be observed to analyse dune dimensions. The DEM was created between the actual cliff-top dune morphology and each calculated base position to which a height of h = 0 m was attributed. This allowed the definition of the geometry and volume of the climbing dunes relative to the position of the dune base.

3.3.2 Ground-Penetrating Radar (GPR) survey

Characterization of the prograded barrier system internal facies was delineated using Ground Penetrating Radar (GPR). Preliminary surveys were undertaken to locate the best area for validated results. The Fonte-da-telha area, located in the southern end of the prograded barrier, was chosen to record the GPR profiles since it preserves the original dune field structure and has less anthropic impact

than the northern area of the barrier. The northern area has been subjected to intense construction and agriculture, and landslide deposits impeded the GPR signal due to the presence of abundant clay.

Images of the subsurface were acquired using an IDS-GPR system RIS MF Hi-Mod #1 with a dual frequency antenna (200 and 600 MHz). GPR has proven to resolve sedimentary facies within the beach profile and the transition towards the adjacent foredune (Bristow and Pucillo, 2006). In addition, GPR was successfully applied to paleo-shoreline reconstruction in prograding coasts by mapping subsurface scarps, which in turn represent the morphological impact of past erosional events (Buynevich et al., 2007). A total of four crosshore and two alongshore GPR profiles 1.2 km-long were surveyed along the barrier complex (Fig. 3.5).

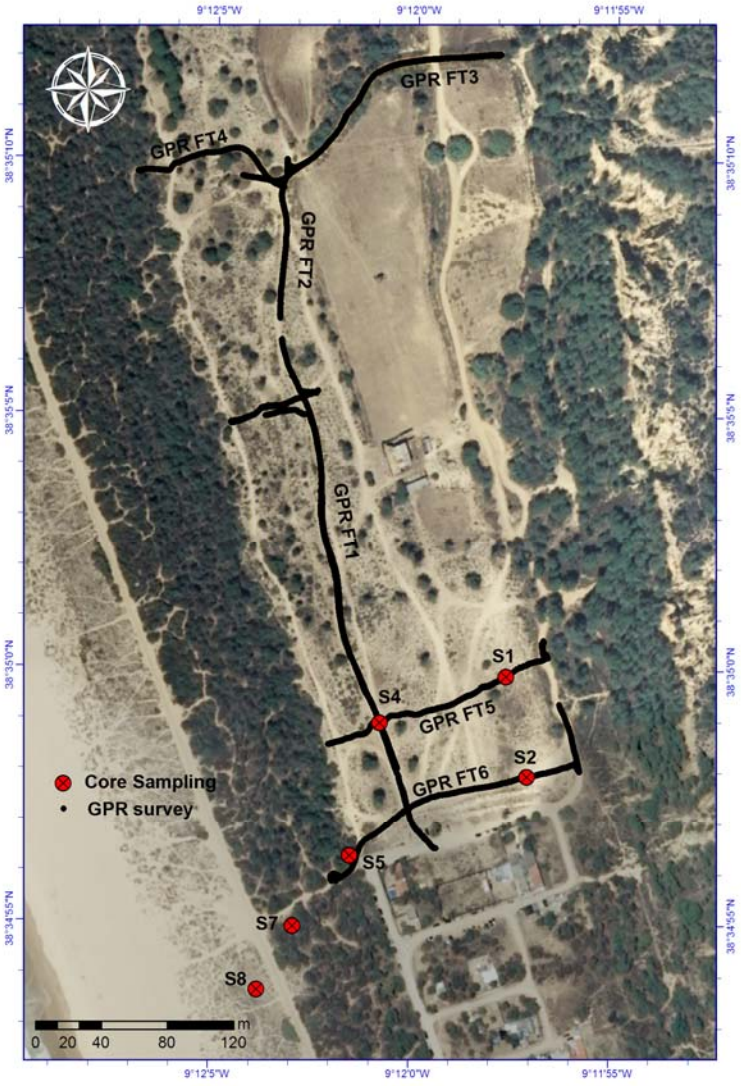

Figure 3.5 - GPR survey lines and core sampling position.

The GPR was synchronized with an RTK-GPS system in order to obtain the topographical information for static correction during the processing of the radargrams. Raw data were processed using Reflex-Win Version 5.0.5 from Sandmeier Software. Processing included time-zero drift, application of filters and gains, velocity profile estimates, migration and static corrections. An average subsurface velocity of 0.16 m/ns was estimated using the interactive hyperbola-adaptation method and is a typical velocity for dry sand.

3.3.3 Core sampling and dating

Core sampling was undertaken based on the geophysical results obtained with the GPR methodology from which the core locations were chosen (Fig. 3.5). Eight cores were collected (S1 to S8) using a TESS-1 suction core operated manually, obtaining different penetrations (Table 3.1).

Table 3.1 – List of samples and corresponding penetration.

Core Sample	Penetration (cm)
S1	386
S2	495
S3	148
S4	337
S5	138
S6	259
S7	360
S8	343

The bottom 40cm (base) from cores S1, S2, S4, S5, S7 and S8 were separated and dated using optically stimulated luminescence (OSL) analyses. Cores S3 and S6 were used as replica cores for dating validation purposes, being collected on a different location of the same dune structure as cores S4 and S5. This infers that results must be similar within the possible range of dune development.

3.4 Results

3.4.1 The dune system morphology

GIS analysis results showed that cliff-top dunes occupy an overall area of 1.0005×10^7 m^2 correspondent to 1.2913×10^8 m^3 over in a 20,662 m cliff length (80% of the overall length of the cliff).

Cliff analysis in GIS shows slopes varying between 5 and 60 degrees. Statistical examination indicates that the most common slopes are between 20 and 40 degrees and only one occurrence is above the 55 degrees (60°) where the presence of landslide deposits comprising Mio-Pleistocene material at the base of the cliff contributed to the reduced angles.

The lower slope angles assist the development of climbing dunes under proper wind conditions. Assuming paleo-winds similar to the predominant direction at present, conditions would have been favourable for the development of climbing dunes. At present, data from the Lavradio meteorological station, located 15km East of the Caparica area, indicates predominant winds from the westerly quadrant occurring 35.1% of the time with relatively constant average annual speeds of 3.9 m/s (CostaPolis, 2005), which exceeds the threshold shear velocity for the dune sand (Fig. 3.6).

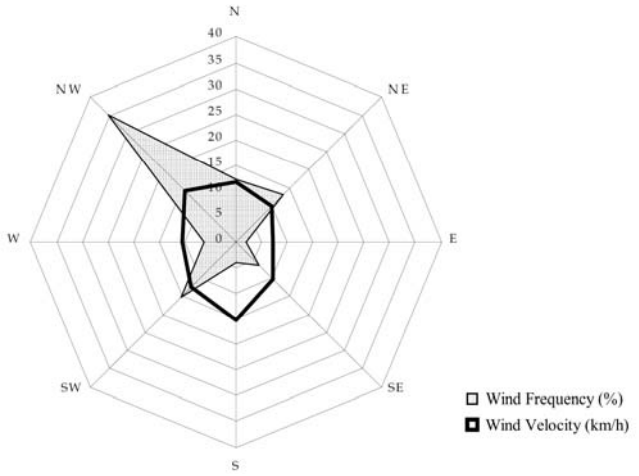

Figure 3.6 – Wind frequency and velocity from Lavradio meteorological station (CostaPolis, 2005).

GIS analysis also indicates that the cliff heights, where cliff-top dunes are present, vary between $5 < h < 80$ m with a mean value of 49m. From Equation 1, the deposition distance from the cliff varies between $10 < d < 280$ m (Fig. 3.7) with repose angles between 16º and 27º. Modelled morphologies (Fig. 3.8) allowed the quantification of the climbing dunes volumes for both scenarios, d/h=2.0 and d/h=3.5, obtaining volumes of 6,033,201m^3 and 15,197,740m^3 respectively (Table 3.2).

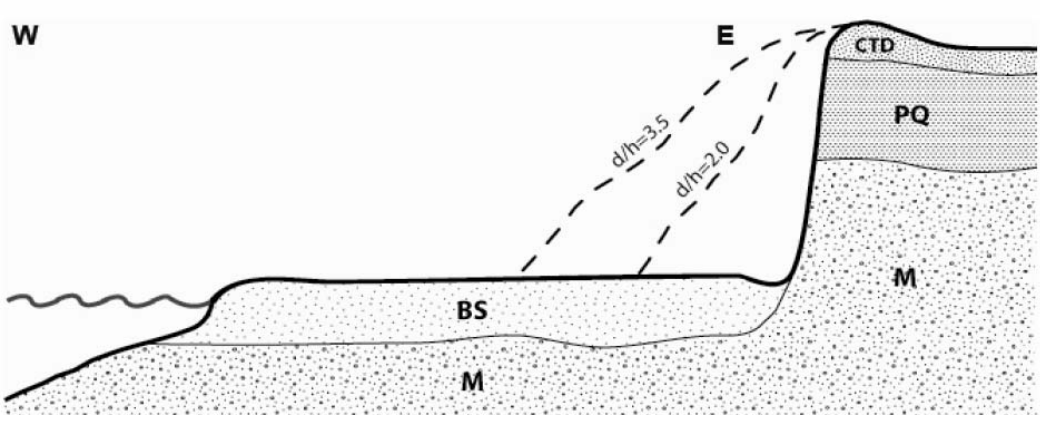

Figure 3.7 - Schematic configuration of both climbing dune scenarios (BS – Barrier System; M – Miocene; PQ – Plio-Quaternary; CTD – Cliff-top dunes).

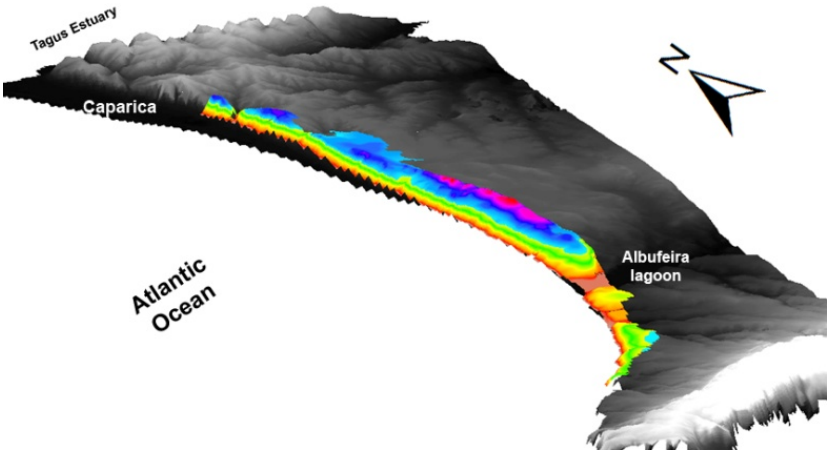

Figure 3.8 - Modelled climbing dune DEM (e.g. d/h=3.5) over the actual topography.

Table 3.2 - Deposition distance (*d)* based on the cliff height (*h*) and the *d/h* ratio. It is also represented the slope value (*α*) of the climbing dune for each case.

d/h	**3.5**			**2.0**		
	Min.	Avg.	Max.	Min.	Avg.	Max.
***h*(m)**	80	49	5	80	49	5
***d*(m)**	280	171	18	160	97	10
***α*(º)**		16			27	
Vol.(m^3)		15,197,740			6,033,201	

Comparison of the modeled climbing dunes with the present-day coastline position indicates that to accommodate these structures coastline had to experience significant changes in most of the area. It is possible to divide the overall cell in two sub cells (Ch. 2) with the division being on Fonte-da-Telha beach. The sub cell south of Fonte-da-Telha at present does not have sufficient physical space to accommodate a climbing dune (Fig. 3.9) because it contains a mainland beach that encroaches directly onto the base of the cliff. It can be inferred from the present lack of space to accommodate a climbing dune that the beach has migrated horizontally inland from a position further seaward resulting in the destruction of the sand ramp portion of the climbing dune.

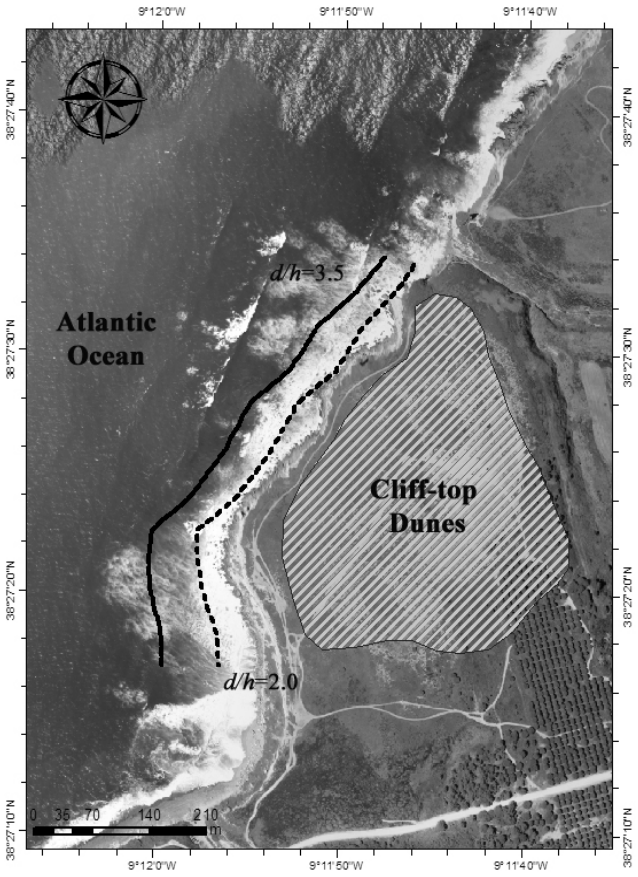

Figure 3.9 - Southern area. Solid and dashed lines represent the different deposition distances and consequent position of the climbing dune base (*d/h*=3.5 – solid line; *d/h*=2.0 – dashed line).

North of Fonte-da-Telha the prograded barrier coastline position has sufficient space for the development of a climbing dune. However, the absence of the structure today implies a past episode of sustained erosion during which the beach migrated inland destroying the sand ramp, redistributing its sediments elsewhere, and leaving the cliff-top dunes isolated from the present coast as evidence of this depositional history (Fig. 3.10). This sediment redistribution could have contributed to the prograded barrier development.

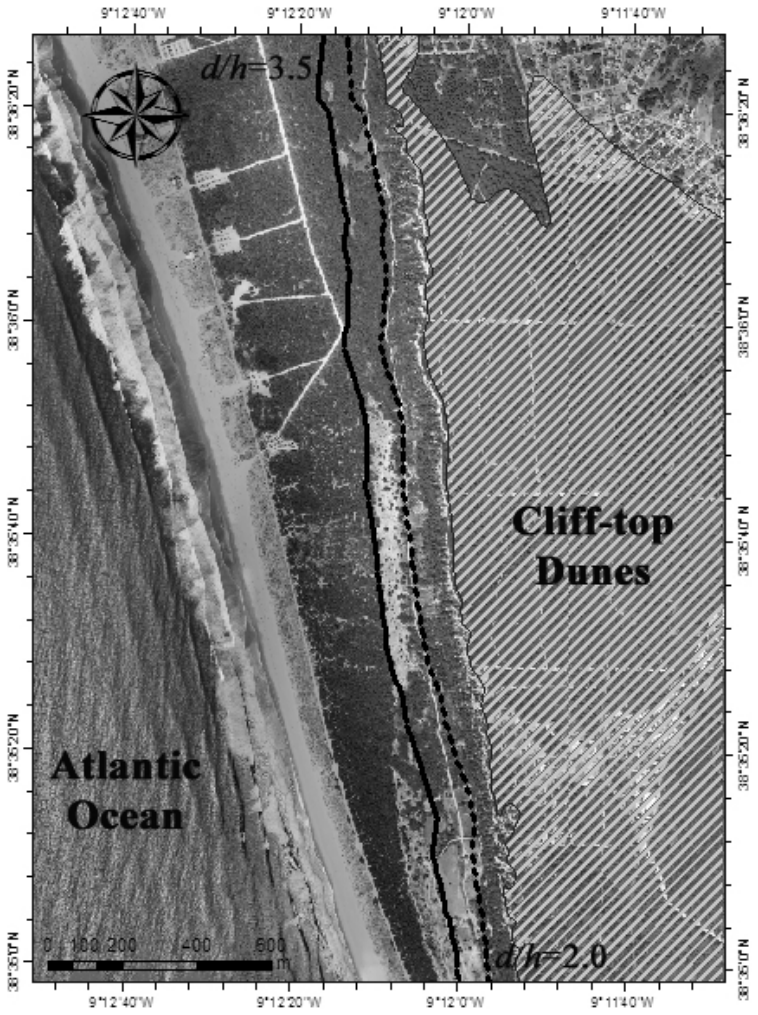

Figure 3.10 - Northern area. Solid and dashed lines represent the different deposition distances and consequent position of the climbing dune base (*d/h*=3.5 – solid line; *d/h*=2.0 – dashed line).

3.4.2 Ground-Penetrating Radar (GPR) profiles and dating

GPR profiles allowed the identification of the prograded barrier internal facies with a structure comprising successive sub-parallel paleo-beach surfaces reflecting a roughly constant barrier progradation. Paleo-beach morphologies are similar to the present beach environment with similar slopes of 2^{o} to 3^{o} typical of dissipative to intermediate type beaches (Short, 1979; Wright and Short,

1984; Sunamura, 1988; Lippmann and Holman, 1990; Short, 1999). In some cases berm crests were slightly higher (6 meters) relative to present day beach environment (3 to 5 meters) reflecting higher energy periods or greater exposure to wave energy. Presently, higher berm crests are observed in the Albufeira lagoon area, where wave energy is more significant for the predominant wave directions that prevail at present (Chapter 2).

Paleo-beach surfaces are overlapped in GPR records by the present dune field in a clear separation between both facies. The dune field mainly comprises successive foredune ridges with an average 2 meters thickness and an internal undulating structure sub parallel to the topography. The beach and dune strata are separated by a semi-horizontal surface that corresponds to the upper limit of the successive swash zones (Fig. 3.11).

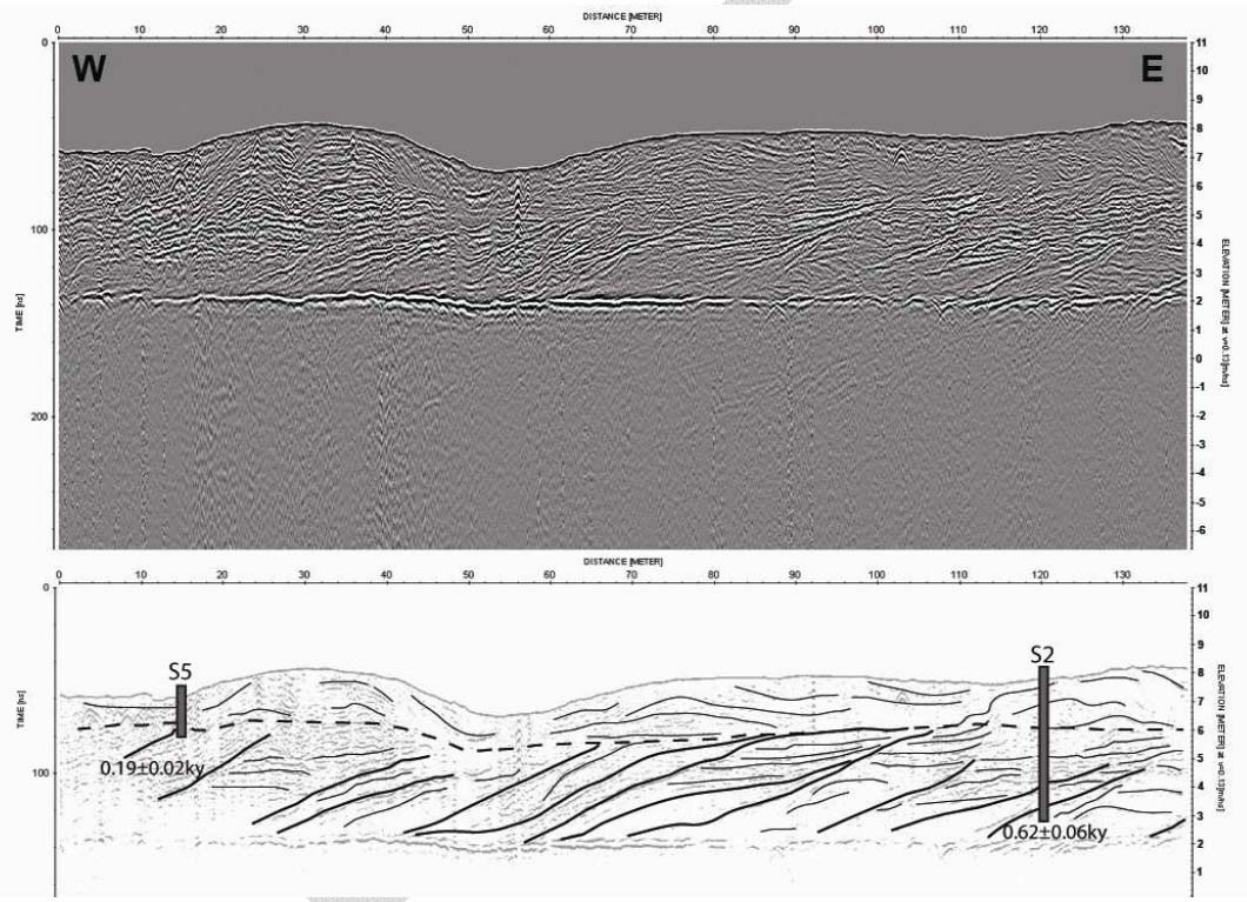

Figure 3.11 - GPR profile obtained (top) and its seismic interpretation (bottom). Core samples S2 and S5 and respective OSL ages. Thick solid lines: paleo-beach surfaces; Thin solid lines: deflation zones; Dashed lines: Separation between beach and transgressive dune environments.

OSL dating results from core samples show that barrier progradation is recent. Samples S1 and S2, obtained near the base of the cliff (Fig. 3.5) to date the older deposits within the barrier present ages of 0.62±0.06ky and 0.62±0.03ky respectively.

The remaining samples show a continuous decrease in age towards the present beach (Table 3.3) indicating a roughly constant progradation rate.

Table 3.3 - OSL dates.

Sample	Age (ky)
S1-2011	0.62±0.06
S2-2011	0.62±0.03
S4-2011	0.36±0.03
S5-2011	0.19±0.02
S7-2011	0.13±0.02
S8-2011	0.11±0.01

3.4.3 Sediment transport and coastline evolution

The results demonstrate that well after sea-level stabilization at approximately 7000 cal BP (Vis et al., 2008), the coastline of the Caparica cell continued to undergo significant morphological change. . During the last 1,000 years, the results indicate that morphological change can be characterised to have occurred in four sedimentary stages: SS1 - active cliff-top dunes period due to the presence of a well-developed climbing dune in the area and considerable sediment supply until 0.98 ± 0.05ky BP (Costas et al., 2012); SS2 - climbing dune erosion period and sediment redistribution followed by barrier progradation until 0.62±0.06 ky BP; SS3 - barrier progradation until 0.13±0.02 ky BP; SS4 - coastline rotation with slight progradation of the Fonte-da-Telha area and significant retreat in the north part.

SS1 and SS2 - active cliff-top dunes period and climbing dune erosion

The latest date for dune activity was 0.98 ± 0.05ky BP according to Costas et al., (2012) and the earliest date for barrier progradation was 0.62 ± 0.06ky BP. These dates leave a 360 year time window for climbing-dune erosion and consequent sediment redistribution. Maximum transport rates inferred from the length of this period and the estimated dune volumes vary between 42,216m^3/m and 16,759m^3/m for the two modelled climbing dune scenarios (Table 3.4).

Table 3.4 - Transport rates for climbing dune erosion and sediment redistribution.

d/h ratio	Climbing dune vol. (m^3)	Complex length (m)	Time (y)	Max. transp. rate (m^3/y)	Transp. Rate (m^3/m/y)
3.5	15,197,740	20,662	360	42,216	2.043
2	6,033,201			16,759	0.811

SS3 - barrier progradation

Dates on the dune deposits located at the base of the cliff show that barrier progradation for this area started ca. 0.62 ± 0.06ky BP. From estimates of the climbing dune volumes, their erosion could have contributed between 5% to 12% of the total barrier volume, assuming no losses to other sinks in the sediment redistribution process. Results from the remaining samples in relation to GPR profiles, in which the absence of erosion scarps indicates no significant erosion events evident, demonstrate that progradation sequence was roughly constant. A time average progradation rate of 0.86m/y occurred until 0.11±0.01ky BP for this area (Fig. 3.12). Rates tend to increase through time towards the most recent samples (Table 3.5).

Figure 3.12 - Core samples S1 to S8 and respective OSL ages.

Table 3.5 - Progradation rates for local barrier development.

Period (ky)	Calendar years	Progradation distance (m)	Time (y)	Progradation rate (m/y)
0.62 - 0.36	1391-1651	80	260	0.31
0.36 - 0.19	1651-1821	50	170	0.29
0.19 - 0.13	1821-1881	50	60	0.83
0.13 - 0.11	1881-1901	40	20	2.00

From the average progradation rate obtained for the entire prograded barrier complex and its corresponding volume, a maximum transport rate of 255,075m^3/y can be inferred (Table 3.6).

Table 3.6 - Transport rates for complete barrier progradation.

Volume (m^3)	Barrier length (m)	Time (y)	Max. transp. rate (m^3/y)	Transp. Rate (m^3/m/y)
130,088,213	12,305	510	255,075	20.73

This alongshore transport rate is significantly higher than the one obtained in relation to climbing dune erosion and redistribution.

SS4 - recent coastline evolution

To validate the progradation tendency, OSL results were related used with results of the aerial photograph analysis (Chapter 2). For the Fonte-da-Telha area, coastline progradation continued until the late 1980's. Adopting 1989 as the end date, progradation occurred in this area for 598 years resulting in an overall distance of 345m for a rate of 0.59m/y. However, in the northern end of the barrier near Caparica, from aerial photos and map comparison, coastal retreat started after 1882. This indicates that a slight clockwise coastline rotation started to affect the evolution of the prograded barrier complex most probably between 1882 and 1901. However, the absence of refined data, especially in the north part of the barrier, does not allow precise inferences to be drawn about the beginning of this period or the magnitude of sediment supply involved.

3.5 Discussion

These results suggest that the coastal cell can be divided into two distinct sub cells: a prograded barrier in the northern sub cell that was strongly dependent on sediment supply variations, and a retrogradational barrier in the southern sub cell that has stabilised in the more recent period.

The presence of cliff-top dunes for which dates indicate activity until 0.98 ± 0.05ky BP (Costas et al., 2012) demonstrates that this coastal cell has undergone significant coastline changes during the last 1000 years. The present coastline morphology is not consistent with the existence of an active climbing dune capable of supplying sediment to the cliff-top dunes complex, especially in the southern sub cell, because there is insufficient space to accommodate the sand ramp. In the north sub cell, the absence of the climbing dune sand ramp today indicates that it was eroded due to coastline retreat followed by a roughly constant barrier progradation that culminated recently in a new coastline retreat episode. This fluctuating behaviour indicates the occurrence alongshore sediment transport rates capable of altering coastline morphology.

Four distinct phases of sedimentary processes were identified where sediment redistribution seems to have involved cyclic retreat/advance patterns in the northern sub cell. The cyclicity requires the existence of an interaction between the several sediment sinks and sources connected by transport pathways. Possible scenarios include changes either in sea-level conditions or in sediment dispersal patterns. For this results were related with findings from other authors (Goy et al., 2003; Vis et al., 2010; Costas et al., 2012).

Global eustatic sea-level variations (Clark et al., 1978; Peltier & Fairbanks, 2006; Siddall et al., 2010) became increasingly dependent in local factors than on eustatic variations in the late Holocene (Dias et al., 2000). Relative sea-level stability in this area was reached ca. 7 Ky cal BP (Vis et al., 2010). However, contrary information from coastline evolution studies for nearby locations, in the SE of the Iberian

Peninsula (Gulf of Almeria), indicate that several sea-level changes occurred for the period between 6 Ky cal BP and today that were capable of causing significant changes in coastline positions (Goy et al., 1996; Goy et al., 2003).

According to Goy et al., (2003) between 1Ky BP and today sea-level variations presented small magnitudes (-0.2m to +0.2m) relative to present day sea level. These variations were probably insufficient to cause sufficient changes in coastline morphology to account for the erosion of the climbing dunes and the sediment redistribution that contributed for barrier progradation. However, the occurrence of two progradation units documented by Goy et al. (2003), H5 and H6, is similar to the occurrence of stages SS1 and SS2 progradation identified in this study. Stage SS1, where cliff-top dunes where active, occurred until 0.98 Ky BP, comparable to Unit H5 (Goy et al., 2003) that occurred between 1.9 and 1.1 Ky cal BP with coastline progradation occurring during a relative sea-level fall. Stage SS2, corresponding to the climbing dune erosion, occurred between 0.98 Ky BP and 0.62 Ky BP. A similar erosion event occurred between Unit H5 and H6 reported by Goy et al., (2003), culminating ca. 0.5Ky cal BP. Since then two progradation phases where identified for both studies: SS3 for the present study with barrier progradation since 0.62 Ky BP; and H6 since ca. 0.5 Ky cal BP for Goy et al., (2003) (Fig. 5.1).

Fluvial studies also indicate similarities with present study sedimentations stages. Vis et al., (2010) identified several phases of high fluvial activity based on lithological changes between 7Ky cal BP and present day for the Lower Tagus Valley. Phase 5, occurred since 1Ky cal BP, includes most of the present study sediment stages. The increased flooding occurred in this phase is attributed to strong human impact on Tagus catchment vegetation that overruled climatic control on sedimentation for the Iberian and Mediterranean regions since then (Fig. 3.13).

Aeolian pulses identified by Costas et al. (2012) for the same area show a close relation to the identified sediment stages. Aeolian pulse 5 (AP5) occurred between 1.2 Ky BP and 0.98 Ky BP reflects cliff-top dune activity coincident with SS1. The lower limit of this aeolian pulse is also an indication for the

beginning of SS1. AP6, occurred between 0.44 Ky BP and 0.3 Ky BP indicates the reactivation of aeolian activity in cliff-top dunes. This aeolian pulse is coincident with the final stage of SS3 where barrier progradation occurred, reflecting sediment availability (Fig. 3.12).

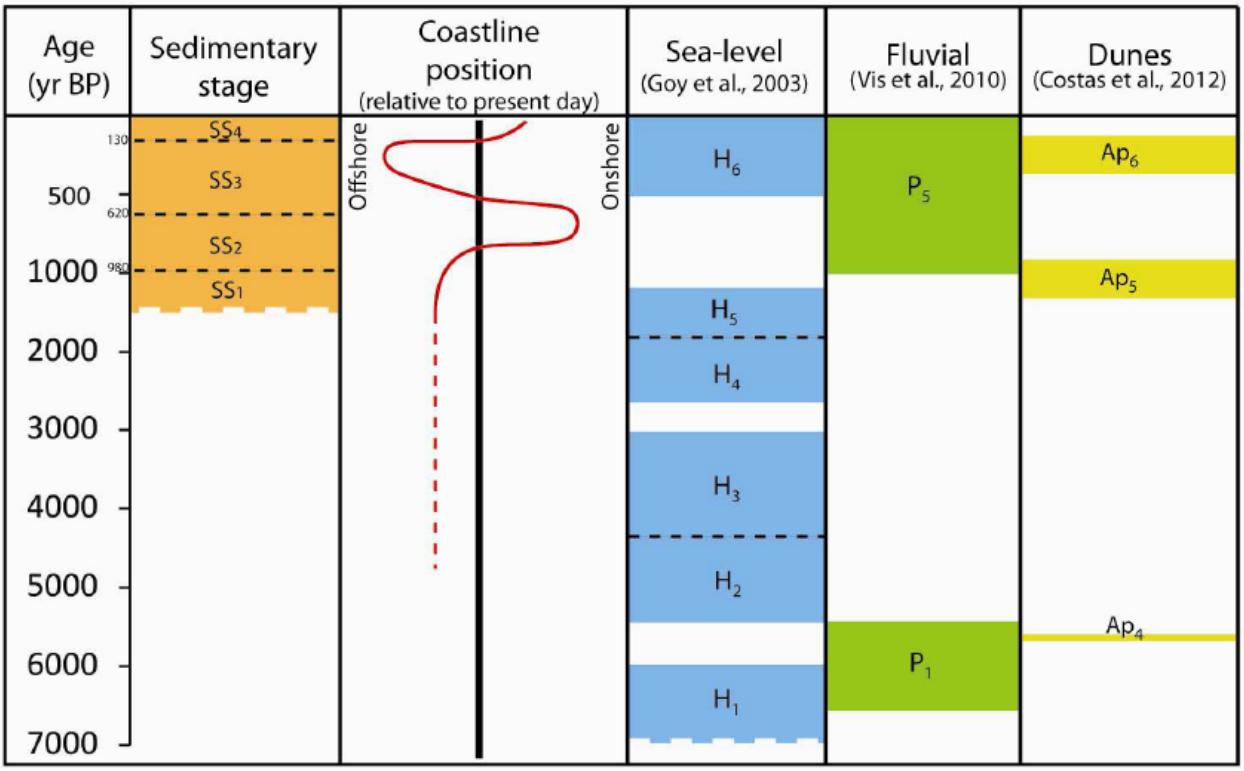

Figure 3.13 - Chronostratigraphy of the local sediment stages in relation with local coastline position, sea-level variations (Goy et al., 2003), fluvial activity (Vis et al., 2010) and Aeolian pulses on dune activity (Costas et al., 2012).

Despite the fluctuations in the North Atlantic Oscillation (NAO) index and/or sunspot oscillations being capable of causing small-scale changes of sea-level (Goy et al., 2003) the low magnitude of these events is probably insufficient to account for the significant coastline changes observed in the Caparica coastal cell. Therefore, by a process of elimination, it seems reasonable to speculate that changes in sediment

availability were responsible for the observed shoreline evolution. This explanation involves a stable sea-level where coastline behaviour patterns were in principle determined by the balance between changes in sediment accommodation space availability (Cowell et al., 2003b). Accommodation changes may be attributed to external factors such as changes in wave climate, variations in storm demand or anthropic impacts such as dredging and harbour-mole construction, as happened in the Tagus estuary during the development of Lisbon as a major port.

3.6 Conclusion

The presence of isolated cliff-top dunes on a Mio-Pleistocene sea-cliff advances a climbing dune scenario in which sediment piles up after finding an obstacle to its aeolian migration inland. The climbing dune activity until 0.98 ± 0.05ky BP indicates that local coastline experienced significant changes in order to completely erode this structure and develop a prograded barrier system between 0.62±0.06ky and the 20th century. Recent morphologic evolution allows identification of two distinct coastal sub cells. The north sub cell, located nearer the local sediment regulation structures (delta and estuary) is affected by larger magnitude coastline changes while the south sub cell is less affected by accommodation variations, and comprises a mainland beach with a stable coastline position.

The quantification of coastline behaviour patterns, determined by the relation between changes in sediment accommodation space and sediment availability, indicate that low order sea-level variations like the ones observed on proximate locations for this period are not sufficient to cause high magnitude coastline changes. This tends to rule out sea-level as the key factor for local coastline development, requiring consideration of changes in other sediment sources and sinks. Anthropic impacts seem the most likely cause of such changes in the Caparica coastal cell, associated with dredging and harbour mole construction in the adjacent Tagus estuary.

The results show conclusively that:

(a) insufficient space exists to accommodate climbing dunes landward on the of the beach in the southern sub cell (south of Fonte-da-Telha), indicating that the shoreline must have been substantially further seaward to permit formation of the sand ramp that supplied the cliff top dunes that have been left as remnants;

(b) although sufficient space exists at present in the northern sub cell to permit format formation of the climbing dunes necessary to account for the remnant cliff top dunes, the removal of the sand ramp through erosion indicates that the space seaward of the cliff line became insufficient in the past between the formation of the climbing dunes and the strandplain progradation evident there at present;

(c) the timing on formation of the climbing dunes places them in more recent period of sea level high stand, so that rather than being attributable to enhanced aeolian activity associated with the destabilising effects of the postglacial marine transgression, climatic anomalies or anthropogenic impacts of medieval settlement.

CHAPTER 4

Deltaic control on embayed beach stability due to changes in wave climate

Photo: Búgio lighthouse

4.1 Introduction

Waves and wave induced currents are dominant mechanisms on long-term sediment dynamics of shorefaces and beaches for wave dominated coasts (Roy et al., 1994; Aagaard & Masselink, 1999). Due to substrate bathymetry waves entering shallow areas are subject to swell direction variations through diffraction and refraction (Komar, 1976) defining local currents that are important sediment transport agents (Aagaard & Masselink, 1999).

Diffraction and refraction are common on embayed beaches, generally considered stable coastline cells (Hesp & Short, 1999; Lausman et al., 2010a) located between fixed structures (natural or artificial) that allow the conservation of the morphodynamic equilibrium (Hsu et al., 2010). The development of the parabolic bay shape equation (PBSE) (Hsu & Evans, 1989) allows definition and quantification of an idealised bay planform for a coastal cell based on the relation between coastline evolution, wave direction and a specific wave diffraction point. Its application is mainly focused on the search for solutions to erosion problems usually related with climate change, anthropic impacts and sediment supply insufficiency (Schiaffino et al., 2011) that create changes on coastal equilibrium. However, the exclusive application of this model to embayed and enclosed headland bay beaches (Hsu & Evans, 1989; Hsu et al., 2010; Lausman et al., 2010a,b) reduces its applicability in morphological coastline evolution studies.

The fact that a headland is the only point considered for variations in wave direction neglects the importance of local bathymetry and the presence of other morphological structures capable of causing significant wave refraction and/or diffraction influencing coastline evolution and stability. Deltaic structures are morphologies that strongly affect swell direction (Fitzgerald, 1996) creating specific wave regimes that regulate sediment dynamics and littoral drift, being more important than headlands in some specific segments.

The purpose of this chapter is to examine the deltaic influence on wave direction patterns in the wave dominated Caparica coastal cell, where previous studies (Ferraz et al., 2011; Costas et al., 2012) and results reported in the preceding chapters of this thesis have demonstrated that coastline equilibrium conditions significantly changed during the last 1000 years. Coastal equilibrium induced through engineering intervention has been sought throughout the last decades to avoid coastal erosion and significant land loss that can affect urbanized areas in the Caparica cell. An example of this was the construction of groin fields in the 1960's and the constant artificial nourishment in the north beaches since the late 1990's.

Empirical application of the PBSE principles based on wave climate variations and coastline position through time was undertaken to address three aims:

(1) to assess whether the delta morphology plays a role in the planform development of the adjacent sandy coastline;

(2) to evaluate whether sub cells identified in the preceding chapters share a common functional shoreline geometry or exhibit the existence of different morphodynamic controls over their planforms; and

(3) to explore the possibility that large changes in the delta morphology evident in historical records may be responsible for changes in shoreline geometry of the adjacent coast.

4.2 Wave climate

The frequency of occurrences and the wave power (P) was characterized based on mean and peak wave periods (T_m and T_p) and significant wave height (H_{Sig}) for each one of the predominant wave directions of the Portuguese Atlantic coast (NW, W and SW) from the work of Costa et al. (2001). For this characterization, two different datasets were used (see Appendix II). Data from the Sines buoy (located approximately 75km south of the study area) from a period between 2003 and 2009 (6 years) was used to characterize mean wave conditions (MWC). A 57 year hindcast (1953-2009) from the Micore project (Morphological impacts and coastal risks induced by extreme storm events) for the same area (Dodet et al., 2010) was used to characterise peak wave conditions (PWC). The use of two distinct datasets also permitted the comparative validation of the data.

Observations from both datasets indicate that NW swell is the most predominant for significant wave heights between 1 and 3 meters and mean periods between 6 and 12 seconds (Fig. 4.1) in mean and peak wave conditions. For MWC statistics, W and SW swell frequencies are not representative of the Caparica wave climate. However, their frequencies are greater in the PWC data indicating relevance to nearshore sediment circulation.

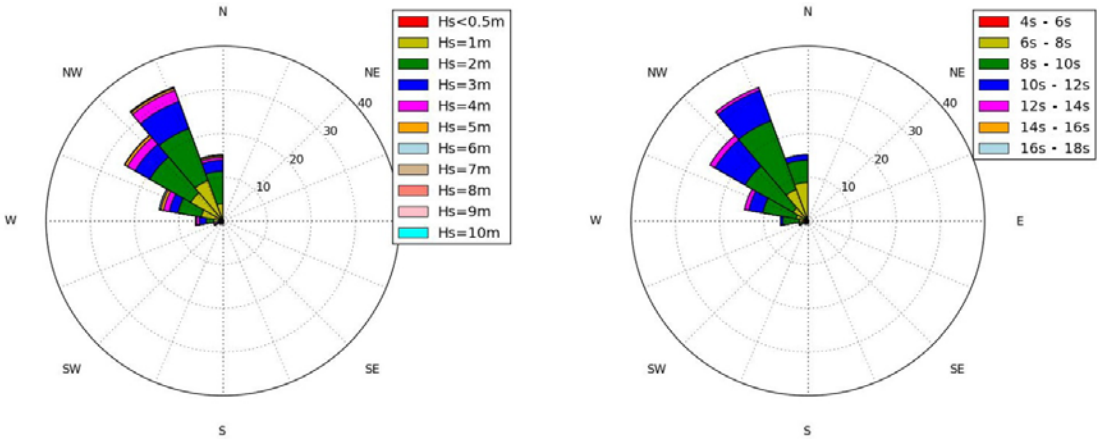

Figure 4.1 - Wave direction in relation with H_{sig} (left) and T_m (right) for MWC

The ratio between the peak frequency (f_p) and wave power, or wave energy flux (P), was calculated for different intervals of peak wave period (T_p) and significant wave height (H_{sig}) according to each direction (NW, W, SW). Wave energy flux was calculated according to

$$P = \frac{\rho g^2}{64\pi} H_{m0}^2 T \approx \left(0.5 \frac{kW}{m^3.s} \right) H_{m0}^2 T \quad (4.1)$$

where P is the wave energy flux per unit of wave-crest length, H_{m0} the significant wave height, T the wave period, ρ the water density and g the acceleration of gravity (Komar, 1976).

NW swell presents a wider range of values in wave height and peak period spectra, showing a greater ratio between peak frequency and wave power particularly for significant wave heights between 6 and 12 meters and peak period values between 2 and 10 seconds.

In either MWC or PWC wave statistics, NW swell predominates in frequency and power, and thus can be expected to dominate wave driven surfzone transport of sediments indicating a net flux from north to south. W and SW swells are not representative for long-term local coastal processes. However, consideration in this study is given to the possibility of their effects play some role due to rare high magnitude occurrence that may cause reversals in the alongshore sediment transport with temporary fluxes from south to north. Although temporary, such fluxes may be of significant if the estuary acts as a sink, and thus a one-way valve for northward sand movements at the northern end of the cell.

4.3 Wave modelling

Local wave conditions were modelled according to main wave directions (NW, W, SW) divided in quadrants using the most frequent values of significant wave height and period. Mean and peak wave conditions were used to relate the wave behaviour to local bathymetry in order to characterize the overall wave propagation and specifically the nearshore wave direction relative to depth-contour and shoreline orientation as an indicator of littoral sediment transport directions.

4.3.1 Mean Wave Conditions (MWC)

The most common directions for the NW, W and SW quadrants in MWC are 330°, 270° and 250° respectively. The T_m intervals vary between 6 and 8 seconds for a H_{sig} of 2 meters for all the considered wave directions (Table 4.1).

Table 4.1 - Wave characteristics in MWC.

Quadrant	Predominant Dir. (°)	T_m (s)	H_{sig} (m)
NW (280° - 360°)	330	6-8	2
W (260° - 280°)	270	6-8	2
SW (180° - 260°)	250	6-8	2

Model results (Fig. 4.2) show that refraction and diffraction mainly affect NW swell due to the morphology of the coast. Waves are first refracted in the northern headland (Roca Cape), with incoming waves changing direction progressively towards East. A second refraction occurs when waves propagate through the delta creating two nearshore circulation cells where wave travel with obliquity near the coast, one in the north part where the waves travel with e SW-NE direction and another where waves travel in a NW-SE direction affecting the south area.

The W swell is only affected by the delta where refraction rotates wave propagation towards north. However, cross-shore wave propagation predominates as wave angles near the coast are perpendicular (90°) or have reduced alongshore-directed components.

The SW swell shows no significant changes in wave direction associated with the presence of the delta or the northern headland, although minor refraction is evident near Espichel cape, at the southern end of the cell. Wave propagation obliquity to the shoreline orientation, in the SW-NE direction, is ubiquitous near the beach.

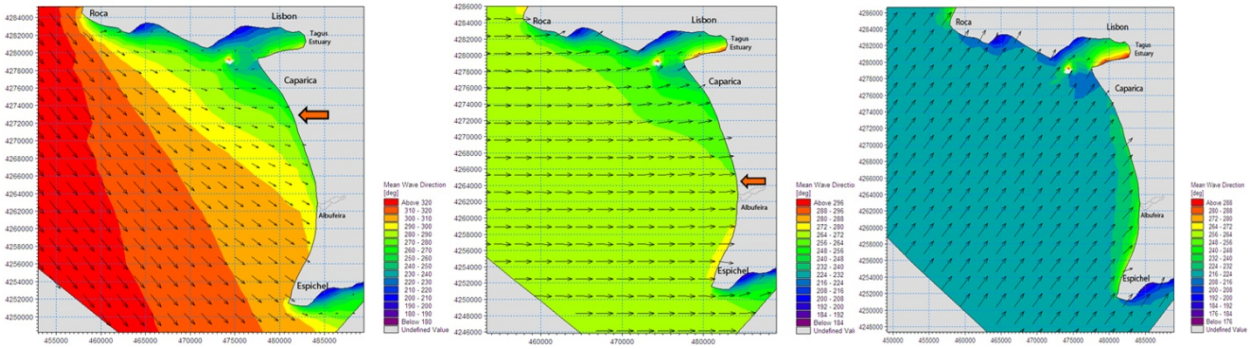

Figure 4.2 - Model results for MWC: NW direction (330°) on the left; W direction (270°) in the middle; SW direction (250°) on the right. Length of black arrows represents wave energy intensity and orange arrow indicates the wave divergence point for each case.

Since nearshore wave obliquity mainly occurs with NW and SW swells, these waves are indicated to be the most important determinants of net alongshore sediment transport. Results show that SW swell has a higher wave power that enhances this transport. However, a reduced annual occurrence (2.4%) (Costa et al., 2001) reduces its importance on a time averaged basis. Despite results for NW swell presenting a lower wave power, and thus a lower alonghsore sediment transport potential on the event timescale, its predominance with 77.3% of the annual occurrences (Costa et al., 2001) gives it a long-term predominance over net sediment dynamics and morphologic evolution.

4.3.2 Peak Wave Conditions (PWC)

The predominant wave directions for PWC are similar to those for MWC. The T_m intervals vary between 12 and 14 seconds for a H_{sig} of 2 meters for the NW and the W quadrant, while for the SW quadrant T_m intervals vary between 10 and 12 seconds for a H_{sig} of 3 meters (Table 4.2).

Table 4.2 - Wave characteristics in PWC.

Quadrant	Predominant Dir. (°)	T_m (s)	H_{sig} (m)
NW (280° - 360°)	330	12-14	2
W (260° - 280°)	270	12-14	2
SW (180° - 260°)	250	10-12	3

Wave model results (Fig. 4.3) for the NW swell are similar to those obtained for MWC. However, a southwards migration of the wave divergence point along the coast is evident in comparison to MWC refraction patterns. This shift increases the extension of the northern nearshore circulation cell in which where inshore wave directions are from SW-NE.

In these conditions the W swell is significantly affected by the presence of the deltaic morphology that enhances wave refraction and diffraction creating a well-defined SW-NE wave propagation pattern for the north part of the cell. The inshore wave obliquity angle decreases toward the south until reaching a cross-shore pattern immediately south of the Albufeira lagoon.

Differences in the results for SW swell compared to that for MWC are negligble. Nevertheless, it is possible to observe stronger directional changes in the wave field nearer ot the delta, demonstrating the importance of this morphology to inshore wave propagation.

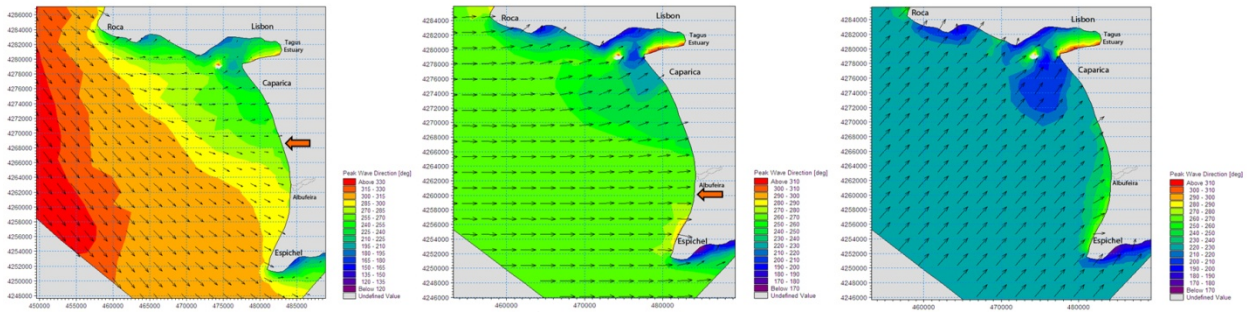

Figure 4.3 - Model results for PWC: NW direction (330°) on the left; W direction (270°) in the middle; SW direction (250°) on the right. Length of black arrows represents wave energy intensity and orange arrow indicates the wave divergence point for each case.

The PWC results show that wave obliquity is not only important for NW an SW swell, as in results when the wave climate is represented using MWC, but also for the W swell where waves tend to refract significantly in the vicinity of the delta. The W and SW swell have a higher wave power than NW swell. However, their annual percentage of occurrences combined reaches only 22.7% (Costa et al., 2001), subordinating their importance in the characterization of the inshore wave climate.

Overall, the wave modelling shows that inshore wave fields both MWC and PWC are similar for the main wave directions (NW, W and SW). However, changes in wave propagation patterns with migration of the wave divergence point can affect nearshore wave driven sediment transport. In either case the northern sub cell is subject to a constant wave obliquity with an approximate SW-NE nearshore direction that enhances sediment transport toward the Tagus estuary. This process indicates net sediment loss from

the prograded barrier into the estuary. The length of beach affected by this process tends to be greater in PWC results than for MWC results as expected.

The southern sub cell is mainly affected by low obliquity and perpendicular angles that enhance cross-shore sediment dynamics. In spite of being affected by higher magnitude wave energy coastline is significantly more stable in this area.

Although NW swell is not the most significant for wave energy on the event timescale, its predominance in the annual percentage of occurrences probably makes it the most important component of the wave climate to consider for long-term coastal evolution.

4.4 Parabolic bay shape model (PBSM) and application rationale

Despite not being a classical headland bay-beach due to the presence of an estuary and a delta within the embayment, the parabolic bay shape model (PBSM) concept was applied to evaluate shoreline geometry of the Caparica cell, in terms of coastline stability, for several stages in the evolution of the cell, as reconstructed in Chapter 2. The analysis was undertaken using MepBay software (Klein et al., 2003). The software applies the parabolic bay shape equation (PBSE) developed by Hsu & Evans (1989) in the form of

$$R_n/R_\beta = C_0+C_1(\beta/\theta_n)+C_2(\beta/\theta_n)^2 \quad (4.2)$$

where there are two primary parameters: the reference wave obliquity angle β and the length of the control line R_β, and R_n is the radius calculated for a point (R_n,θ_n) along the static equilibrium planform (SEP) that can be calculated based on a value of θ_n from the same wave crest line radiating out from the point of wave diffraction. The three C constants vary with angle β and were generated by regression analysis to fit the bay planform (Hsu et al., 2010) (Fig. 4.4).

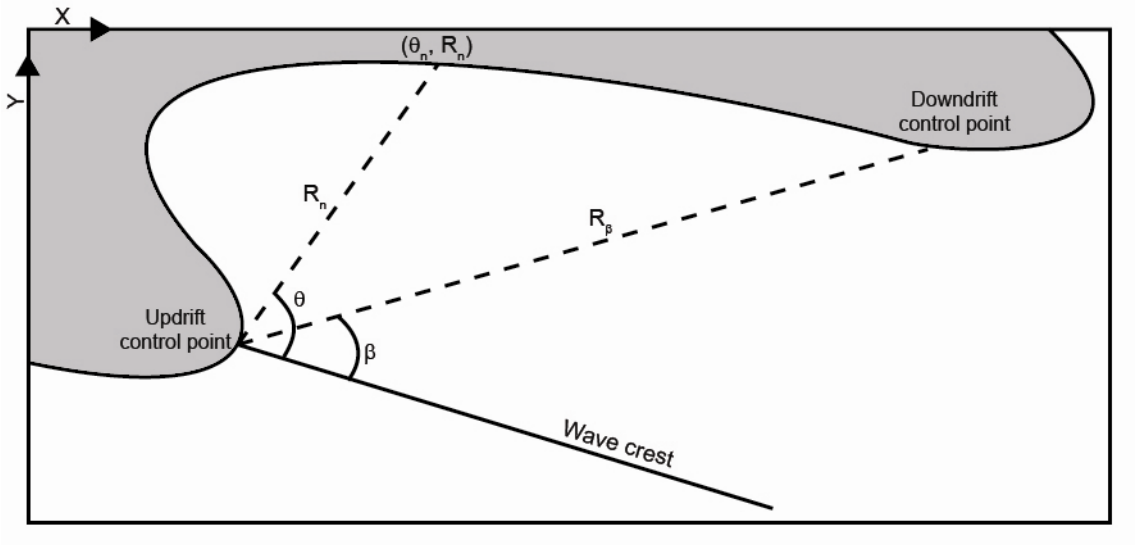

Figure 4.4 - Major physical parameters for the PBSM developed by Hsu & Evans (1989).

In this chapter the classical use of the updrift control point (Hsu & Evans, 1989; Klein et al., 2003; Hsu et al., 2010) was replaced by an empirical approximation where every change in wave direction was considered including wave refraction, as explained in the following.

Since wave propagation within the embayment is dominated by the presence of the delta, the updrift control point (Hsu et al., 2010) was positioned on the deltaic structure, according to local wave propagation previously modelled, instead using waves passing the prominent northern headland. For this, to define the position of the updrift control point, the seaward limit to significant wave effects was calculated according to Hallermeier's (1981) principles:

$$h_i = \left(\overline{H}_{sig} - 0.3\sigma\right)\overline{T}_{sig}\left(g/5000D\right)^{1/2} \tag{4.3}$$

where H_s represents the mean significant wave height, σ the standard deviation of mean significant wave height, T_s the mean period, g the acceleration of gravity and D the typical mean grainsize at or near 1.5h_i. Calculations according to local wave conditions (Costa, et al., 2001) and sediment grainsize on the shoreface (Monteiro and Moita, 1971; IH, 2005) place this limit at $-h_i$ = 33.4 m in the Caparica cell.

Therefore, the parabolic bay planform was modelled according to the predominant wave direction from NW (330°) (Costa, et al., 2001) with the upstream control point located along the refraction depth contour considering the preceding refraction caused by the north headland (Sec. 4.3). Uncertainty analysis was not included in this chapter since it is mainly related with bathymetric data acquisition which is out of the scope of this study.

4.5 Planform model results

4.5.1 Single bay shape

The model was initially applied to the entire Caparica coastal cell using the apex of the Tagus ebb delta as the control point (as defined in Figure 4.4) for the present day and 1882 shorelines. Results show that the modelled parabolic bay shape is located seawards of the actual shoreline (Fig. 4.5). Based on this result, according to Hsu et al. (2010), the embayment would be classified as being in natural beach reshaping or as an unstable bay. Comparing the same result with the 1882 coastline, when the prograded barrier extended near the Búgio lighthouse, the gap between the predicted bay shape planform and the coastline in 1882 (Fig. 4.6) was less than at present. From 1882 to present a coastline retrogradation of 800 meters occurred.

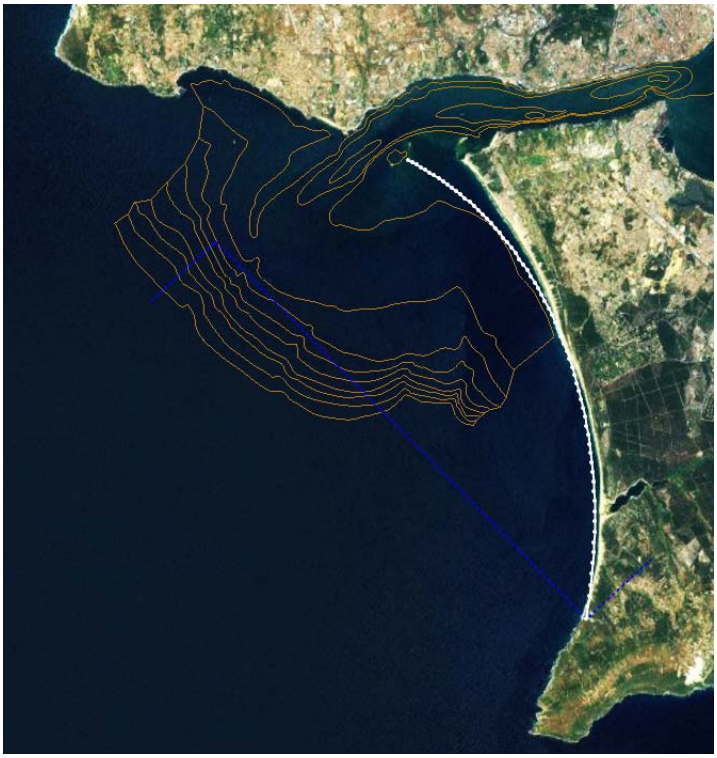

Figure 4.5 - Modelled bay shape planform compared with the present coastline of the entire Caparica coastal cell.

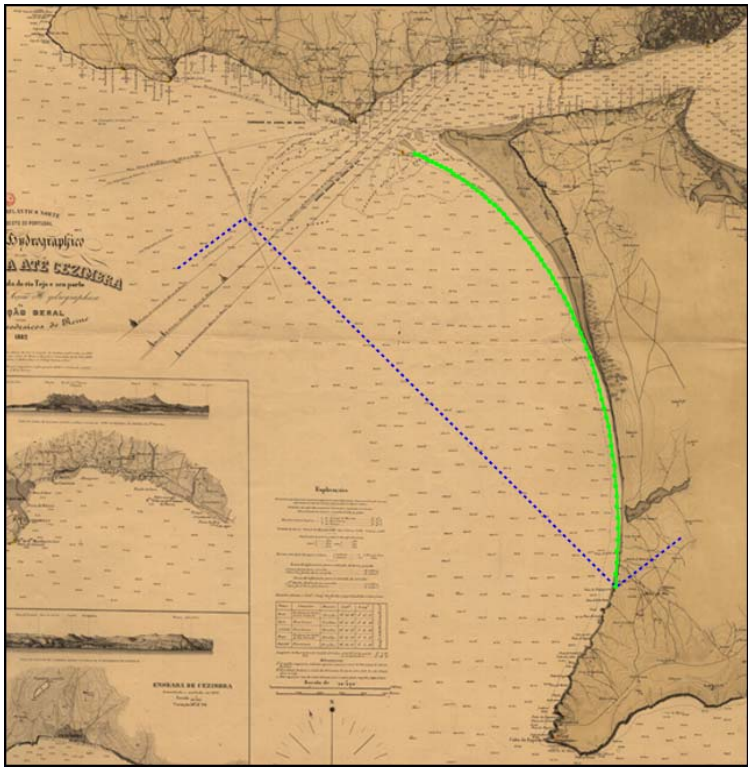

Figure 4.6 - Modelled bay shape planform compared with the 1882 coastline for the entire Caparica coastal cell.

4.5.2 Compound bay shape

The delta influence on the coastline evident from the two sub cells was identified Chapter 2 from littoral transport divergence, and in both chapters 2 and 3 through the contrasting evolutionary histories reconstructed for the sub cells. The sub cells are also subtly evident in the shoreline morphology which features a protrusion located on the central part of the Caparica cell in the vicinity of the littoral-transport divergence point that marks sub-cell process boundary. Since there is no obvious classical morphological control, this protrusion may indicate the evolution of the embayment into two distinct bays with the delta being the main cause for wave refraction (*i.e.*,the updrift control point).

Treating the sub cells as two distinct embayments, the bay shape model planform was applied separately to each. The results show that for the southern sub cell the bay shape is very similar to the

coastline in nature (Fig. 4.7) consistent with a static equilibrium at present (Hsu et al., 2010). However, if the curve is extended further north it is similar to the single bay shape planform (Fig. 4.5). For the northern sub cell, results show that the existing shoreline is landward of the predicted bay shape resulting in an unstable or in natural beach reshaping bay (Hsu et al., 2010) (Fig. 4.8).

Figure 4.7 - Modelled bay shape planform for the southern sub cell.

Figure 4.8 - Modelled bay shape planform for the northern sub cell.

Coastline retrogradation is evident for the northern sub cell. The application of the PBSM to the entire Caparica cell indicates an unstable or in natural beach reshaping classification for the northern sub cell (Hsu et al., 2010), whereas the southern sub cell is closer to static equilibrium. A compound shoreline model of the Caparica cell that couples the separate models for the two sub cells (Fig. 4.7 and 4.8) provides a superior visual fit to the present shoreline than evident when applying the single model to the entire cell (Fig. 4.5). Nevertheless, the compound model still confirms the instability of the northern sub cell (*i.e.*, the modelled shoreline lies seaward of the natural shoreline).

4.6 Climatic control change - Wave rotation

Changes in wave climate that produces different swell refraction over time has been demonstrated a potential cause of shoreline planform rotation (Ashton et al., 2011). According to Dodet et al. (2010), winter mean wave direction (MWD) has rotated clockwise up to 8° between 1953 and 2009 (57 years) off the SW European coast. This wave climate rotation increased longshore drift and disturbed coastal sediment budget causing erosion (Andrade et al., 2007). Model results based on this trend suggest that by the end of the 21st century the wave climate affecting the Portuguese west coast may experience an additional 7° clockwise rotation (Andrade et al., 2007).

Based on the approach applied to the present historical coasts above (Sec. 4.3 and 4.4), the coastline equilibrium can be related either with changes in wave direction, significant changes in delta morphology. The latter could be expected to exert an effect by modifying the position of the updrift control point for wave refraction. Changes in the wave height and period statistics of the wave climate, or changes in typical grain sizes of sediments supplied to the delta can also modify the location of the control point, and thereby the shoreline geometry, via the effects implicit in Equation 4.3.

Since grainsize variations and small morphologic changes are difficult to trace through time, changes in wave direction alone were assumed to characterise past climatic and morphologic conditions of the Caparica cell between 1Ky and present using model results (Andrade et al., 2007; Dodet et al., 2010). These factors were therefore used to examine effects of climate variability on shoreline geometry, together with inverse interpolation based on the coastline position inferred by the presence of cliff-top dunes (Ferraz, et al., 2011). The model was applied using the predominant MWD waves (NW – 330°) and the results compared to results from the model using the PWC statistics since these are the dominant conditions for long-term coastal evolution.

4.6.1 1953 wave conditions

Wave modelling results

To understand the implications of wave rotation in the Caparica cell, an 8° counterclockwise rotation was applied to the predominant wave direction (330°-8°) for characterization of wave conditions in 1953 based on work reported by Dodet et al. (2010). Results show that either in general refraction for MWC and PWC there are no significant changes. However, it is important to consider small changes in wave propagation patterns near the delta edge (Fig. 4.9).

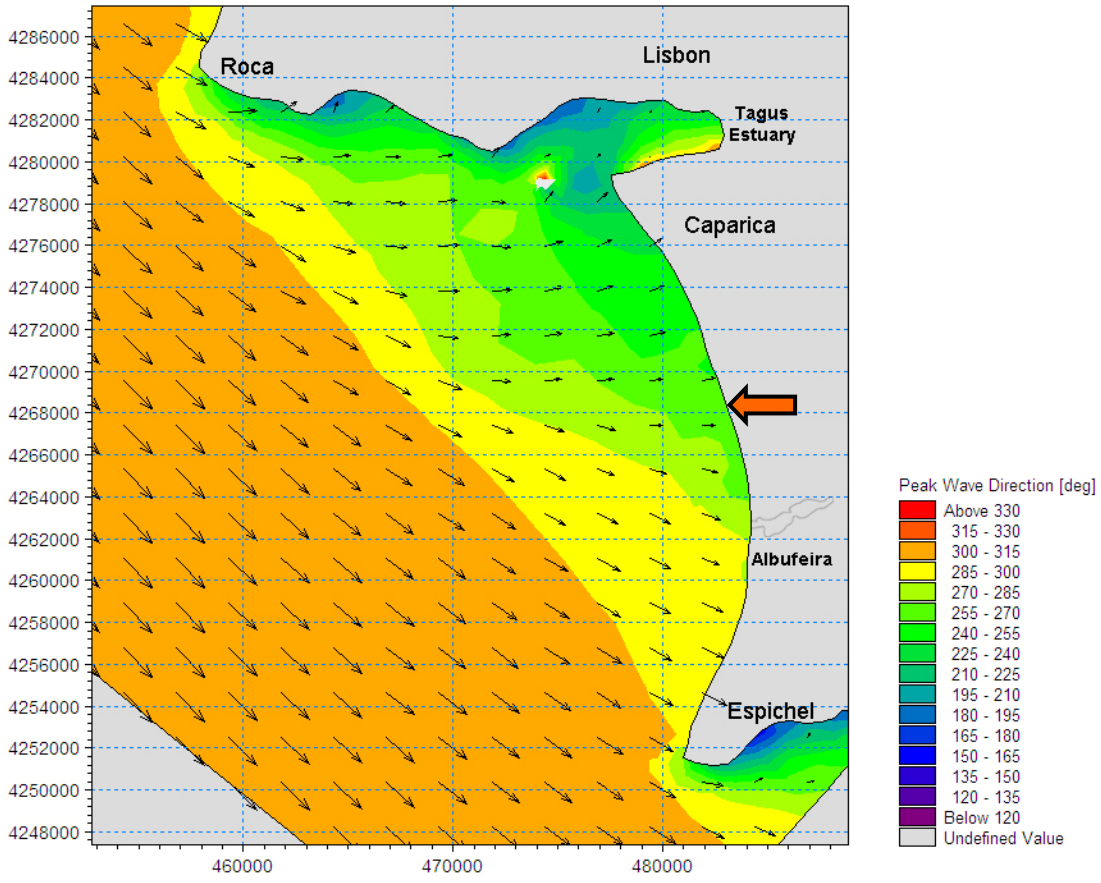

Figure 4.9 - Model results for NW direction (322° - with adopted wave rotation) in PWC (length of black arrows represents wave energy intensity and the big orange arrow indicates the wave divergence point).

Bay shape model results

For 1953 wave conditions (Dodet et al., 2010), application of the bay shape model shows a pronounced landward migration of each modelled planform: i.e., the modelled planform is relocated inland relative to the present day coastline (Fig. 4.10, 4.11 and 4.12). This relocation, mainly due to the changes in wave propagation patterns on the delta, allows to classify the coastline as being in dynamic equilibrium, more stable than in present day wave conditions.

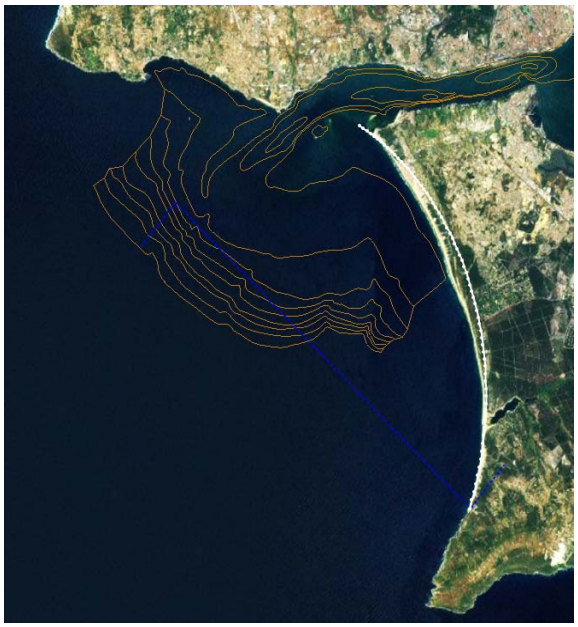

Figure 4.10 - Modelled bay shape planform compared with the present coastline after adopted wave rotation.

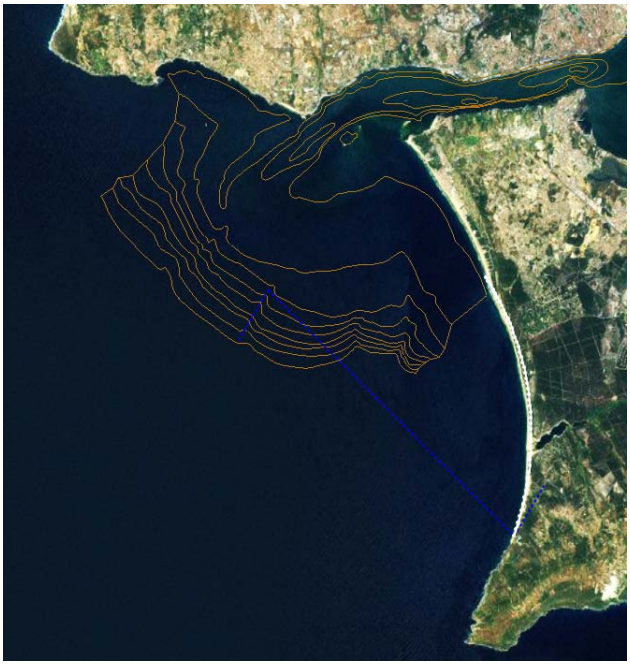

Figure 4.11 - Modelled bay shape planform for the southern sub cell after adopted wave rotation.

Figure 4.12 - Modelled bay shape planform for the northern sub cell after adopted wave rotation.

4.6.2 2100 wave conditions

Wave modelling results

After applying the 7° magnitude clockwise rotation in the predominant wave direction (330°+7°) results show that in MWC there are no significant changes to inshore wave patterns. However, the same rotation applied in PWC caused a migration of the wave divergence point to south (Fig. 4.13) enhancing SW-NE nearshore wave obliquity in the northern sub cell, thus indicating the possibility of an increased potential for sediment transport from the prograded barrier into the estuary.

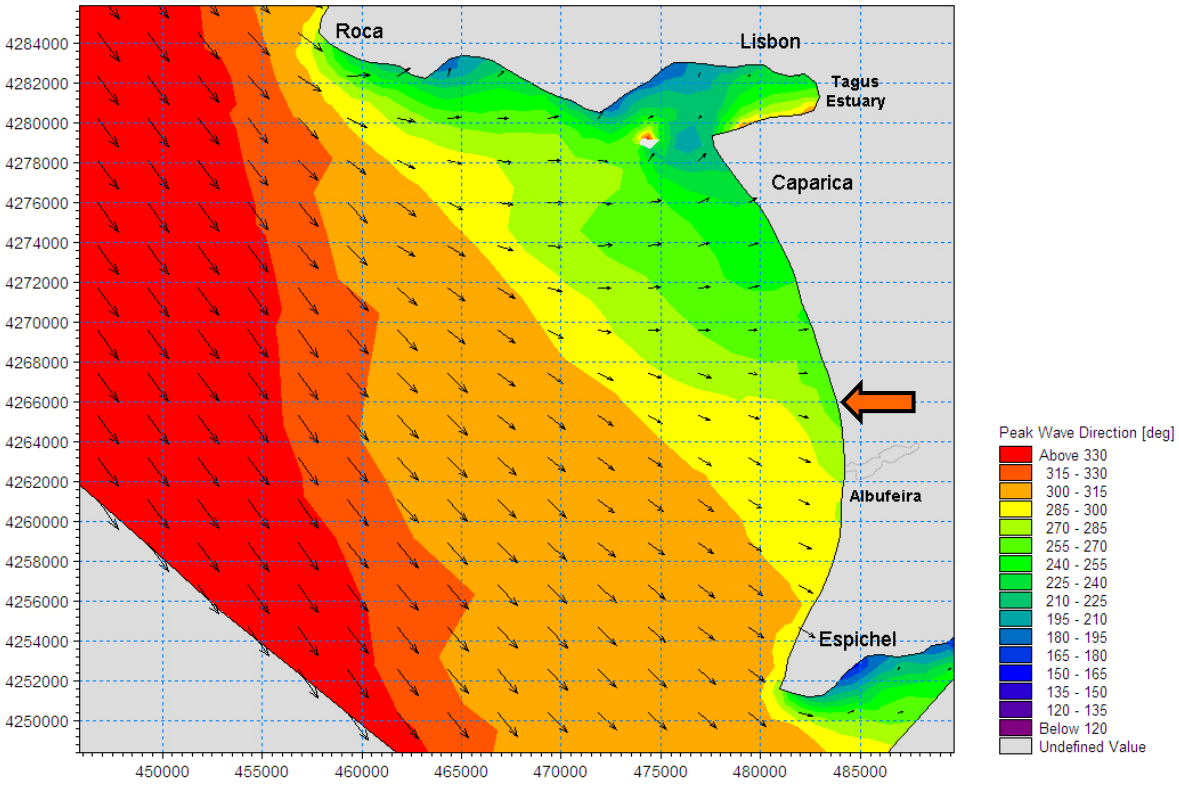

Figure 4.13 - Model results for NW direction (337° - with adopted wave rotation) in PWC (length of black arrows represents wave energy intensity and orange arrow indicates the wave divergence point).

Bay shape model results

For the 2100 wave conditions (Andrade et al., 2007), application of the bay shape model shows an offshore migration of each of the modelled future shorelines relative to the present coastline. The northern sub cell potentially becomes more unstable (Fig. 4.14 and 4.15) while the southern sub cell loses its static equilibrium, to become characterise by the Hsu unstable classification (Fig. 4.16). It can be concluded that with clockwise wave rotation modelled coastline instability increases.

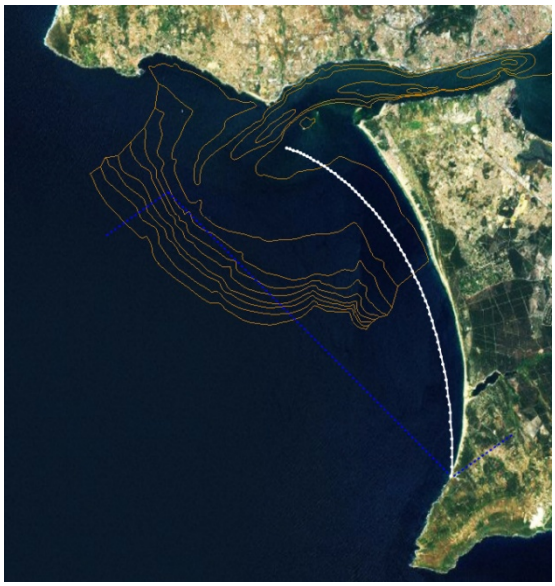

Figure 4.14 - Modelled bay shape planform compared with the present coastline after adopted wave rotation.

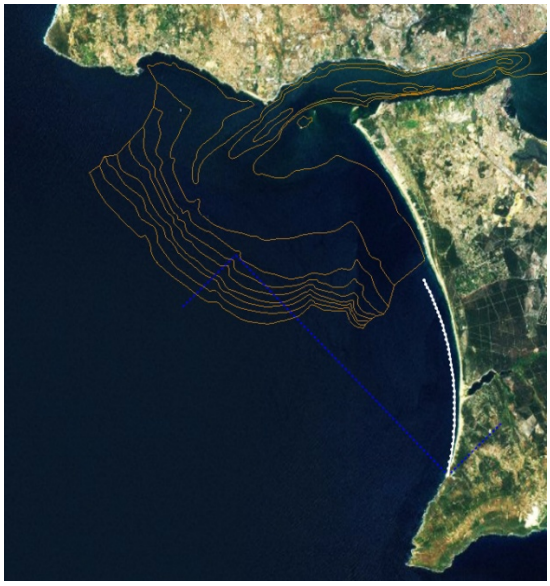

Figure 4.15 - Modelled bay shape planform for the southern sub cell after adopted wave rotation.

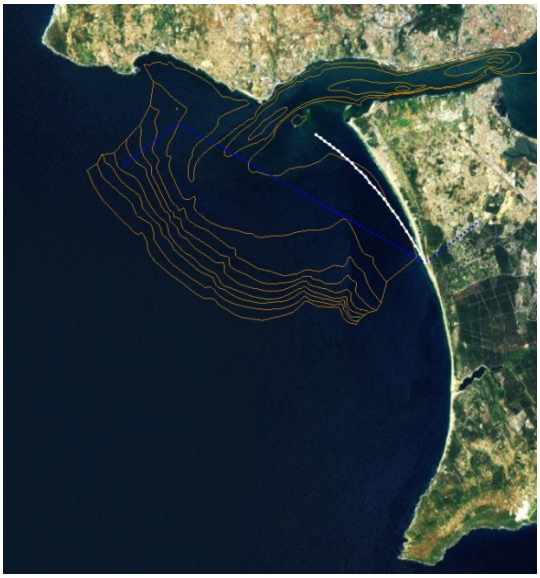

Figure 4.16 - Modelled bay shape planform for the northern sub cell after adopted wave rotation.

4.7 Cliff-top dunes coastline position

4.7.1 Bay shape model

The bay shape model was applied to the hypothetical shoreline position occurred in the period when the climbing dunes, evident through the presence of remnant cliff-top dunes (Ch.3), were active in the Caparica coastal cell (Ferraz et al., 2011). This application of the model involved an inverse interpolation from the present position of the updrift control point assumed for wave refraction in the PBSM. The objective was reverse model the swell direction based on coastline position assumed to be in static equilibrium during climbing dunes activity.

Model results for the entire Caparica cell indicate that a 25^{o} counter-clockwise swell rotation, relative to present day average observations would have been necessary to obtain an equilibrium profile coherent with the coastline position at the time (Fig. 4.17).

In the unlikely event that wave climate did not change during this period, the attainment of an equilibrium shoreline geometry in principle could attained by a repositioning of the updrift control point for wave refraction due to changes in the delta morphology or local sea-level variations. Alternative model results show that such a scenario would require the updrift control to be shifted significantly shoreward such a scenario would require relative the present one, to a very improbable position (Fig. 4.18). Alternatively, a sea level more than 20 meters higher than present would have been necessary to relocate the seaward limit for significant wave effects by the required distance. Since both scenarios are implausible, the modelling favours a directional rotation in the wave climate as the most likely explanation for the planform rotation required to explain the limited range of distances between the beach and cliff (Eq. 3.1) necessary to satisfy required physical conditions required for the formation of climbing dunes.

Figure 4.17 - Wave-climate rotation (25^{o} counter clockwise) required for a best fit of the bay-shape planform position to the coastline location inferred for the period when climbing dunes were active (black line represents coastline position at the time).

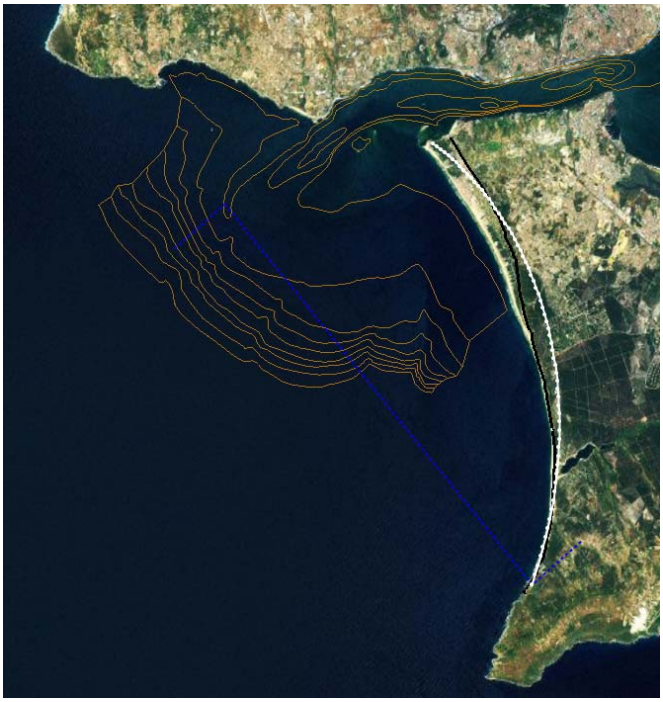

Figure 4.18 - Updrift control point relocation due to modified delta bathymetry required for a best fit of the bay shape planform with the coastline location inferred for the period when climbing dunes were active (black line represents coastline position at the time).

Applying a compound shoreline model showed that for the northern sub cell a 16^{o} counter-clockwise wave rotation would be necessary to satisfy paleo climbing-dune requirements (Fig. 4.19). Otherwise, if the change in delta morphology was responsible for the coastline rotation, an implausible relocation of the updrift control point is required: *i.e*, toward the right-hand margin of the estuary (Fig. 4.20).

Figure 4.19 - Wave-climate rotation (16º counter clockwise) required for a best fit of the bay shape planform position with the paleo coastline inferred for climbing dune formation in the northern sub cell (black line represents coastline position at the time).

Figure 4.20 - Updrift control point relocation due to modified delta bathymetry required for a best fit of bay shape planform position with the paleo coastline inferred for climbing dune formation in the northern sub cell (black line represents coastline position at the time).

In the case of the southern sub cell, a wave rotation of 7^{o} counter clockwise would be necessary to support the coastline position necessary for climbing dune formation (Fig. 4.21). A relocation of the updrift control point due to modified delta bathymetry would not be significant relative to the control point for the present shoreline (Fig. 4.22).

Figure 4.21 - Wave climate rotation (7^{o} counter clockwise) required for a best fit of the bay shape planform with the paleo coastline inferred for climbing dune formation in the southern sub cell (black line represents coastline position at the time).

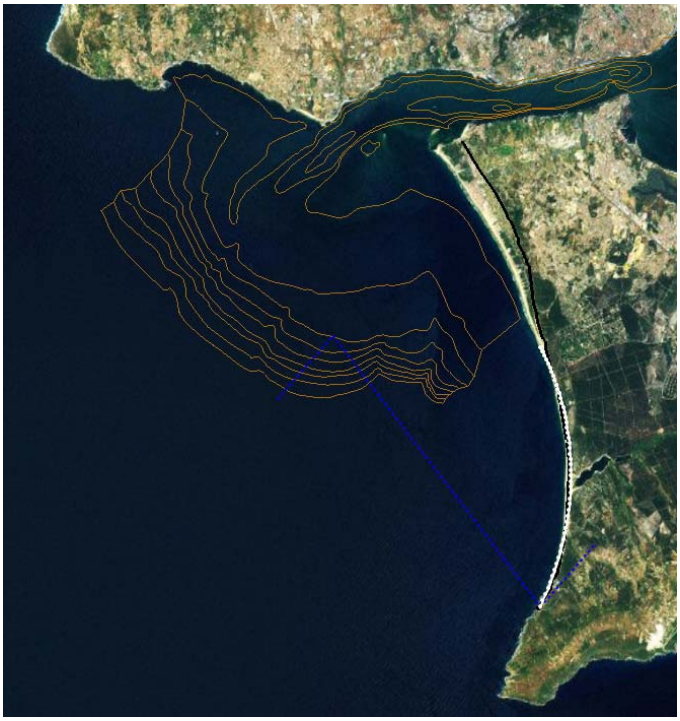

Figure 4.22 - Updrift control point relocation due to modified delta bathymetry required for a best fit of the bay shape planform with the paleo coastline inferred for climbing dune formation in the southern sub cell (black line represents coastline position at the time).

Wave modelling

To examine the effects of counter-clockwise wave rotation, wave modelling was performed with the maximum rotation value (25^{o}) obtained with the PBSM (Fig. 4.17) for mean and peak wave conditions. Results show a considerable north migration of the wave divergence point in MWC (Fig. 4.23) while in PWC the position is preserved (Fig. 4.24). This suggests that past wave conditions, previous to wave rotation, were more appropriate for coastline stability in this area as the area affected by SW-NE nearshore wave direction was considerably minor as well as erosion potential.

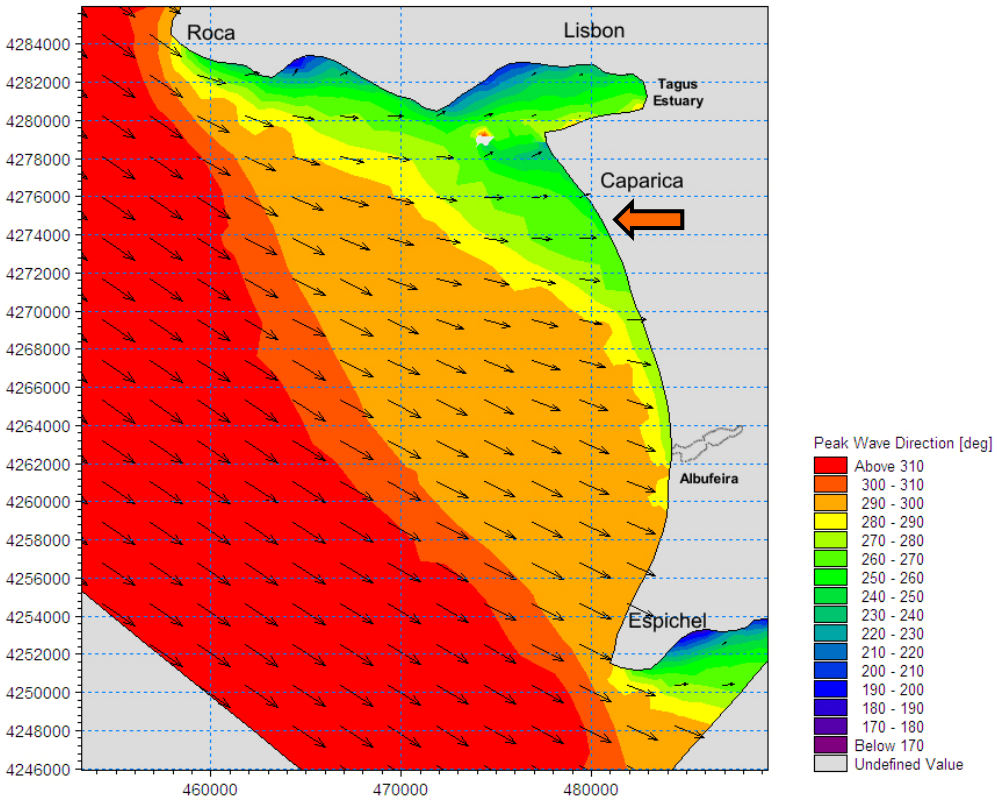

Figure 4.23 - Model results for 305° direction in MWC (black arrows length represents wave energy intensity; large orange arrow indicates the wave divergence point).

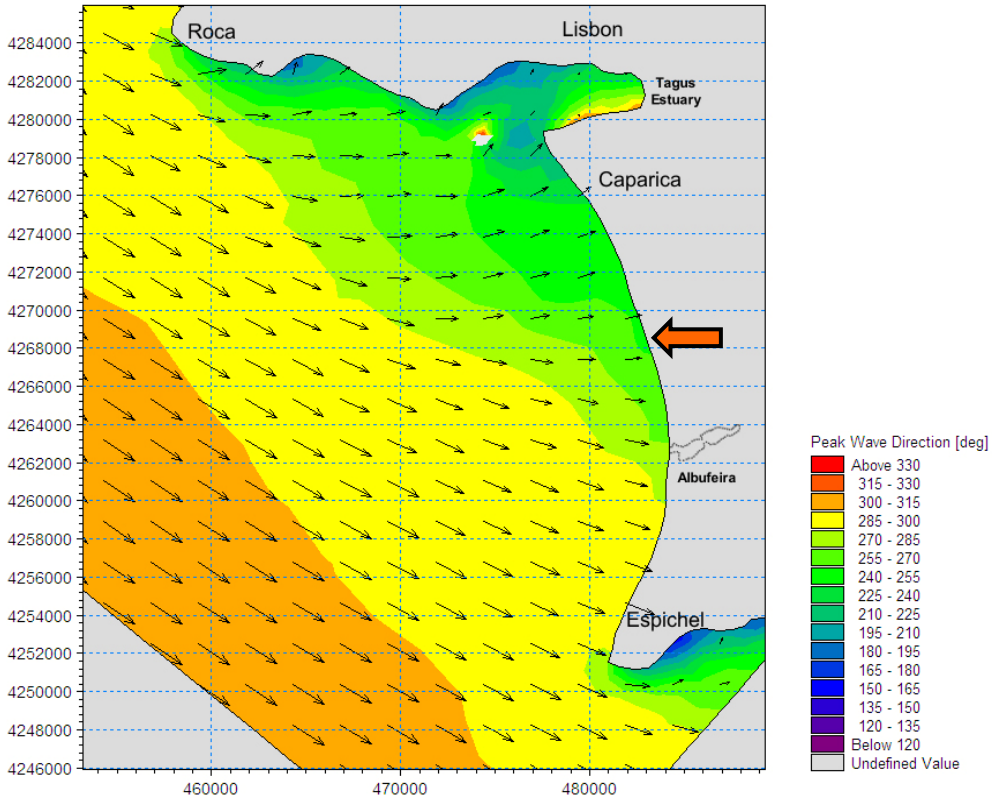

Figure 4.24 - Model results for 305° direction in PWC (black arrows length represents wave energy intensity; large orange arrow indicates the wave divergence point).

4.8 Conclusions

Results from application of the shoreline model support the three fundamental conclusions:

1. Delta morphology plays a key role in the planform development of the adjacent sandy coastline in the Caparica coastal cell. This conclusion holds for the shoreline that actively shares sediment with the delta, but also holds for the shoreline beyond region of active sediment exchange with the delta. The former case involves the beach that extends along the flanks of the delta margin. That this shoreline and the delta are coupled is not a new conclusion, and the modelling results are entirely consistent with a much earlier demonstration of modelled morphodynamic adjustment by the shoreline planform to sand discharged at rivermouths and redistributed alongshore in the surfzone (Komar, 1976). For the shoreline beyond region of active sediment exchange with the delta the conclusion is novel because it relates to the shoreline along the beach that is not part of the delta margin and can thus be regarded as the adjacent coast in a stricter sense than the former case. There is nothing about the coast studied to suggest that this conclusion would not be valid elsewhere.

2. The delta margin shoreline and the shoreline beyond the immediate influence of the delta have distinctly different planform alignments, consistent with evidence presented in preceding chapters that these two shoreline segments operate physically as separate, although connected, sub cells within the Caparica embayment. Although it might be concluded from model results that different morphodynamic controls over the planfroms exist for the two sub cells, paradioxically the distal shoreline is better aligned with the delta than is the proximal shoreline. It might also be concluded that the paradox reflects a greater sensitivity of the proximal shoreline to changes in the delta to which it is more directly connected.

3. Changes in delta morphology over the historical period have less effect on shoreline planform along the adjacent coast than do direction changes in the wave climate. The wave rotation process plays an important role on coastline stability since it establishes sediment dispersal patterns according to nearshore wave propagation on a long-term approach for wave dominated coasts. Variations in swell direction are proven to cause changes in nearshore sediment transport affecting coastline stability and often enhancing erosion and retrogradation rates when associated with insufficient sediment supply.

These conclusions remain tentative because they depend on the validity of the parabolic bay shape equation (PBSE) when applied to shorelines affected by deltaic processes. The applicability of the PBSE in such environments has not been systematically evaluated.

Nevertheless, the conclusions are consistent with reasoning from physical principles. The wave modelling results from the present study, based on local wave conditions, demonstrate that wave propagation is strongly affected by local morphology and bathymetry. The presence of a delta creates significant wave refraction that can be expected to condition nearshore wave currents and alongshore transport of sand that affect the adjacent coastline evolution. The refraction patters induced by the delta bathymetry produce two distinct sub cells whose mutual boundary shifts along the beach according to swell direction variations. It can be concluded that the northern sub cell, which is frequently affected by SW-NE nearshore wave direction, has an erosive tendency because alongshore transport of sediment from the prograded barrier into the estuary may operate as a one way valve. Such a net transfer of sediment is especially likely if the accommodation capacity of the estuary has been increased, for example, artificially by dredging works for Port development, or naturally through sea level rise. In contrast, the southern sub cell is frequently affected by nearshore wave directions oriented perpendicular to the beach alignment, promoting a stable coastline associated with minimal net alongshore transport of sand.

CHAPTER 5

How sediment supply rules coastal response to climate change

Photo: Meco beach

5.1 Introduction

Coasts are naturally vulnerable areas to external influences as climatic changes, storm events and anthropic impacts. Throughout the 20th century global sea-level rise contributed to coastal inundation, erosion and coastline retreat (IPCC, 2007) affecting coastal populations and representing significant property damage. Anticipated predictions indicate that climatic changes include a significant sea-level rise (IPCC, 2007; Rahmstorf, 2007) and intensification of storm conditions (IPCC, 2007). Considerable variations in these events will be experienced at local scales, but negative impacts are generally expected. People and coastal assets are probably therefore subject to additional stresses due to land-use and changes in river catchments including dams that reduce sediment supply to the coast (IPCC, 2007).

Long-term characterization (decadal to centennial) is most applicable to investigations on coastal response to climatic changes in relation to planning and risk mitigation (Capobianco et al., 1999). Aggregated coastal modelling adopts the parameterization of the relevant processes involved in coastal evolution using a deterministic approach to exploit uncertainties (Cowell et al., 1995, Cowell et al., 2003a,b). This allows quantitative estimates to be derived to forecast coastal evolution at timescales relevant to climate change (Cowell et al., 2006).

This chapter documents application of aggregated coastal modelling techniques to investigate the response of the Caparica coastal cell (Fig. 5.1) to changes in external conditions comprising sediment supply variations and effects of climatic changes that include sea-level rise and variations in storm demand. The modelling techniques reported in this chapter draw from geological evidence and its interpretation regarding coastal change presented in the preceding chapters to provide context and calibration for model generated forecasts applicable to the Caparica coastal cell. The geomorphic setting is described in chapter 2.

The objective of this chapter is to forecast coastal change through to future the decades, 2030, 2050 and 2100 (Sec. 5.4.5). In developing these forecasts, the chapter addresses four questions:

1) Which factor is determinant for local coastline recession?

2) What is the expected recession magnitude in the future?

3) Does recession involve permanent land-loss and property damage?

4) Which mitigation procedures are valid for this area on a long-term basis?

Results provide quantitative estimates of the inevitable uncertainty (Cowell, 2002) associated with the recession forecasts.

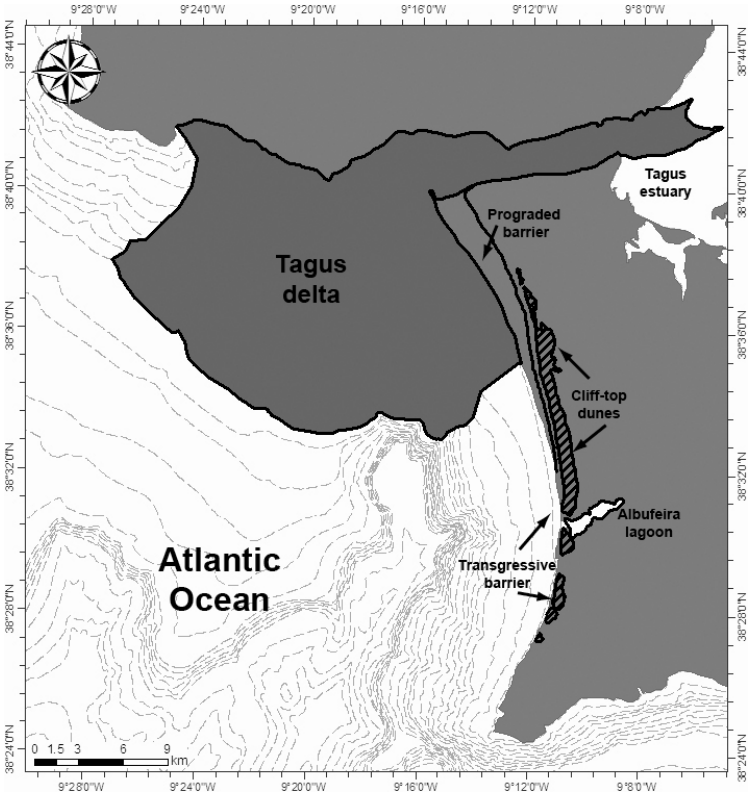

Figure 5.1 - Main morphological features of the Caparica coastal cell.

5.2 Low order coastal modelling and management of uncertainty

Low order coastal behaviour is defined by long-term (centennial) and large scale (kilometres) changes that entail problems of chronic erosion important to coastal management (Cowell et al., 2003a; Kinsela, 2007). This type problem involves parts of the coast usually not considered for management purposes (behaviour of the continental shelf) (Cowell et al., 2003a), and relates to the climate change time scale.

Aggregation procedures for coastal modelling avoid issues that arise with attempts to scale up short-term processes in quantitatively estimating for long term behaviour by undertaking the analysis directly on the long term time scale by focusing directly on time averaged and spatially averaged behaviour (Kinsela, 2007). The Shoreface Translation Model (STM) applied in this study is a means of analysing sediment budgets to quantify coastal changes (Cowell et al., 1995). Because processes are represented in an aggregated form the STM is readily adaptable to stochastic simulation techniques involving the sampling of different input values from probability distributions that characterize the input variables and uncertainty about them (Cowell et al., 2006). Outputs are generated as probabilistic forecasts suitable to risk analysis and quantification of uncertainty.

The introduction of the coastal tract concept by Cowell et al., (2003a,b) defined the composite morphology which provides guidelines on scale and aggregation problems for climate change predictions. This concept deals with morphologic change on coasts through the definition of coupled sediment sharing systems in which volumetric exchanges form the basis for analysing morphological change (Cowell et al., 2003a; Kinsela, 2007).

Due to the complex dynamics of coastal areas, uncertainty is unavoidable in morphologic evolution studies (Cowell et al., 2006).

5.3 Model parameterization

5.3.1 Coastal cell delineation for sediment budget model application

According to the coastal tract concept (Cowell et al., 2003a) coastal cell boundaries need to be delineated to define the sediment budget control volume. The alongshore extent of the Cell needs to be large enough to allow averaging out of details that can be assumed to constitute higher order noise in long-term analysis, but not so large that alongshore homogeneity cannot be assumed, while cell width needs to include the different morphological environments (Kinsela, 2007).

Based on the results contained in the previous chapters the Caparica cell was divided in two distinct sub cells. The northern sub cell is essentially influenced directly by the delta (and its estuary) through sediment exchanges with it, while the sediment budget of southern sub cell is more isolated from sediment exchanges with delta and more connect to potential sand sinks on the continental shelf. The southern sub cells also has a steeper shoreface with a narrow shelf and a close proximity to the Lisbon Canyon (Fig. 5.2), so homogeneity cannot be assumed for the entire Caparica coastal cell in relation to characteristic morphology.

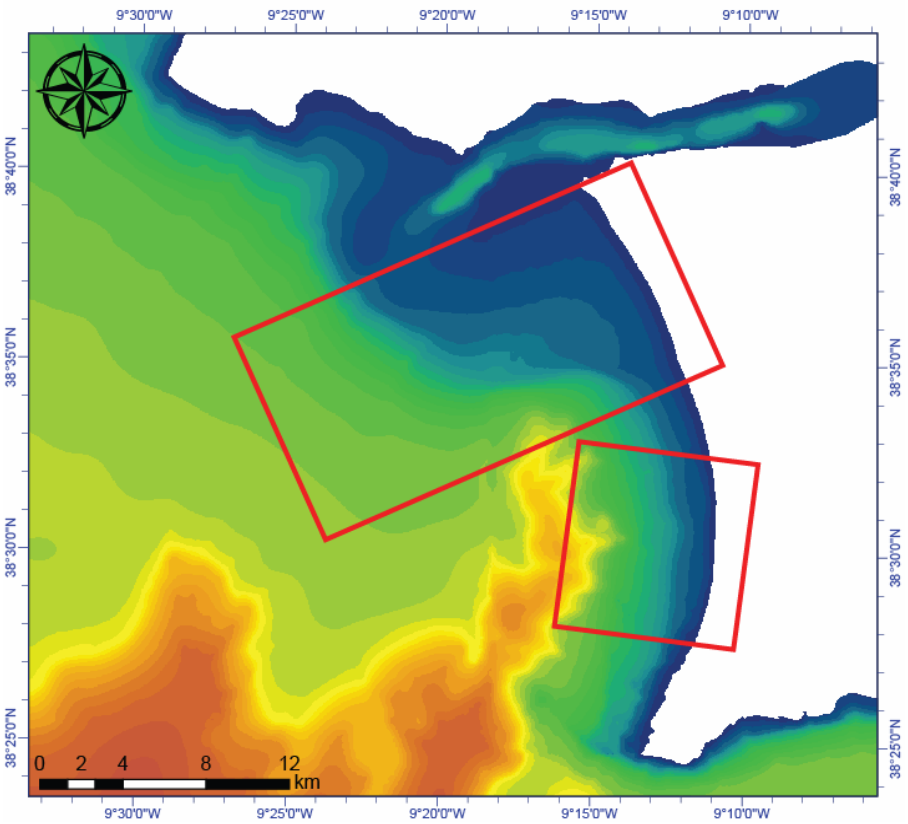

Figure 5.2 - Sub cell delineation

Cell extent

In the alongshore direction the northern sub cell as delineated extends from the estuary mouth to the protrusion in the coastline that expresses morphologically the end of the deltaic influence (Fig. 5.3). The southern sub cell was defined as extending between Fonte da Telha and the southern limit of the continuous beach segment (beginning of rocky coastline).

In a cross-shore direction the inland limit for both sub cells was defined at the Mio-Pleistocene sea-cliff whose changes within the time frame of this work were assumed to be improbable. No artificial structures were considered in the model. A conservative seaward limit of 100 meters depth was assumed in both cells since significant sediment transport beyond these depths is unlikely to occur on a

millennial timescale based on Hallermeier (1981) considerations encapsulated in Equation 4.3 (Cowell et al., 2001; Cowell et al., 2003b).

Cell orientation

To obtain a more accurate one dimensional representation of the shoreface, alongshore cell boundaries need to have an orthogonal alignment with the bathymetric contours so the morphology can be averaged as profiles to obtain unbiased representation of the shoreface (Daley, 2005; Kinsela, 2007; Adlam, 2008; Figueiredo, 2010). However, the presence of a delta and a canyon in the Caparica cell causes systematic irregularity in bathymetric contours incompatible with the aggregation principles underlying alongshore-averaging procedures. The possibility of aligning sub cells with the present coastline was also not possible due to the significant changes occurred that have occurred the northern sub cell during the last century (Ch. 2). The base of the Mio-Pleistocene sea-cliff was therefore adopted as the reference line for cell orientation because, according to maps and aerial photographs, the cliff line has been relatively stable during the last few centuries.

Using ArcGIS™, the cliff base line was cropped within each cell and sampled into points that were exported to Microsoft Excel™ and where a linear least squares fit was applied to optimise sub-cell orientation (Fig. 5.3 and 5.4).

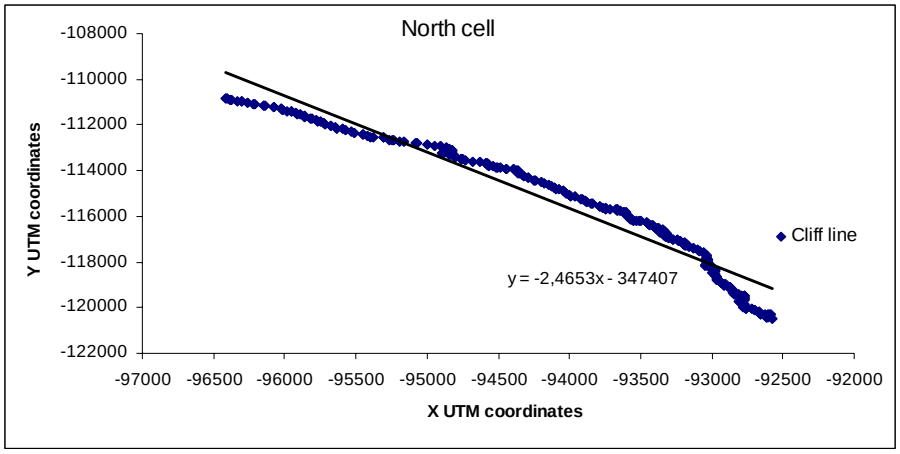

Figure 5.3 - Cliff line configuration and line of best fit for northern sub cell.

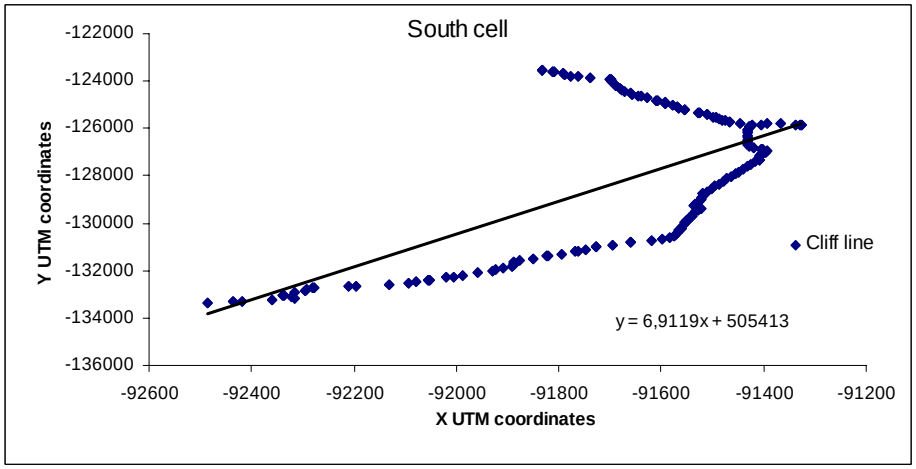

Figure 5.4 - Cliff line configuration and line of best fit for southern sub cell.

The angle between the cliff base line and the cross shore boundaries of each cell was obtained by trigonometric calculations and then applied to shapefiles for each sub cell in ArcGIS™ through the ArcEditor tool.

5.3.2 Spatial aggregation

Offshore morphological characterisation

The offshore morphology was characterised using a range bathymetric sets from different sources (see chapter 2). The data was compiled and combined into the same dataset in order to create a DEM using ArcGIS™ spatial analyst tool.

Bathymetric representation inside each cell was based on the hypsometric curve concept (Kinsela, 2007) where the cell-averaged profiles represent the cumulative frequency plot of the areas of the shoreface that share the same depth value. The procedure relies on the assumption that the shoreface is a monotonic surface, an assumption that is reasonably applicable in the Caparica cell (Kinsela, 2007).

Spatial averaging calculations were performed after transforming each cell value into integer data and determine the shoreface area (P_A) for each depth value according to the following equation:

$$P_A = \frac{D_A}{W_C} \tag{5.1}$$

where W_C is the width (alongshore direction) of the coastal cell and D_A the number of raster cells for each depth value.

Onshore profile characterisation

According to the local 1:50.000 geology chart (Manuppella et al., 1999) the geological setting of the area comprises a homogeneous prograded sand barrier limited inland by a semi-consolidated sandstone Mio-Pleistocene sea-cliff. Geotechnical surveys show that the barrier has an average thickness of 12m, over a Miocene substrate. Morphologically the barrier becomes narrower towards south with a monotonic surface sloping down from the cliff toe to the coastline. Onshore morphology and elevation was defined through alongshore averaging of the Digital Elevation Model (DEM) within each sub cell. Beach profiles

surveyed after a regular winter storm, allowed the location of the erosion scarp to be defined as the initial landward limit of the shoreface and beach for modelling purposes.

For each sub cell, buffers were defined in ArcGIS™ at variable intervals (Kinsela, 2007) (Fig. 5.5). The average elevation was then computed for each buffer interval landward of the beach using values extracted from the local DEM cells within each buffer separately for each sub cell (Tables 5.1 and 5.2).

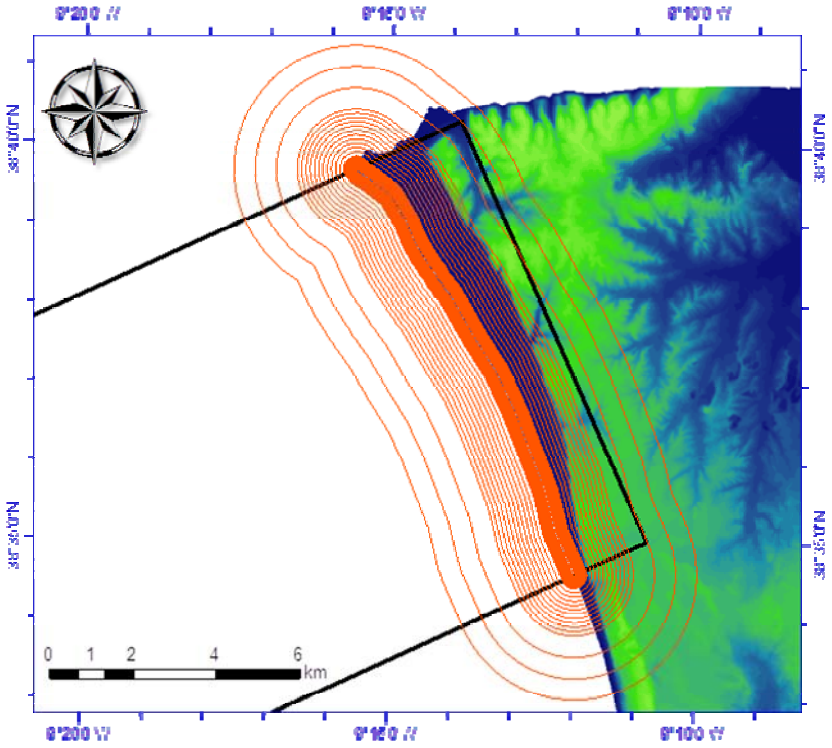

Figure 5.5 - GIS buffers applied for computing alongshore average elevations with distance inland from the beach, exemplified for the northern sub cell. Mean elevation was computer only for the buffer intervals landward of the beach.

Table 5.1 - Buffer intervals used for alongshore averaging of elevations as a function of distance inland from the beach for the northern sub cell.

Distance landward from coastline (m)	Buffer interval (m)	Morphological features
0-300	20	Beach + Foredunes
300-1400	100	Prograded barrier + Sea-cliff
>1400	500	Cliff top

Table 5.2 - Buffer intervals used for alongshore averaging of elevations as a function of distance inland from the beach for the southern sub cell.

Distance landward from coastline (m)	Buffer interval (m)	Morphological features
0-100	10	Beach + Dunes + Cliff face
100-250	50	Cliff top +Lagoon + Dunes
>250	500	Cliff top +Lagoon

The average distance between the cliff toe and the defined coastline was calculated using the Digital Shoreline Analysis System (DSAS) from the United States Geological Survey (USGS) (Thieler et al., 2009) drawing several profiles along each cell and averaging it.

5.4 Model calibration

5.4.1 Substrate profiles

The substrate characterised by the aggregation procedure described above (Sec. 5.3.2) defines initial morphological conditions related to the shoreface and backshore as they exist at present in each sub cell. In STM, the substrate profile comprises a surface profile representative of the mobile sediment and an underlying profile that represents the bedrock. The elevation difference between profiles represents the sediment thickness available for reworking in the model constituting one of the sediment sources. A representative sediment thickness of 20 meters was applied based on geotechnical survey data (Figs. 5.6 and 5.7).

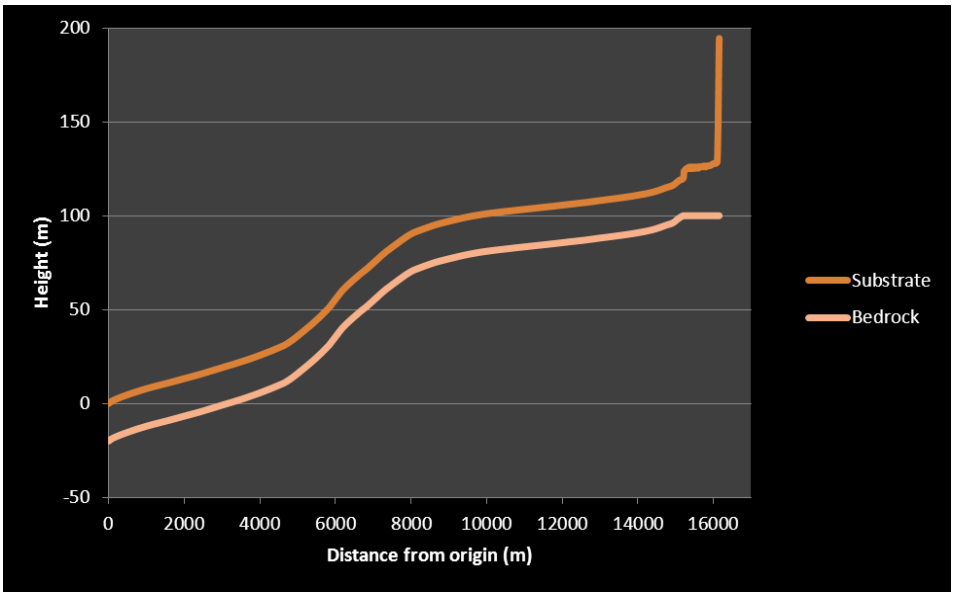

Figure 5.6 - Alongshore averaged profile and bedrock substrate for the northern sub cell. (Axes are in the STM reference frame.)

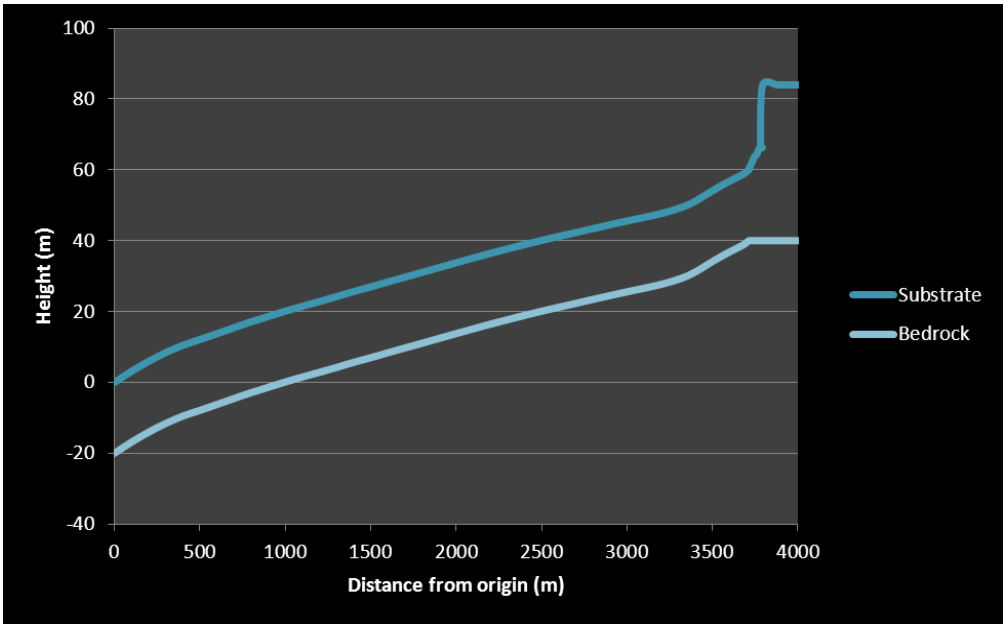

Figure 5.7 - Alongshore averaged profile and bedrock substrate for the southern sub cell. (Axes are in the STM reference frame.)

5.4.2 Compound shoreface curve fitting

After merging the onshore and offshore profiles and converting them into the STM axis frame of reference (Figs. 5.6 and 5.7), the compound shoreface for each sub cell is ready for the modelling procedure. However, the profile must be transformed into a mathematical function (the 'active profile') that allows the model to compute the coastal response to the external factors. The evolution of the active profile may change through time from its initial form, representative of the shoreface as it exists at present within each sub cell. Time dependent changes to profile geometry can be imposed to reflect environmental changes (e.g. changes in wave climate or sediment characteristics over time) or simply to take into account uncertainty about future profile geometry. The initial profile geometry was defined by fitting to the sub-cell averaged substrate profiles (Figs. 5.6 and 5.7) the compound shoreface model proposed by Cowell et al., (1999):

$$h = WA_c x^{mc} + (1 - w)A_i x^{mi} \tag{5.2}$$

where

$$W = exp\left\{-\left[\frac{|\lambda - x| - (\lambda - x)}{\lambda c}\right]^{\alpha}\right\} \tag{5.3}$$

The profile fitting was undertaken numerically through iterative optimisation separately for the northern and southern sub cells (Fig. 5.8 and 5.9).

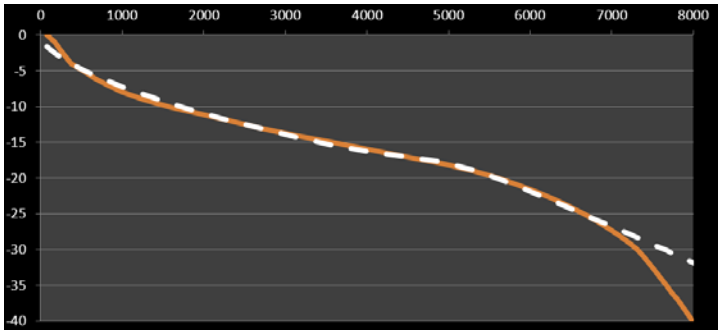

Figure 5.8 - Theoretical compound shoreface (Eq. 5.2) fitted to spatially averaged bathymetry for the northern sub cell (orange line – substrate profile; dashed line – fitted profile).

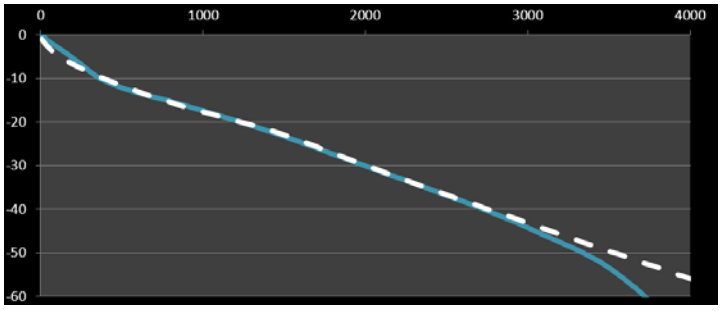

Figure 5.9 - Theoretical compound shoreface (Eq. 5.2) fitted to spatially averaged bathymetry for the southern sub cell (blue line – substrate profile; dashed line – fitted profile).

In the STM the shoreface origin is set horizontally to the landward limit of erosion estimated for “mean storm” conditions, identified in this study for practical purposes the base of the erosion scarp on the sub-aerial beach from surveys undertaken after a typical winter storm event.

The offshore limit of the active shoreface was defined using Equation 4.3 according to the Hallermeier (1981) approach which relates to the maximum water depth for significant sand movements over 12 hours in a typical year (Fig. 5.10). According to Hallermeier (1981) This limiting depth, h_i, is more applicable to analysis of sediment budgets on the climate change time scale (many decades) than the closure depth, *hc*, that is defined as the seaward limit of bed height changes that are detectable ins survey during a typical year..

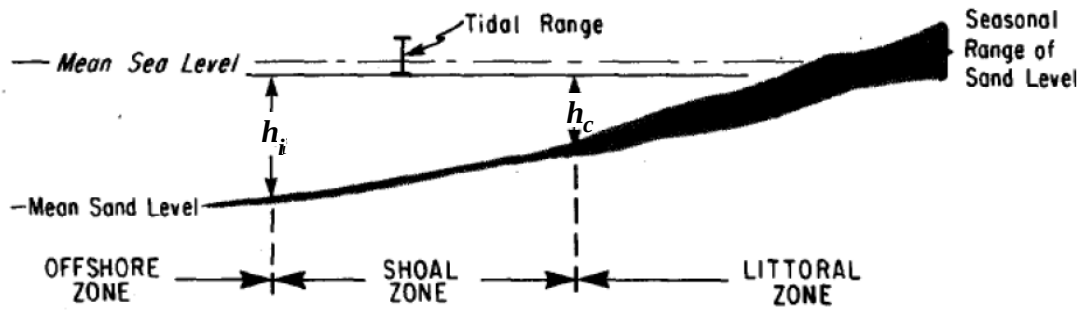

Figure 5.10 - Seaward limit, h_i, (Eq. 4.3) for morphologic change on shoreface over the climate-change timescale based on the rationale of Hallermeier (1981). (Adapted from Hallermeier, 1981).

The medium grainsize (*D50*) strongly influences estimates of h_i in Equation 4.3. For that it is important to prepare a strong sediment characterization before the actual calculation (Sec. 5.4.4).

5.4.3 Wave parameters

Costa et al., (2001) characterized the wave parameters on this area using Sines wave measurement buoy to obtain H_s, σ, and T_s mean values (Table 5.3).

Table 5.3 - Wave parameter values for the study area (Costa et al., 2001).

H_s(m)	1.70
σ(m)	0.90
T_s(s)	6.60
g(m/s^2)	9.80

5.4.4 Sediment size and sorting

Since there were no sediment samples available for this study, three different data sources were taken into consideration: Continental shelf characterization off the Caparica cell between Búgio and Espichel (Monteiro et al., 1971); sediment data from Setúbal Peninsula beach characterization (Teixeira, 1990); and the surficial sediment map of the area (IH, 2005).

Teixeira (1990) characterized the Setúbal peninsula beach sediments at nine locations along the cell in different seasons for the upper, middle and lower beach environment. For h_i calculation, mean grainsize values of the entire beach environment as well as values for the lower beach area were used. The lower beach sediment is closer to the depth for grain size measurements recommended by Hallermeier (1981) for application in Equation 4.3: *i.e.*, a sample depth of h = 1.5 h_c (Fig. 5.10). However, the natural surf zone sediment sorting can exclude part of the fine sediments fraction leaving the mean grainsize values from the entire beach as representative of a more realistic distribution of the sediment without surf zone sorting. Regardless, the possibility exists that beach sediments are poorly representative of the shoreface sand, making it preferable to use samples from the shoreface where these are available.

Monteiro et al., (1971) described the continental shelf sediments of the study area including from the shoreface. He found that shoreface sediment between Búgio and Espichel is composed of fine (D < 0.125mm) well sorted sand (Fig. 5.11).

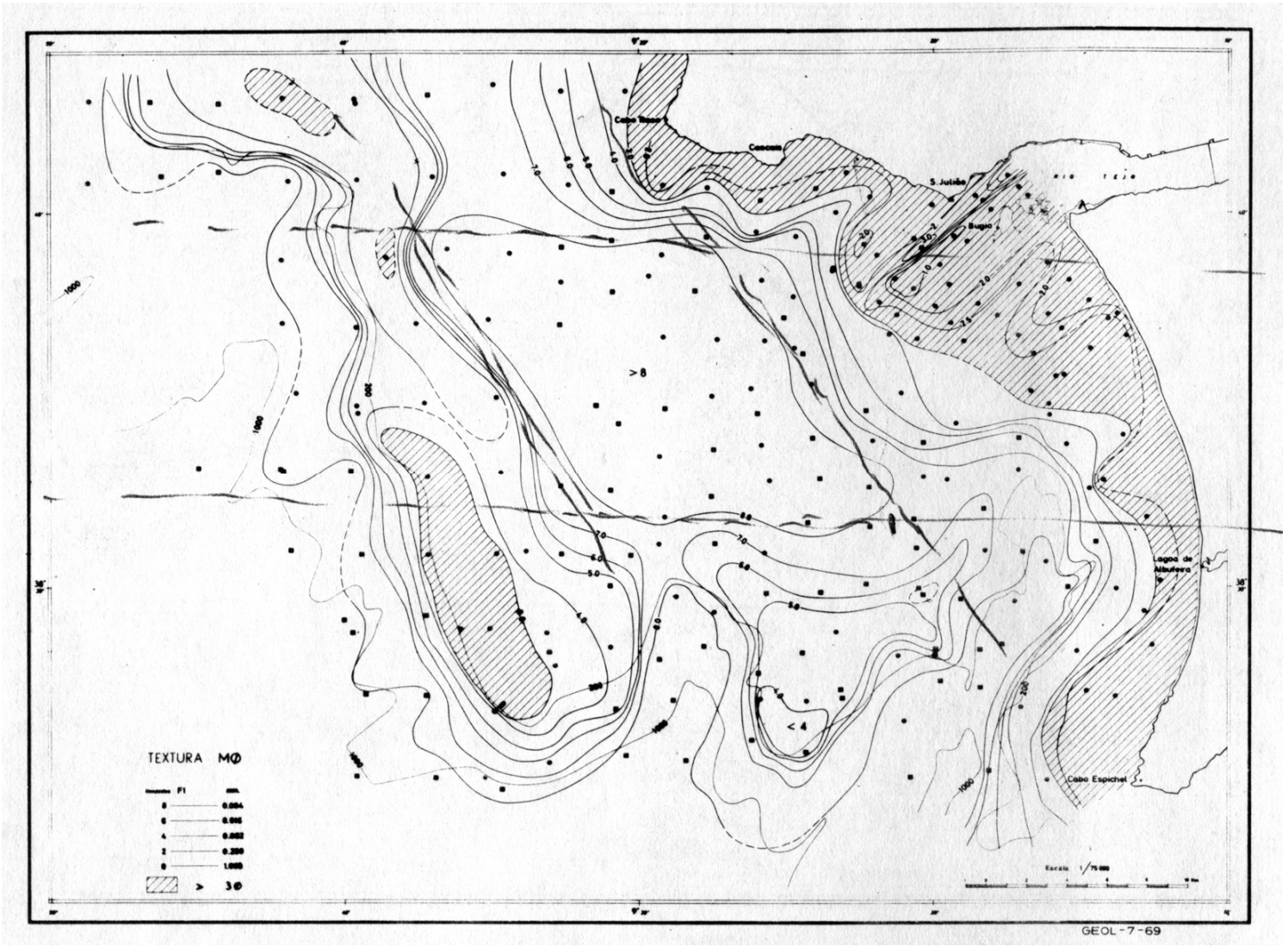

Figure 5.11 - Sediment grainsize map (Monteiro et al., 1971).

Unfortunately Monteiro et al, specified sediment grainsize only in descriptive size classes. However, sediment characterization from the superficial sediment map of the area (IH, 2005) allowed confirmation of the sediment distribution proposed by Monteiro et al., (1971) as well as to obtain a narrower grainsize range for each of the sediment classes. Mean grainsize was calculated for each class and used to characterize the shoreface grainsize.

Since the shoreface is mostly composed by fine sands (class AF1 on the map) the grainsize range varies between $0.062 \geq D \geq 0.2$ 5mm (Fig. 5.12) with a mean value used to approximate D_{50} = 0.156 mm.

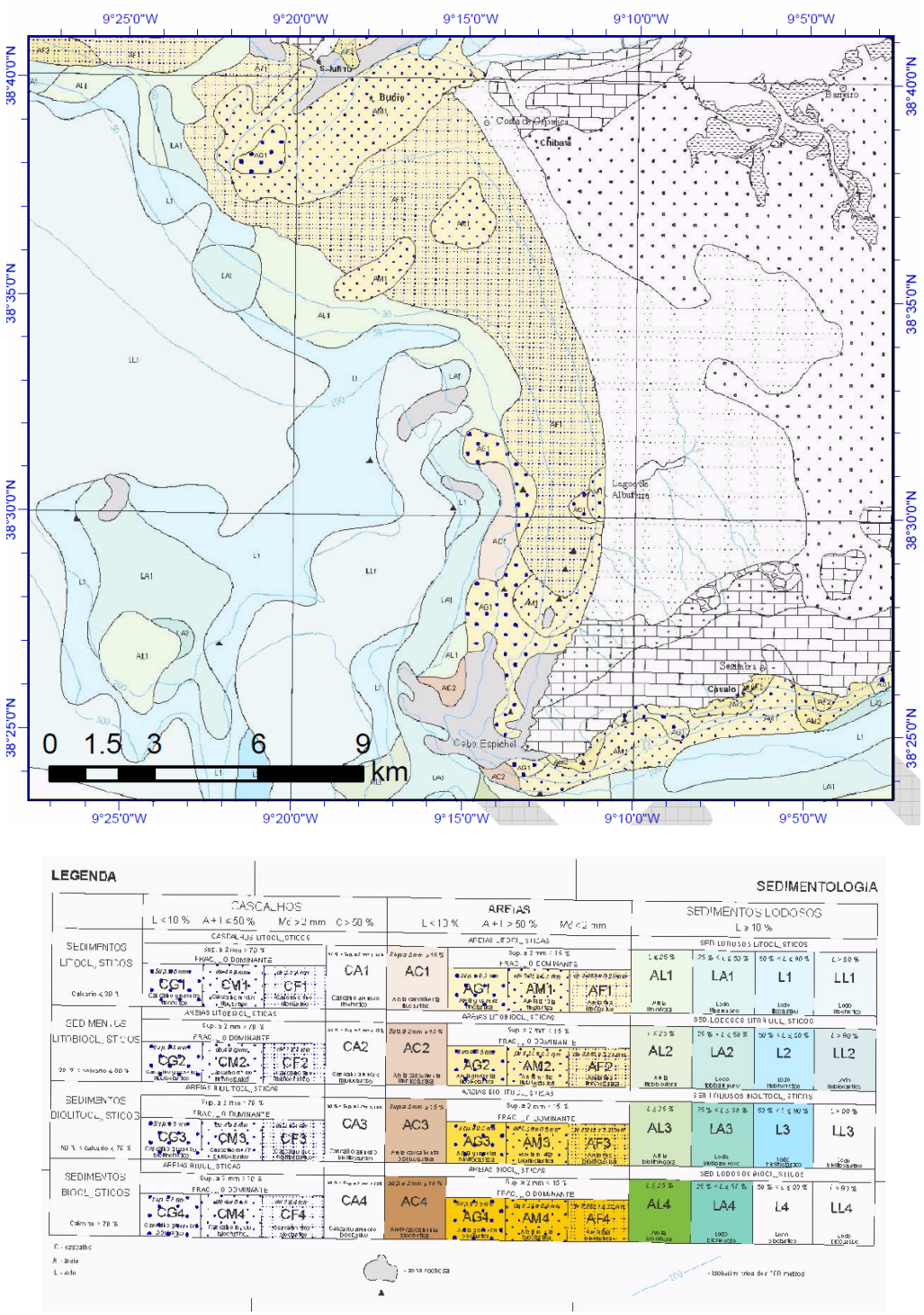

Figure 5.12 - Superficial sediment map (IH, 2005).

Both Foz and Fonte da Telha beach were ruled out for estimating $D50$ because Foz is a perched beach in the southern end of the area outside the southern cell. In the case of Fonte da Telha beach, is located in between northern and southern cell.

Estimates for h_i were therefore based on the mean grainsize for the entire beach environment using grainsize measurements from Teixeira (1990) (Table 5.4) for which the mean grainsize for the northern sub cell gives $D50 \approx 0.261$ mm, while the equivalent estimate for the southern sub cell is $D50 \approx 0.781$ mm.

Table 5.4 - Mean grainsize values for the entire beach environment (based on Teixeira, 1990)

	South cell				North cell				
	Foz	Pipa	L.Albufeira	F. Telha	Belavista	Rainha	Saude	C. Caparica	S. Joao da Caparica
Mean beach grainsize (mm)	1.110	0.916	0.647	0.414	0.304	*0.279*	0.276	0.223	0.226
Mean cell grainsize (mm)		0.781			0.261				

Estimates based on the grainsize values of the lower beach environment from Teixeira (1990) (Table 5.5) indicates that from the mean grainsize for the northern sub cell is $D50 \approx 0.252$ mm while the equivalent estimate for the southern sub cell is $D50 \approx 0.674$ mm.

Table 5.5 - Lower beach environment grainsize (based on Teixeira, 1990).

	South cell				North cell				
	Foz	Pipa	L.Albufeira	F. Telha	Belavista	Rainha	Saude	C. Caparica	S. Joao da Caparica
Grainsize (mm)	-0.110	-0.120	0.205	1.396	1.303	1.833	1.742	1.973	2.023
	-0.250	1.000	1.146	1.713	2.253	1.861	2.283	2.091	1.995
	-0.100	0.487	0.888	1.472	1.715	1.740	1.784	2.289	2.201
	-0.160	0.180	1.049	1.333	2.092	2.171	2.116	2.412	2.299
	-0.060	0.324	0.673	1.379	1.600	1.973	1.914	2.147	2.000
Mean grainsize (mm)	1.099	0.772	0.577	0.364	0.289	0.265	0.256	0.220	0.233
Mean cell grainsize (mm)		0.674			0.252				

The surficial sediment map prepared by IH (2005) characterises grainsize values as being similar in the entire all the shoreface: fine sands (class AF1) with a mean value of 0.156 mm (Table 5.6)

Table 5.6 - Grainsize values according to the superficial sediment map (based on IH, 2005).

	South cell				North cell				
	Foz	Pipa	L.Albufeira	F. Telha	Belavista	Rainha	Saude	C. Caparica	S. Joao da Caparica
Min grainsize (mm)	>0.5	0.062	0.062	0.062	0.062	0.062	0.062	0.062	0.062
Max grainsize (mm)		0.250	0.250	0.250	0.250	0.250	0.250	0.250	0.250
Mean grainsize (mm)	–	0.156		–	0.156				
Sediment type (mm)	–	AF1		–	AF1				

The values in Table 5.7 are consistent with the sediment distribution proposed by Monteiro et al. (1971) where the shoreface sediments were characterised as D < 0.125mm.

Applying Equation 4.3 using these estimates of $D50$ indicates that between $26.9 \leq h_i \leq 33.5$ m for the northern sub cell and between $15.0 \leq h_i \leq 33.5$ m for the southern sub cell (Table 5.7).

Table 5.7 - Limiting shoreface depth h_i (m) estimated from to *D*50 for each data set via Eq. 4.3.

Data from	Cell	*D50* (m)	h_i (m)
Mean grainsize (all beach)	North cell	2.61E-04	25.9
	South cell	7.81E-04	15.0
Mean grainsize (low beach)	North cell	2.52E-04	26.3
	South cell	6.74E-04	16.1
Sediment Map	North cell	1.56E-04	**33. 5**
	South cell	1.56E-04	**33. 5**

The graded shoreface, described by Johnson (1919), entails the fining of sand across the shoreface eventually passing through mud into the continental shelf (Cowell et al., 1999). It is usually associated with prograding coasts that have abundant deltaic sediment supply and that often develop strandplains during weak sea-level rise (*e.g.*, toward the end of the post glacial marine transgression), dependent on the sediment input rate over the relative sea-level change (Swift et al., 1991). As sediment is sorted by wave action over the delta, fine sediment is eroded, transported and redeposited in a series of decreasing grainsize lithofacies (Swift et al., 1991).

In the Caparica case, the sediment sorted in the delta, due to waves and tides, is transported to the adjacent shoreface by wave currents. This is entirely consistent with surficial sediment textures mapped in Figure 3.12, where the fine sediment layer fades out towards south.

Under such circumstances, the shoreface can be characterized as comprising allochthonous, fine, well-sorted sand on top of a coarser, less well-graded substrate that interpreted to be a lag deposit (Roy, 1981).

Based on the above considerations and the grain size evaluation, the shoreface sediment the Caparica cell is probably finer than the beach sediment. The grainsize difference between the beach and the

shoreface relates to the presence of local sediment sources especially in the southern cell where the mean grainsize values are significantly larger due to the proximity of a Mio-Pleistocene sea-cliff as well as a Cretaceous limestone rocky shoreline in the southern end. The coarser material also indicates that the beach has eroded into the Mio-Pleistocene cliff in the past.

With this, the shoreface sediment grainsize, based on the sediment map was used to calculate the seaward limit to significant wave effects, obtaining a value of 33.45 meters for each one of the cells.

5.4.5 Input of the Probability Density Functions

Sea-level rise

Global sea-level rise projections (e.g. IPCC, 2007; Rahmstorf, 2007) are based on averages from modelling results and data from different parts of the globe. In principle, however, sea level projections for specific regions can be improved through inclusion of localise trends in vertical movements of the land as well as regional anomalies in the global sea level projections themslelves.

The European Atlantic coast has geographically variable linear trends in mean relative relative sea levels (IPCC, 2007). For the Caparica coast, adjusted regional sea-level projections were used to define the probability density function (PDF) for sea level rise projected to2030 and to 2050, relative to the base year 2000. These regional adjustments were based on data presented by Antunes (2010) from the tide gauge at Cascais, Portugal (Fig. 5.13). These projections were also compared with Rahmstorf (2007) projections, which show strong similarity. Since there are no local projections for 2100, IPCC (2007) and Rahmstorf (2007) projections were used (Table 5.8).

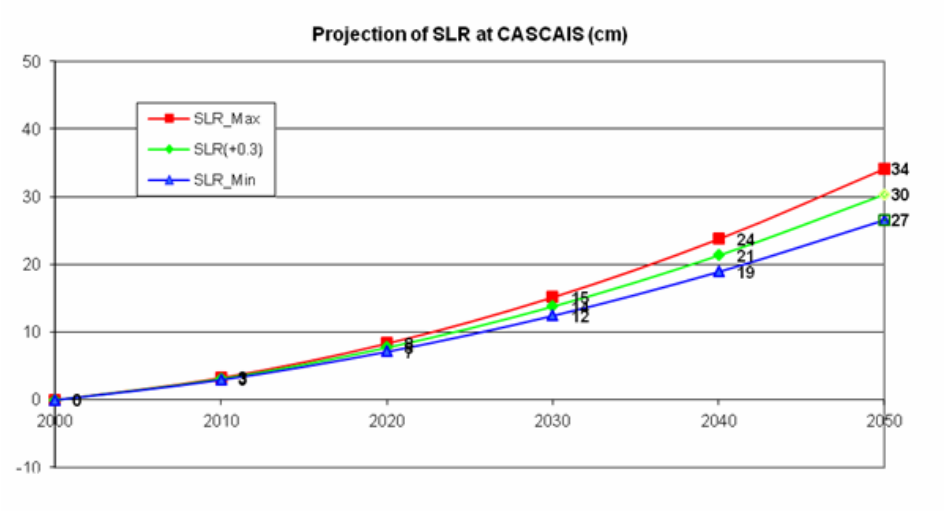

Figure 5.13 - Sea-level rise projection for Cascais based on actual values of rising speed and acceleration (adapted from Antunes, 2010).

Table 5.8 - Sea-level rise projections used to construct PDFs used to model coastal recession forecasts (*Antunes, 2010; **IPCC 2007; ***Rahmstorf 2007).

	2030	**2050**	**2100**
Min. (m)	0.125*	0.266*	0.180**
Prob. (m)	0.138*	0.304*	0.485**
Max. (m)	0.152*	0.341*	1.400***

Littoral sediment supply

The sediment balance governs coastal evolution due to net gains and losses associated with sediment sinks and sources within or connected to the coastal cell (Cowell et al., 2003a). Characterization of the sources and sinks affecting the Caparica coastal cell were examined in chapters 2 – 4 based on geological

evidence. Because of geohistorical differences between the evolution of the northern and southern sub cells documented in those chapters, estimates of sources and sinks were derived differently. For the northern sub cell, source and sink volume estimates were derived from data drawn heuristically from two different time scales; the geological time-scale (millennia) and historical time scale (centuries). For the southern sub cell, only the evidence for historical evolution was taken into consideration due to its perched nature of the coastal deposits and lack of long-term characterization data.

Estimates for rates of supply and loss to the sources and sinks for the northern sub cell were based on the dating results obtained from the prograded-barrier complex (chapter 2). These show that progradation started at 0.62±0.06ky with a roughly constant progradation rate. The estimate for rates of sediment supply was based on the volume of the present barrier and the period inferred for its accumulation.

Since the historical period is dominated by erosive events, the evidence of coastal change relates to demand on the shoreface from sand sinks. Rates estimated for sink demand in the historical evolution were derived from the comparison historical maps (1882) and aerial photographs (1958 and 2007). The sediment budget fluctuations (noise) were averaged out by comparing the 1882 historical map with the 2007 aerial photographs for a maximum erosion volume and the 1957 with the 2007 for the minimum value. The same procedure was applied to the southern sub cell. The results for both sub cells are given in Table 5.9.

Table 5.9 - Sediment supply for the modelled cells (negative supply is net loss) expressed in cubic metres per year per metre of coastline.

Cell	Sed. Supply	Min. $m^3/m/yr$	Prob. $m^3/m/yr$	Max. $m^3/m/yr$
North	Geologic	1.705	3.836	5.967
	Recent	-86.053	-64.960	-32.245
South	Recent	-4.598	-3.221	-1.844

Storm erosion demand

The storm demand is an estimated reference volume of the amount of sediment eroded from the beach and dune environment during a storm event or a series of event. Ferreira & Dias (2000) predicted the storm impacts and the consequent shoreline retreat on the oceanic northwest coast of Portugal. They characterized “mean storm” (return period of 0.7 years) and the “century storm” (return period of 100 years). Their “mean storm” predictions show beach erosion volumes between 70 and 110m^3/m without dune retreat, while the “century storm” would be expected to cause erosion volumes between 390 and 680m^3/m with dune retreat. Marcos et al. (2011) concluded, based on the outputs of a numerical barotropic regional model, that future storm demand in the Atlantic Iberian coast will be similar to that of the present, ruling out modified use of storm demand in forecasts.

In the case of the Caparica cell, the prominent headland to the north of the cell protects the coast against direct wave action for 77 percent of the time during which waves arrive from NW (Costa et al., 2001). The presence of the delta also affords semi protection due to wave refraction (Ch. 4).

The “century storm demand” was applied in simulations to forecast evolution of northern sub cell, whereas applied “mean storm demand” conditions to test modelled sensitivity of barrier progradation to variations in this parameter. The “mean storm demand” values from Ferreira & Dias (2000) were applied as reported since they do not involve dune erosion. However, the “century storm demand” was modified heuristically to account for the semi-sheltered location: a minimum value of 390m^3/m and an average value of 535m^3/m were applied.

Based on this, simulations using the STM were repeated with all the parameters fixed except for the upper shoreface and transition-zone parameters selected to examine effects varying erosion demand. To provide volume comparison, the horizontal component of beach movements, Δx_e, obtained from the STM results must be converted to aggregated dune-erosion volumes, V_e:

$$\Delta x_e = f\left(V_e\right) \tag{5.4}$$

A storm-demand transfer function was obtained from the alongshore-averaged dune profile of the northern sub cell to calculate sand volumes, V, above mean sea level for the dune as a function of the distance, x, inland from the initial location of the beach applied in the simulations:

$$V = x/0.103 \tag{5.5}$$

For the southern sub cell, storm demand was not taken into consideration due to the perched nature of the beaches and small sediment volume above sea-level. In “mean storm” conditions it is common that the coastline is located at the base of the cliff (Fig. 5.14).

Figure 5.14 - Coastline migration to the cliff toe due to storm surge.

Shoreface dilation

Despite the widespread use of simplistic assumptions based on Bruun (1962) about the response of the shoreface to sea level rise, little is really known about shoreface evolution under stable sea levels, much less under conditions of changing sea level (Cowell and Thom, 1994; Cowell et al., 2001). The shoreface may therefore serve as a sink or source for beach sand under present conditions, and neither possibility can be ruled out with rising sea level. Either of these possibilities implies that the geometry of the shoreface varies through time as it either gains or loses sand.

Evaluation of uncertainty about shoreface behaviour as either source or sink can be managed through perturbation of the shoreface parameters in the STM (Cowell et al., 1995; 2006). The possibility also exists that the lower shoreface response may be negligible on the climate change time scale which, with sea level rise would manifest as shoreface dilation as the upper shoreface and beach is translated upwards and landwards with sea level rise (Cowell et al., 2006). To account for this uncertainty in

modelling forecast for both sub cells, a probability density function for the dilation parameter was applied to allow for the possibility of full dilation ranging through to no dilation. The derived PDF was skewed toward less dilation to ensure forecasts are consistent with a risk-averse approach in relation to application of such forecasts to coastal management (the 'precautionary principle').

5.5 Risk analysis

The outcomes of the STM simulations are presented for each of the sub cells taking into account their different settings and sediment-budget indicators derived from geological evidence. The morphologic response to local and global variations of environmental conditions (climate change) and its sensitivity to effects of the potential sources and sinks that characterise each of the sub cells is compared for the three forecast periods. Sources of uncertainty identified through model calibration procedures were applied to identify the contribution of the PDF for each variable to about probabilities for coastal recession distance, R, (*i.e.*, retreat of the coast from its present location). The R probabilities were generated from Monte Carlo simulations, each run 2,000 times using independently sampled values of all parameters from their PDFs for each set of forecasts.

5.5.1 Northern sub cell

Risk forecast

Forecast simulations show a significant recession tendency for all the forecast horizons. For the 2030 and 2050 horizons, the minimum certain recession distance is 80 and 150 m respectively beyond which the probability of excedence tends do drop abruptly as recession distance increases (Fig. 5.15). For the 2100 horizon, the most probable recession distance is $R(p{=}0.5) = 215$ m, with the probability of occurrence progressively dropping to a of $R(p{\rightarrow}0) = 816$ m (Fig. 5.15). Table 5.10 lists the recession distances exceeded at four different risk thresholds.

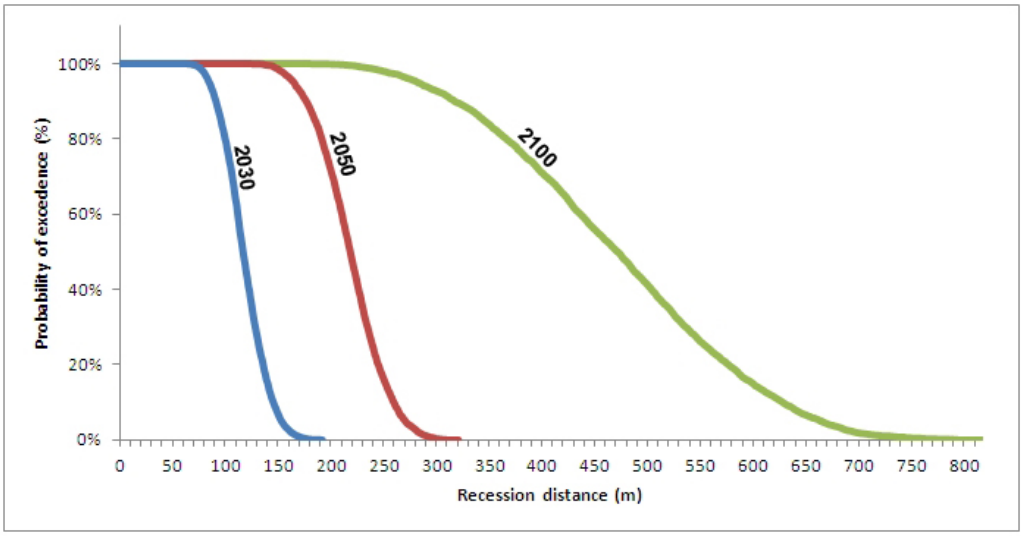

Figure 5.15 - Risk (or probability of excedence) curves for recession distance, R, forecast in the northern sub cell for 2030 (blue), 2050 (red) and 2100 (green).

Table 5.10 - Probable recession distance, $R(p)$ m, under various risk scenarios for each forecast horizon.

Risk level	2030	2050	2100
50%	117	218	472
25%	132	240	555
10%	146	260	628
0,1%	184	308	793

Uncertainty assessment

Uncertainty was assessed in relation to sensitivity of recession distance to each model parameter by replacing the PDF for one of the parameters with zero values in the simulation. This procedure was repeated for all parameters one a time to observe the change in output uncertainty, $R(p)$, due to the removal of all influence on the simulation by the given parameter. The results are shown in risk curves plotted in Figures 5.16, 5.17 and 5.18.

Sensitivity to uncertainty in future sea-level tends to increase towards 2100 with differences in $R(p)$ between the test (fixed zero sea level rise) and the standard simulations (*i.e.*, with all parameters fully stochastic) that varying between 37 and 376 m for the 2100 simulations, with the fully stochastic simulation giving larger recession distances across the full range of probabilities.

Tests reveal significantly greater sensitivity to uncertainty in sediment-supply estimates than to uncertainty in sea level rise. Differences in $R(p)$ between the test (zero sediment supply) and the standard simulations vary between 60 and 399 m across the full range of probabilities and forecast horizons. Because these differences are larger than for those of the sea level test over all time horizons, sediment supply for the Caparica cell is demonstrated to play a greater role in coastal vulnerability that sea level rise projected due to global warming.

For the case of storm demand, test simulations applied the "mean storm" conditions (most common storm events) as fixed value, rather the removing the effect by setting the parameter to zero, as applied in the preceding tests. This approach was adopted because removing storm demand completely would significantly distort shoreline behaviour. Differences between recession for this test simulation and standard simulation that included "century storm" conditions gave a decrease in $R(p)$ ranging 20 and 55 m for all forecast horizons. These differences are significantly less than for the tests on effects of either sea level rise or sediment supply.

Figures 5.16, 5.17 and 5.18 graphically compare the uncertainty related to each PDF for the three considered forecast horizons. With effects of sediment supply excluded, recession probability decreases in all cases. With "century storm" demand substituted by "mean storm" demand, the probability of recession increases significantly for all forecasts. This ranking of parameter uncertainty in the response of the northern sub cell, with sediment supply being the most relevant followed by sea-level for which

importance tends to increase for longer forecast horizons. . Sensitivity of recession to uncertainty in storm demand appears to be weak for the northern sub cell.

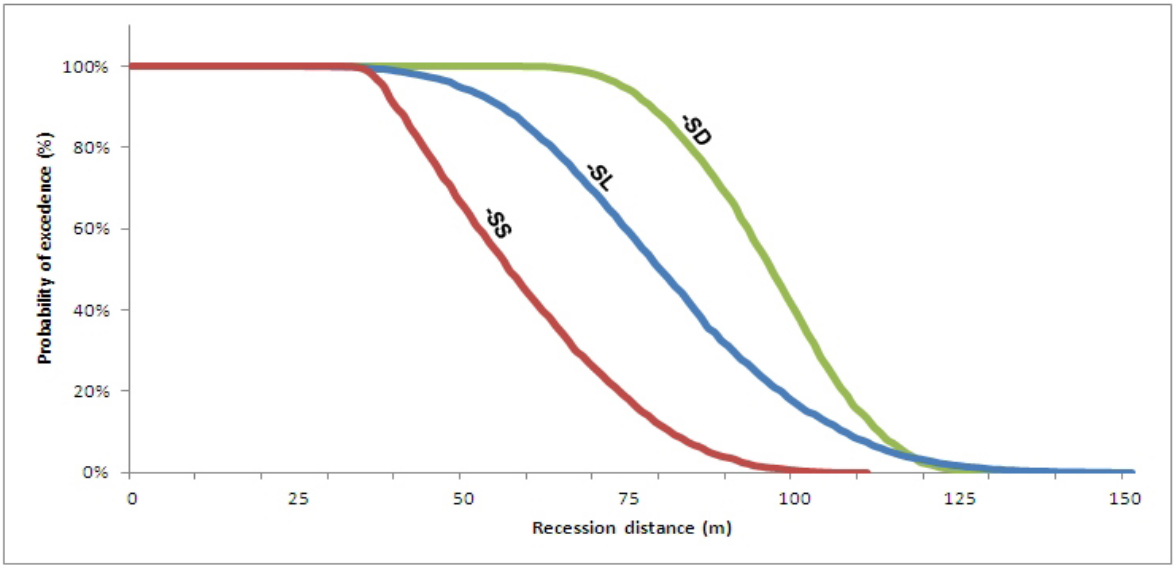

Figure 5.16 - Graphical comparison of the uncertainty related to each PDF for 2030 in the northern sub cell with the effects removed for sediment supply (red) and sea-level (blue), and with “mean storm” demand applied (green).

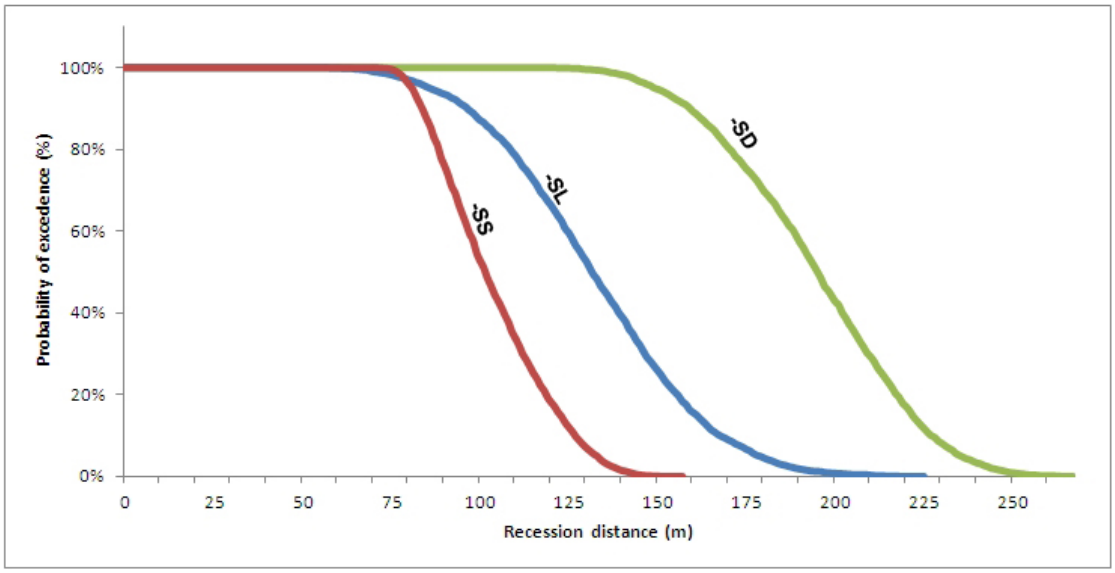

Figure 5.17 - Graphical comparison of the uncertainty related to each PDF for 2050 in the northern sub cell with effects removed for sediment supply (red) and sea-level (blue), and with "mean storm" demand applied (green).

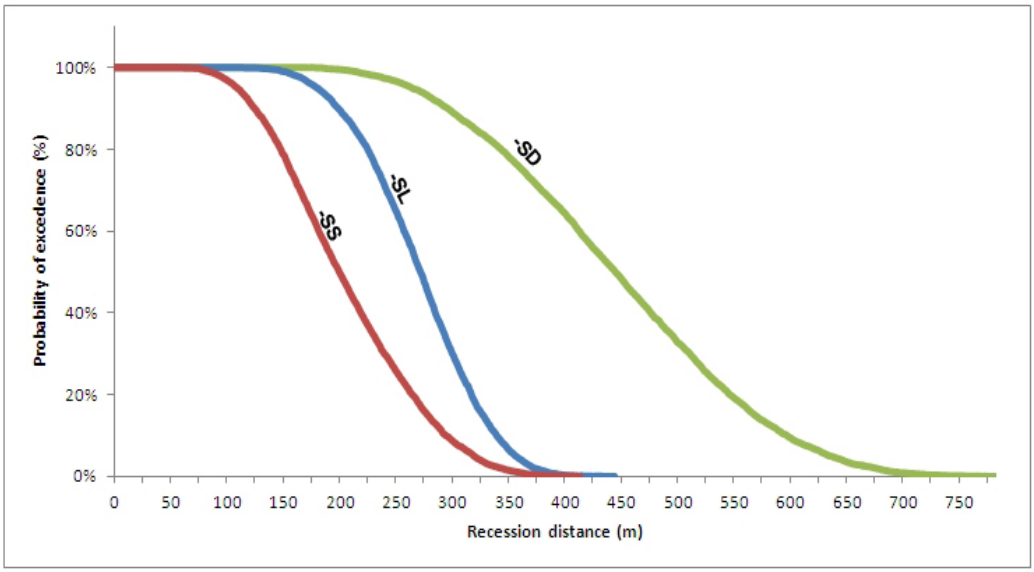

Figure 5.18 - Graphical comparison of the uncertainty related to each PDF for 2100 in the northern sub cell with effects removed for sediment supply (red) and sea-level (blue), and with "mean storm" demand applied (green).

5.5.2 Southern sub cell

Risk forecast

Forecast simulations show a recession tendency for all the forecast horizons. For 2030 and 2050, the minimum certain recession distance is 13 and 30 m beyond which the probability of excedence tends do drop abruptly as recession distance increases (Fig. 5.19). For the 2100 horizon this tendency is smoother with a maximum probable recession of 97 m (Fig. 5.19). For this forecasted horizon, a prominent drop of the probability of excedence (by about 6%) occurs at the R = 70 m which is explained by the presence of the Mio-Pleistocene sea-cliff, the inland limit of the beach environment. Model results also show a 17% probability of cliff erosion that can reach a maximum recession value of 26 m due to its friable nature and consequent vulnerability to oceanic influence. However, cliff-erosion problems are out of the scope of this study. Table 5.11 lists the recession distances exceeded at four different risk thresholds. .

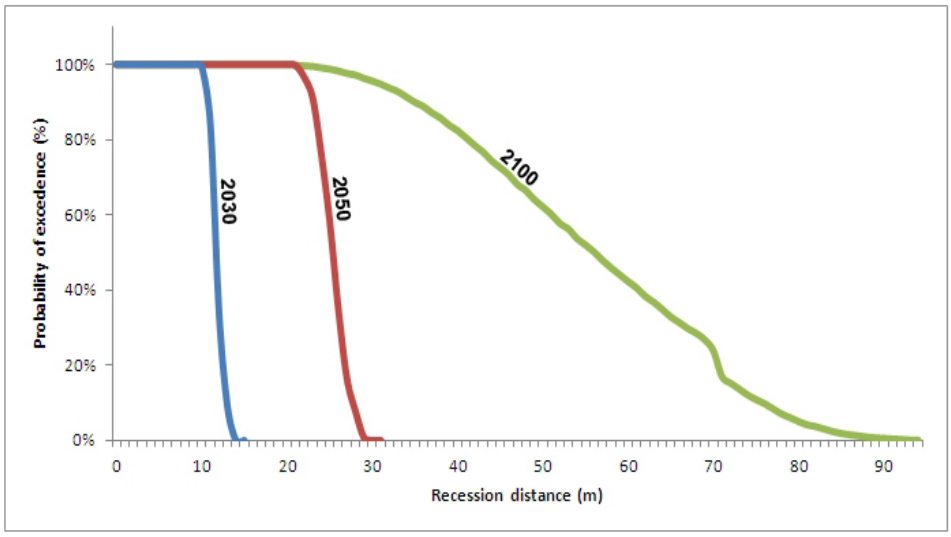

Figure 5.19 - Probability of excedence curves for recession distance, R, in the southern sub cell for 2030 (blue), 2050 (red) and 2100 (green).

Table 5.11 - Probable recession distance (m) at various risk levels for each forecast horizon.

Risk level	2030	2050	2100
50%	12	25	56
25%	12	26	69
10%	13	28	75
0,1%	14	30	98

The forecasts indicate that by 2100 recession will have caused the disappearance of the beach within the sub cell, with the cliff descending directly into the surf zone.

Uncertainty assessment

The procedures for testing sensitivity to uncertainty in some of the individual parameters documented above for the northern sub cell (Sec. 5.1.1) where also applied to forecast simulations for the southern sub cell, except for effects of storm demand which was not considered for the southern sub cell for reasons given above (Sec. 5.4.5 under 'storm erosion demand').

Sensitivity to uncertainty in future sea-level rise for the southern sub cell tends to increase through time. Differences in $R(p)$ between the test (fixed zero sea level rise) and the standard simulations (*i.e.*, with all parameters fully stochastic) very between 9 and 78 m .

Tests show that sensitivity to uncertainty in sediment supply is weak indicating that this factor has little significant influence on the morphologic evolution of the southern sub cell. Differences n $R(p)$ between the test and standard simulations vary as little as 3 and 14 m.

Figures 5.20, 5.21 and 5.22 graphically compare the uncertainty related to each PDF for the three forecast horizons. The plots demonstrate that the effect on $R(p)$ from sea level rise in forecasts is much greater than that due to sediment supply.

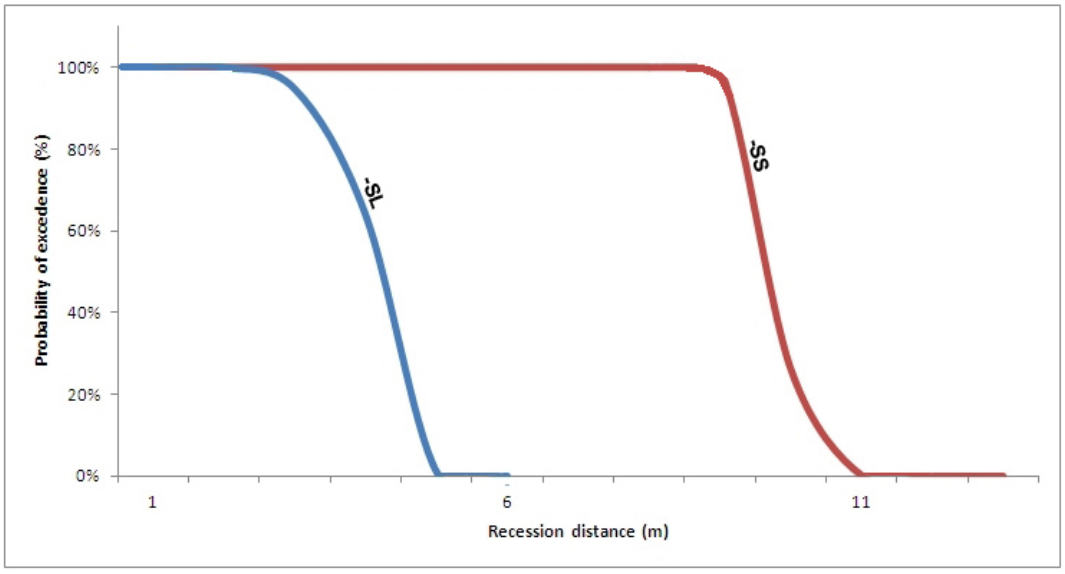

Figure 5.20 - Graphical comparison of the uncertainty related to each PDF for 2030 in the southern sub cell with effects removed separately for sea-level (blue) and sediment supply (red).

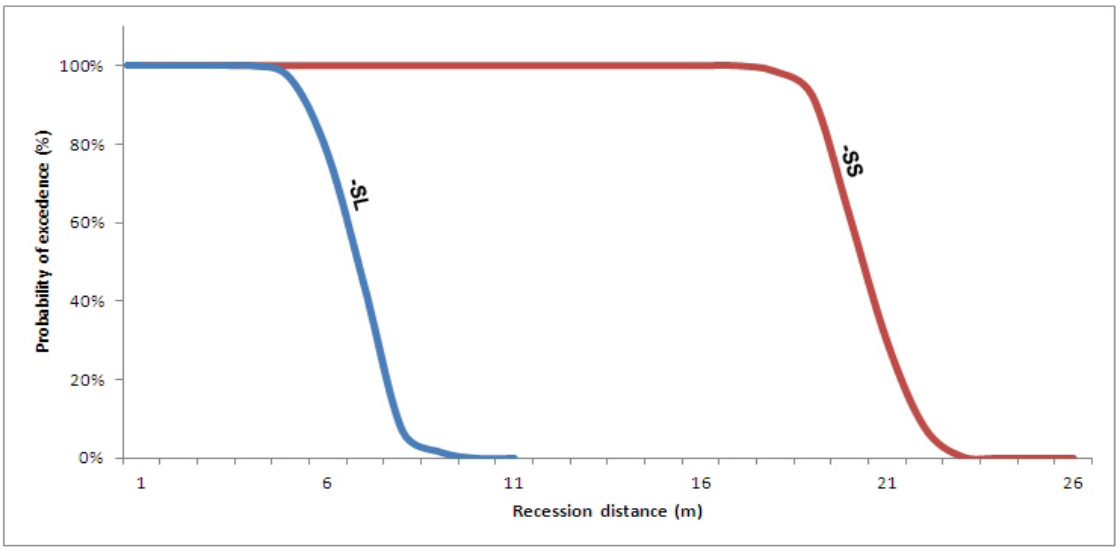

Figure 5.21 - Graphical comparison of the uncertainty related to each PDF for 2050 in the southern sub cell with effects removed separately for sea-level (blue) and sediment supply (red).

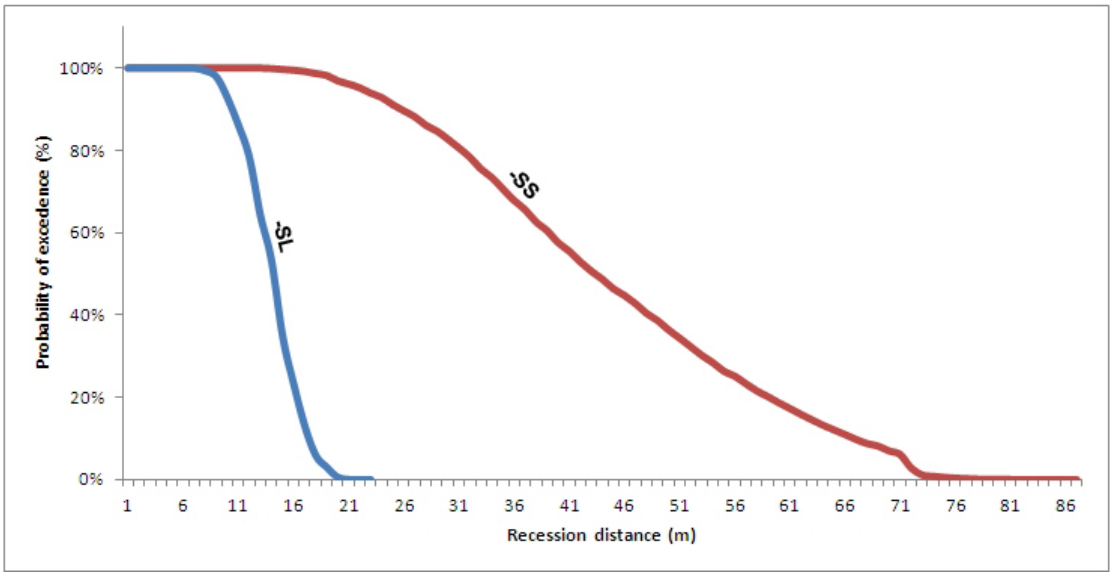

Figure 5.22 - Graphical comparison of the uncertainty related to each PDF for 2100 in the southern sub cell with effects removed separately for sea-level (blue) and sediment supply (red).

5.6 Coastline position forecast

5.6.1 Northern sub cell

The morphologic evolution of the north cell and the consequent preservation of the prograded barrier is strongly dependent on sediment supply conditions. The close proximity of the area to the main sediment regulators (the Tagus estuary and delta) makes this sub cell particularly vulnerable to changes in sediment dynamics and climatic changes. Climate change contributions are mainly driven by sea-level rise which tends to become more important for long-term forecasts while storm demand contributions do not show significant recession rates even for extreme storm conditions with longer average return intervals (ARI ≥ 100 years).

For the 2030 forecast, recession distances lead to considerable land loss and thus potential for propriety damage on the urban areas of the coast near Caparica (Fig. 5.23). The narrow width of the northern beaches and the absence of a dune system due to construction place this area within the envelope of higher level risk contours with respect to coastal recession hazard. South of the urban area recession risk contours mainly intersect the vegetated dune field where only small tourism structures are exposed to the hazard.

Figure 5.23 - Risk contours for the 2030 forecast indicating the extent of recession for different probabilities of excedence.

Recession distances tend to increase in the 2050 forecast increasing land loss and property vulnerability within the urban areas. Property assets in the northern area once again full within the contour envelope that includes high risk of recession, while in the south risk contours span the dune field, thus limiting exposure of property to the recession hazard (Fig. 5.24).

Figure 5.24 - Risk contours for the 2050 forecast indicating the extent of recession for different probabilities of excedence.

Significant changes in risk contours are evident for the 2100 forecast, with a growth in uncertainty about recession distances evident in the spreading of successive risk contours (Fig. 5.25). For this forecast, the risk envelope spans most of the urbanized areas, for which exposure to recession occurs with probabilities between 50% and 10%. The 0.1% probability of recession hazard affects most of the prograded barrier area extending approximately to the cliff (blue line in Fig. 5.25).

Figure 5.25 - Risk contours for the 2100 forecast indicating the extent of recession for different probabilities of excedence.

The risk contours mapped in the above diagrams do not consider mitigation procedures that may reduce recession rates. Artificial nourishment and/or sea-walls, similar to the ones that already exist near the urbanized areas of the northern sub cell (Fig. 5.26), may reduce recession rates and in some cases preserve coastline position. Recent artificial nourishments performed in the north area of the cell using 1 million m^3/yr (André et al., 2010) have been insufficient to stem existing retreat rates (Ch. 1).

Figure 5.26 - Sea-wall structure composed by loose rocks in the northern part of the northern sub cell, constructed under emergency conditions when severe storms threatened urbanized areas in 2007.

Based on the evolutionary characterization undertaken in this study, the sediment retention capacity of the northern sub cell is mostly dependent on the accommodation space available in the nearby sedimentary sinks and the transport pathways connecting these to the sub cell. The sand-spit erosion at the northern end of the sub cell enhanced sediment transport towards the Tagus estuary (chapter 2).

5.6.2 Southern sub cell

The morphologic evolution of the southern sub cell is characterized by greater stability than the northern sub cell. This sub cell is less affected by sediment supply uncertainty due to its distance from, and lack of direct connection to the Tagus delta, responsible for the majority of instability in the Caparica cell. Besides the markedly steeper shoreface of southern sub cell compared to the northern sub cell, and the narrow continental-shelf platform, sediment becomes entrapped in narrow reflective beaches that prevent permanent losses to the Lisbon canyon. Climate change contributions are mainly

related to sea-level variations that will probably become more relevant through time and which may produce recession that results in complete loss of the local beaches.

For the 2030 and 2050 forecasts, likely recession distances are comparable to erosion distances that occur during storm events. However, for the 2100 forecast, recession distances may become large enough in some areas to place the coastline directly against the base of the cliff causing the disappearance of the beach (Fig. 5.27). Some small, isolated perched beaches may persist, similar to the ones that can already be seen in the southern end of the southern sub cell, near Espichel headland.

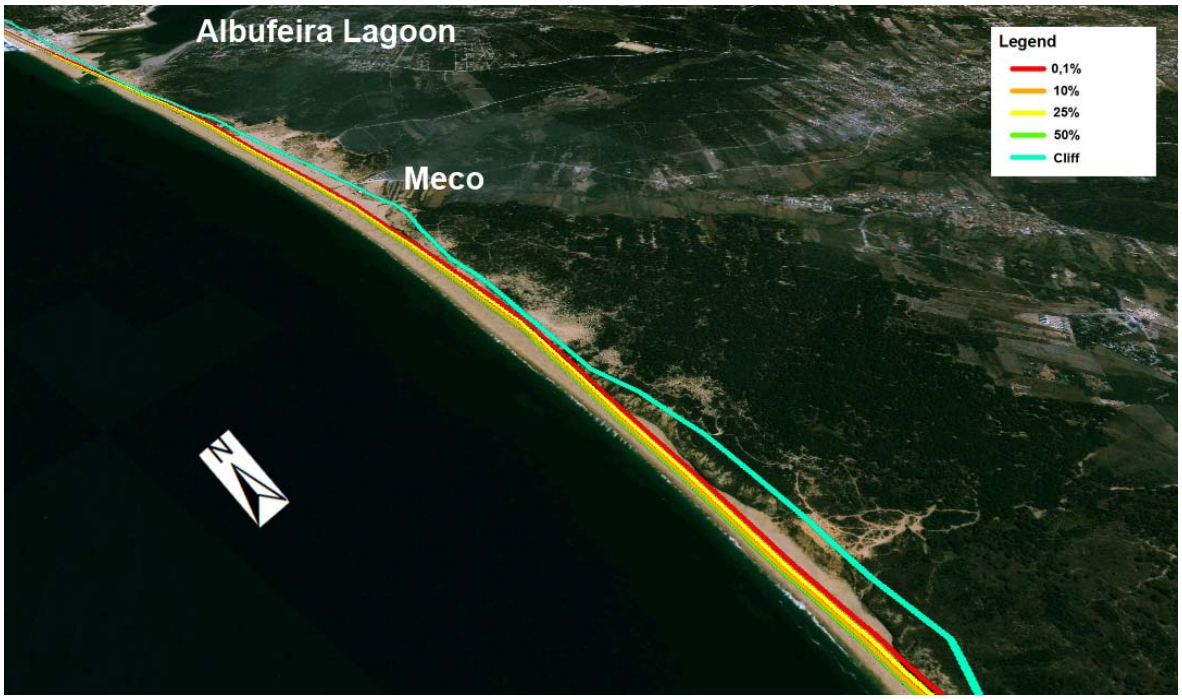

Figure 5.27 - Risk contours for the 2100 forecast indicating the extent of recession for different probabilities of excedence.

Despite not having significant erosion problems related to a negative sediment supply, the southern sub cell is vulnerable to changes on climatic conditions. The association of sea-level rise and more frequent storms may cause a permanent recession sooner than 2100. Coastal protection through engineering

procedures is improbable as the cliff impedes further significant recession and no urban areas are directly affected. The Albufeira Lagoon area is the only low relief zone of the south cell. However, its morphology will probably be maintained through barrier rollover (Leatherman, 1983) that causes the lagoon inlet and associated beach to recede.

5.7 Conclusions

It can be concluded from the modelled forecasts that the presence of the delta and associated estuary tends to make sediment exchanges between the delta and adjacent coast a destabilising factor in morphological change that may cause comparable or greater recession than sea level rise projected due to global warming? This proposition however is confirmed only for the northern sub cell which connected directly to (and is part of) the Tagus delta. The sediment budget in the southern sub cell is on weakly linked to the delta, so that the proposition is unlikely to hold for this sub cell: sea level rise creates a much higher probability of coastal recession exceeding a given magnitude than the corresponding effects of negative anomalies in sediment supply in the southern sub cell.

Forecast magnitudes of coastal recession increases with time horizon throughout the Caparica cell, as does the uncertainty about these magnitudes, although both are an order of magnitude greater in the northern and sub cell than for the southern sub cell. Recession distances of hundreds of metres are indicated in forecasts for the northern sub cell with probabilities of excedence of 50% or less for all forecast horizons, whereas recession forecasts for the southern sub cell are limited to tens of metres for the correspond levels of risk and projected date.

Forecast recession indicate permanent land and property loss in part of northern sub cell, but in other parts the designation of coastal dunes as reserve lands means the forecast recession hazard will probably cause loss of land but not developed property assets. However, there is a significant risk that beach will be lost due to recession of the coast to the paleo cliff line in the southern sub cell.

In complex morphologic settings the management of uncertainty becomes fundamental to understand the key drivers in coastal evolution. Geomorphic variability due to sea-level variations is significantly

affected by shoreface behaviour. However, other factors as variations in storm demand and sediment supply conditions can overcome sea-level importance on morphologic evolution.

CHAPTER 6

Conclusions

Photo: Artificial groin at Caparica

The results of this study demonstrate that the Caparica coastal cell, located adjacent to the Tagus delta, turns out to be an even better natural laboratory to address the overarching aim of the thesis than first thought. The research showed the cell is naturally split into two sub cells:

(1) the proximal adjacent-coast that forms part of the delta itself, the delta margin, intimately sharing sediments with the ebb- and flood-tidal deposits, with the morphology responding accordingly; and

(2) the distal adjacent-coast that is not part of the delta, and has a negligible sediment-sharing relationship with the delta.

The results of the investigation on relationships between a delta and its adjacent coast support the fundamental conclusion that,

(a) the morphology and stability of the proximal adjacent-coast is governed by its direct, coupled sediment exchanges with the delta, because of which its shoreline geometry is paradoxically out of alignment with the delta morphology; whereas

(b) the sediment budget and associated morphological responses of the distal adjacent-coast are largely independent of the delta, but the shoreline of the distal adjacent-coast is well aligned with and controlled by the delta morphology, not through sediment exchanges (because there are none), but through effects of the deltaic bathymetry on refraction patterns in the dominant swell wave field.

This overarching conclusion has as its corollary the conclusion that the effects of projected sea level rise due to global warming are completely different for the proximal and distal adjacent-coast:

(c) effects of sediment exchanges with the delta on future morphological change for the proximal adjacent-coast seem likely to dominate over the direct effects of sea level rise on the morphology of the proximal-adjacent coast; whereas

(d) effects of sea level rise will likely be the dominant factor governing morphological change in coming decades on the distal adjacent-coast.

The relationships between the Caparica coastal cell and the adjacent Tagus delta and estuary not only hold in modelled future change (Chapter 5), they are also apparent in past coastal behaviour reconstructed from geohistorical evidence (Chapters 2- 4) from coastal evolution since the end of the Holocene after local sea-level stabilization (<7ky BP). Chronologic information for existing cliff-top dunes (1190 BP) indicates that the recent development of a prograded barrier complex in the northern sub cell is not coeval with deltaic evolution driven by sea-level variations. This evidence made it possible to rule out sea level as the main agent for local coastal evolution, thus advancing sediment supply as responsible for significant coastline migrations in stable sea-level conditions.

The northern sub cell has had an unstable coastline, since the onset of the Holocene stillstand, currently comprising a well-developed, prograded barrier with a recent evolution (<1.19 ky BP). The geological evidence indicates that this proximal-adjacent coast has always been strongly dependent on the deltaic supply of sediment (both positive and negative supply).

The southern sub cell has a stable coastline comprising a mainland beach encroaching up the base of a sea-cliff. This distal adjacent-coast may have received a net alongshore sand supply from the delta early in the stillstand, but not now and probably not during the past millennium based on evidence inferred from remnant cliff-top dunes about the formation and destruction of their climbing dune counterparts (Chapter 4). It is also possible that this distal adjacent-coast never received a significant alonghore supply of sand from the delta during the stillstand nor in the later stages of the marine transgression. Rather, it is just as possible that the sub cell

inherited its sand from the narrow continental shelf that fronts it, through the eastward migration of a transgressive barrier that eventually encroached upon the cliffs, as sea level approached its present elevation, to form the mainland beach evident at present.

Both the sub cells comprising the proximal and distal adjacent-coast are morphologically sensitive to changes in wave direction that in turn is partly subject to significant deltaic influence. This influence is exerted through the effects on wave refraction over the bathymetry of the delta lobe (Chapter 4). Clockwise wave rotation due to climatic variations tends to increase coastline instability and consequent vulnerability enhancing erosion rates in both sub cells, but the instability effect has been enhanced in the northern sub cell by the non-return valve created in littoral transport sediment exchanges with the estuary. The creation of such a valve is in principle consistent with the generation of a large volume of additional accommodation available for sand deposition due to dredging undertaken for port development (Chapter 2 and 4). Risk based forecast modelling for each cell indicates that for the area directly affected by deltaic influence (the northern sub cell) recession distance is fundamentally dependent on sediment supply conditions capable of changing shoreface geometry and consequently coastline position. In this case, climatic variations have a secondary importance on morphologic behaviour with a smaller contribution to coastal vulnerability. However, modelled sea level rise exerts a strong effect in forecasts for 2100 because of the increased magnitude of sea level rise projected for then.

List of references

Aagaard, T., Masselink, G. (1999). *The Surf Zone*. Handbook of Beach and Shoreface Morphodynamics. A. D. Short. Chichester, Wiley: 72-118.

Adlam, K. (2008) *Shoreface Dilation in Response to Sea Level Rise – Tiber Delta Reference Site*. BSc (Honours), The University of Sydney, Sydney. 99 pp.

André, J. N., Cordeiro, M. F. N. (2010) *Human interventions responsible for the coastal destabilization Cova do Vapor-Coast Caparica coastal reach*. Proceedings do V Congresso Nacional de Geomorfologia. Porto 305-310. ISBN: 978-989-96462-2-3.

Andrade, C., Pires, H. O., Taborda, R., Freiras, C. (2007). *Projecting future changes in wave climate and coastal response in Portugal by the end of the 21st century*. Journal of Coastal Research(SI 50): 253-257.

Antunes, C. (2010) *Monitorização da variação do nível médio do mar*. 1as Jornadas de Engenharia Hidrográfica. Lisboa.

Ashton, A. D., Giosan, L. (2011). *Wave-angle control of delta evolution*. Geophys. Res. Lett. 38(13): L13405.

Azevedo, M. T. (1983). *O Sinclinal de Albufeira - Evolução Pós-Miocénica E Reconstituição Paleogeográfica*. PhD, Universidade de Lisboa.

Bristow, C. S., Pucillo K. (2006). *Quantifying rates of coastal progradation from sediment volume using GPR and OSL: the Holocene fill of Guichen Bay, south-east South Australia.* Sedimentology 53(4): 769-788.

Bruun, P. (1962) *Sea level rise as a cause of shore erosion*. *Journal of Waterways and Harbors Division*, ASCE, 88, 117-130.

Buynevich, I., Bitinas, A., Pupienis, D. (2007). *Reactivation of Coastal Dunes Documented by Subsurface Imaging of the Great Dune Ridge, Lithuania*. Journal of Coastal Research SI 50: 226 - 230.

Cabral, J., Dias, R. P. Brum, A. (1984). *Estudo das falhas afectando formações Plio-Quaternárias na zona da Fonte da Telha (Península de Setúbal)*. Comunicações dos Serviços Geológicos de Portugal 70(1): 83-91.

Capobianco, M., De Vriend, H. J., Nicholls, R. J., Stive, M. J. F. (1999) *Coastal area impact and vulnerability assessment: The point of view of a morphodynamic modeller*. Journal of Coastal Research, 15, 701-716.

Carter, R. W. G. Woodroffe, C.D. (1997). *Coastal evolution: An introduction*. Coastal evolution - Late Quaternary shoreline morphodynamics. R. W. G. W. Carter, C.D., Cambridge University Press: 1-31.

Church, J.A., White, N.J., Hunter, J.R., McInnes, K.L, Cowell, P.J., O'Farrell, S.P. (2008). *Sea-level rise and the vulnerability of coastal environments*. Newton, P.W. (ed.), Transitions: Pathways Towards Sustainable Urban Development in Australia. CSIRO Publishing, Melbourne, 191-209.

Clark, J. A., Farrell, W. E., Peltier, W. R. (1978). "Global changes in postglacial sea level: A numerical calculation." Quaternary Research 9(3): 265-287.

Costa, M., Silva, R., Vitorino, J. (2001). *Contribuição para o estudo do clima de agitação marítima na costa portuguesa.* 2ª Jornadas portuguesas de engenharia costeira e portuária. Sines, Associação Internacional de Navegação.

Costapolis (2005). *Estudo de Impacte Ambiental do Projecto dos Novos Parques de Campismo da Área de Intervenção do Programa Polis da Costa de Caparica*. Environmental Resources Management - ERM.

Costas, S., Brito, P., Ferraz, M., González-Villanueva, R., Novo, A., Rebêlo, L. (2010). *The cliff-top dune of Costa da Caparica: Possible scenarios of formation and evolution*. Coastal Hope 2010, Lisbon, Faculdade de Ciências, Universidade de Lisboa.

Costas, S., Jerez, S., Trigo, R. M., Goble, R., Rebêlo, L. (2012). *Sand invasion along the Portuguese coast forced by westerly shifts during cold climate events*. Quaternary Science Reviews 42(0): 15-28.

Cowell, P. J., Thom, B.G. (1994*). Morphodynamics of coastal evolution.* Coastal Evolution: Late quaternary shoreline morphodynamics. R. W. G. Carter & C. D. Woodrofee., Cambridge University Press: 33-86.

Cowell, P. J., Roy, P. S., Jones, R. A. (1995) *Simulation of large-scale coastal change using a morphological behavior model*. Marine Geology, 126, 45-61.

Cowell, P. J., Hanslow, D. J., Meleo, J. F. (1999). The shoreface. Hanbook of beach and shoreface morphodynamics A. D. Short. New York, Wiley: 37-71.

Cowell, P. J., Stive, M. J. F., Roy, P. S., Kaminsky, G. M., Buijsman, M. C., Thom, B. G., Wright, L. D. (2001) *Shoreface sand supply to beaches*. Proceedings 27th International Coastal Engineering Conference, 2495-2508.

Cowell, P. J. (2002). *Columbia-River cell coastal erosion project: Limits to knowledge*. USGS open-file report. USGS: 278-296.

Cowell, P. J., Stive, M.J.F., Niedoroda, A.W., De Vriend, H.J. Swift, D.J.P., Kaminsky, G.M., and Capobianco, M. (2003a). *The coastal tract (Part 1): A conceptual approach to aggregated modelling of low-order coastal change*. Journal of Coastal Research 19(4): 812-827.

Cowell, P. J., Stive, M.J.F., Niedoroda, A.W., Swift, D.J.P., De Vriend, H.J., Buijsman, M.C., Reed, C.W., De Boer, P.L. (2003b). *The coastal tract (part 2): applications of aggregated modelling of low-order coastal change*. Journal of Coastal Research 19(4): 828-848.

Cowell, P. J., Thorn, B.G., Jones, R.A., Everts, C.H., Simanovic, D. (2006). *Management of Uncertainty in Predicting Climate-Change Impacts on Beaches*. Journal of Coastal Research 22(1): 232-245.

Daley, M. (2005) *Effects of rock truncation on shoreface profile geometry*. BSc (Honours), The University of Sydney, Sydney. 121 pp.

Davis, R. A., Hayes, M.O. (1984). *What is a wave-dominated coast?* Marine Geology 60(1–4): 313-329.

Dias, J. M. A., Boski, T., Rodrigues, A., Magalhães, F. (2000). *Coast line evolution in Portugal since the Last Glacial Maximum until present - a synthesis*. Marine Geology 170(1-2): 177-186.

Dodet, G., Bertin, X.,Taborda, R. (2010). *Wave climate variability in the North-East Atlantic Ocean over the last six decades.* Ocean Modelling 31(3–4): 120-131.

Emery, D., Myers, K. (1996). Sequence Stratigraphy, Blackwell Science.

Ferraz, M., Cowell, P., Rebêlo, L. (2011). *Coastal-change estimates inferred from remnant cliff-top dunes*. Journal of Coastal Research 1(64): 661-665.

Ferreira, Ó., Dias, J.A. (2000). *Prediction of storm impacts and shoreline retreat induced by hypothetical storms on open coastlines*. *In:* G. R. Rodríguez, C. A. Brebbia e E. Pérez-Martell (eds), *Environmental Coastal Regions* III, p.137-147, WIT Press - Wessex Institute of Technology. ISBN: 1853128279.

Figueiredo, S. (2010). *External Forcing and Internal Controls on Coastal Response to Climate Change at Rio Grande do Sul, Southern Brazil*. PhD. The University of Sydney, Sydney. 136 pp.

Fisher, J. J., Simpson, E.J. (1979). *Washover and tidal sedimentation rates as environmental factors in development of a transgressive barrier shoreline*. Barrier Islands from the Gulf of St. Lawrence to Gulf of Mexico. S. P. Leatherman. New York, Academic Press.

Fitzgerald, D. (1996). *Geomorphic Variability and Morphologic and Sedimentologic Controls on Tidal Inlets*. Journal of Coastal Research(SI 23): 47-71.

Fleming, K., Johnston, P., Zwartz, D., Yokoyama, Y., Lambeck, K., Chappell, J. (1998). *Refining the eustatic sea-level curve since the Last Glacial Maximum using far- and intermediate-field sites*. Earth and Planetary Science Letters 163(1–4): 327-342.

Folk R.L., Ward. W. C. (1957). *Brazos river bar : a study of significante of grain size parameters*. Journal of Sedimentary Petrology 27: 3-26.

Fortunato, A. B., Oliveira, A., Baptista, A.M. (1999). *On the effect of tidal flats on the hydrodynamics of the Tagus estuary*. Oceanologica Acta 22(1): 31-44.

Fox, T. (1978). *Modeling Coastal Environments*. Coastal Sedimentary Environments. A. Davis (ed) Springer: ch 1. 385-413.

Freire, P. (1993). *Caracterização e dinâmica de sedimentos em sistemas de canais do estuário do Tejo cala do Norte (Portugal)*. MSc. Universidade de Lisboa.

Freire, P. (1999). *Evolução morfo-sedimentar de margens estuarinas (Estuário do Tejo - Portugal).*PhD. Universidade de Lisboa.

Freitas, M. C. (1995). *A Laguna de Albufeira (Península de Setúbal). Sedimentologia, morfologia e morfodinâmica.* PhD. Universidade de Lisboa.

Freitas, C., Ferreira, T. (2004). *Geologia*. Lagoa de Albufeira. Instituto da Conservação da Natureza - Centro de Zonas Húmidas: 11-52.

Goodwin, I.D, Stables, M.A., Olley, J.M. (2006). *Wave climate, sand budget and shoreline alignment evolution of the Iluka–Woody Bay sand barrier, northern New South Wales, Australia, since 3000 yr BP*. Marine Geology, 226, 127-144.

Goy, J. L., Zazo, C., Dabrio, C. J., Lario, J., Borja, F., Sierro, F. J., Flores, J. A. (1996). *Global and regional factors controlling changes of coastlines in Southern Iberia (Spain) during the holocene*. Quaternary Science Reviews 15(8-9): 773-780.

Goy, J. L., Zazo, C., Dabrio, C. J. (2003). *A beach-ridge progradation complex reflecting periodical sea-level and climate variability during the Holocene (Gulf of Almería, Western Mediterranean)*. Geomorphology 50(1-3): 251-268.

Guerra, S., Pires, H. O., Taborda, R. P. (2000). *Mean sea-level, North Atlantic Oscillation and climate variability in Portugal*. 3rd Symposium on the Iberian Atlantic Margin, Faro.

Hallermeier, R. J. (1981). *A profile zonation for seasonal sand beaches from wave climate*. Coastal Engineering 4(0): 253-277.

Haslett, S. K., Davies, P., Curr, R. H. F. (2000). *Geomorphologic and paleoenvironmental development of Holocene perched coastal dune systems in Brittany, France*. Geogr. Ann. 82A(1): 79-88.

Hayes, M. O. (1979). *Barrier island morphology as a function of tidal ad wave regime*. Barrier Islands from the Gulf of St. Lawrence to the Gulf of Mexico. S. P. Leatherman. New York, Academic Press: 1-27.

Hayes, M. O. (1980). *General morphology and sediment patterns in tidal inlets*. Sedimentary Geology 26: 139-156.

Hesp, P., Thom, B. (1990). *Geomorphology and evolution of erosional dunefields*. Coastal Dunes: processes and morphology. K. F. Nordstrom, N. P. Psutty, R. W. G. Carter. Chichester, J. Wiley & Sons: 253-288.

Hesp, P., Short, A.D. (1999). *Barrier Morphodynamics.* Handbook of Beach and Shoreface Morphodynamics. A. D. Short. New York, Wiley: 307-333.

Hicks, D. M., Hume, T. M. (1996). *Morphology and Size of Ebb Tidal Deltas at Natural Inlets on Open-sea and Pocket-bay Coasts, North Island, New Zealand*. Journal of Coastal Research 12(1): 47-63.

Hidroprojecto (2001). *Equilibrio hidrodinâmico das barras do Tejo. Estudo prévio*. Hidroprojecto S.A. TomoI/II.

Hsu, J. R. C., Evans, C. (1989). *Parabolic bay shapes and applications*. Proceedings of the Institution of Civil Engineers London, Thomas Telford Ltd.

Hsu, J. R. C., Yu, M. J., Lee, F. C., Benedet, L. (2010). *Static bay beach concept for scientists and engineers: A review*. Coastal Engineering 57(2): 76-91.

Hunt, J. C. R., Richards, K. J., Brighton, P. W. M. (1988). *Stably stratified shear flow over low hills*. *Q. J. R. Meteorol. Soc.* (114): 859-886.

IH (2005). *Carta SED5, Cabo da Roca ao Cabo de Sines. Folha 5. Sedimentos Superficiais da Plataforma Continental*. Maria Manuela Matos. Lisboa, Marinha - Instituto Hidrográfico.

Jennings, J.N. (1967). *Cliff-top dunes*. Australian Geographical Studies, 5: 40-49.

Jiménez, J. A., Arcilla, A.S., Valdemoro, H. I., Gracia, V., Nieto, F. (1997). *Processes reshaping the Ebro delta*. Marine Geology 144: 59-79.

Johnson, D. W. (1919) *Shore processes and shoreline development*. Wiley. New York. 584p.

Kinsela, M. A. (2007). *Topographic control of dune response to climate-change impacts*. BSc (Honours), University of Sydney.

Klein, A. H. F., Vargas, A., Raabe, A. L. A., Hsu, J. R. C. (2003). *Visual assessment of bayed beach stability with computer software*. Computers & Geosciences 29(10): 1249-1257.

Komar, P.D. (1973). *Computer models for delta growth due to sediment input from rivers and longshore transport*. Geological Society of America Bulletin, 84, 2217-26.

Komar, P. D. (1976). Beach processes and sedimentation. New Jersey, Prentice Hall.

Lausman, R., Klein, A. H. F., Stive, M. J. F. (2010)a. *Uncertainty in the application of the Parabolic Bay Shape Equation: Part 1*. Coastal Engineering 57(2): 132-141.

Lausman, R., Klein, A. H. F., Stive, M. J. F. (2010)b. *Uncertainty in the application of the parabolic bay shape equation: Part 2*. Coastal Engineering 57(2): 142-151.

Leatherman, S. P. (1983) *Barrier Dynamics and Landward Migration With Holocene Sea-Level Rise*. Nature, 301, 415-417.

Leatherman, S. P. (2003). *Shoreline Change Mapping and Management Along the U.S. East Coast*. Journal of Coastal Research. Shoreline Mapping and Change Analysis: Technical Considerations and Management Implications(SI 38): 5-13.

Lippman, T. C., Holman, R.A. (1990). *The spatial and temporal variability of sand bar morphology*. *Journal of Geophysical Research* 95: 1575-1590.

Liu, X., Dong, Z., Wang, X. (2006). *Wind tunnel modeling and measurements of the flux of wind-blown sand.* Journal of Arid Environments(66): 657–672.

Marcos, M., Jordà, G., Gomis, D., Pérez, B. (2011). *Changes in storm surges in southern Europe from a regional model under climate change scenarios*. Global and Planetary Change 77: 116-128.

Manuppella, G., Antunes, M.T., Pais, J., Ramalho, M.M., Rey, J. (1999). *Notícia explicativa da Folha 38-B (Setúbal) – Carta Geológica de Portugal à escala 1:50.000*. Instituto Geológico e Mineiro, Departamento de Geologia, Lisboa, 143 p.

Monteiro, Moita (1971). *Morfologia e sedimentos da plataforma continental e vertente superior ao largo da Península de Setúbal*. 1º Congresso Luso Hispânico de Geologia Económico. Madrid/Lisboa.

Morton, R. A., Speed, F.M. (1998). *Evaluation of Shorelines and Legal Boundaries Controlled by Water Levels on Sandy Beaches*. Journal of Coastal Research 14(4): 1373-1384.

Nabais, A. (2009). *Barcos do Tejo*. AÇFA online 2.

Nicholls, R.J., P.P. Wong, V.R. Burkett, J.O. Codignotto, J.E. Hay, R.F. McLean, S. Ragoonaden, C.D. Woodroffe, (2007). *Coastal systems and low-lying areas*. Climate Change 2007: Impacts, Adaptation and Vulnerability. Contribution of Working Group II to the Fourth Assessment Report of the Intergovernmental Panel on Climate Change, M.L. Parry, O.F. Canziani, J.P. Palutikof, P.J. van der Linden and C.E. Hanson, Eds., Cambridge University Press, Cambridge, UK, 315-356.

Oertel, G. F., Henry, V.J., Foyle, A.M. (1991). *Implications of tide-dominated lagoonal processes on the preservation of buried channels on a sediment-starved continental shelf*. Shelf and sandstone bodies. Geometry, facies and sequence stratigraphy. D. J. P. Swift, Oertel, G. F., Tilman, R. W., Thorne, J. A., Blackwell scientific publications: 379-394.

Pais, J., Moniz, C., Cabral, J., Cardoso, J. L., Legoinha, P., Machado, S., Morais, M. A., Lourenco, C., Ribeiro, M. L., Henriques, P., Falé, P. (2006). *Notícia Explicativa da Folha 34-D Lisboa*. Carta Geológica de Portugal. INETI. Lisboa, Ministério da Economia.

Pajak, M. J., Leatherman, S. (2002). *The High Water Line as Shoreline Indicator*. Journal of Coastal Research 18(2): 329-337.

Peltier, W. R. and Fairbanks, R. G. (2006). *Global glacial ice volume and Last Glacial Maximum duration from an extended Barbados sea level record*. Quaternary Science Reviews 25(23-24): 3322-3337.

Pimenta, J., Calado, M., Leitão, M. (2005). *Novos dados sobre a ocupação pré-romana da cidade de Lisboa: as ânforas da sondagem n.º 2 da Rua de São João da Praça*. Revista Portuguesa de Arqueologia 8(2): 313-334.

Pye, K., Bowman, G. M. (1984). *The Holocene marine transgression as a forcing function in episodic dune activity on the Eastern Australian Coast*. Coastal Geomorphology in Australia. B. G. Thom, Academic Press: 179-196.

Pye, K., Tsoar,H. (2009). Aeolian Sand and Sand Dunes. Berlin, Springer.

Rahmstorf, S. (2007). *A semi-empirical approach to projecting future sea-level rise*. Science, 315, 368-370.

Roy, P. S., Thom, B. G. (1981). *Late Quaternary marine deposition in New South Wales and southern Queensland - An evolutionary model*. Journal of the Geological Society of Australia, 28, 471-489

Roy, P. S., Cowell, P.J., Ferland, M.A., Thom, B.G. (1994). *Wave-dominated coasts.* Coastal Evolution - Late Quaternary shoreline morphodynamics. R. W. G. Carter & C. D. Woodrofee., Cambridge University Press: 121-186.

Roy, P. (1994). Holocene Estuary Evolution - *Stratigraphic studies from southeastern Australia*. Incised Valey systems: Origin and sedimentary sequences. R. B. a. Z. Z. R. Dalrymple. Sydney, SEPM (Society for Sedimentary Geology). Special publication 51: 241-263.

Roy, P.S., Boyd, R. (1997). *Quaternary Geology of Southeast Australia: a Tectonically Stable, Wave dominated, Sediment-deficient Margin*. International Geological Correlation Program, Project 367.

Schiaffino, C. F., Brignone, M., Ferrari, M. (2011). *Application of the parabolic bay shape equation to sand and gravel beaches on Mediterranean coasts*. Coastal Engineering 59(1): 57-63.

Short, A. D. (1979). *Three dimensional beach stage model*. Journal of Geology 87: 553-571.

Short, A. D. (1987). Modes, timing and volume of Holocene cross-shore and aeolian sediment transport, Southern Australia. Coastal sediments '87, New Orleans.

Short, A. D. (1988). *Holocene coastal dune formation in Southern Australia: A case study*. Sedimentary Geology 55: 121-142.

Short, A. D. (1999). *Wave-dominated beaches*. Hanbook of beach and shoreface morphodynamics. A. D. Short, Wiley: 173-203.

Siddall, M., Kaplan, M. R., Schaefer, J. M., Putnam, A., Kelly, M. A., Goehring, B. (2010). *Changing influence of Antarctic and Greenlandic temperature records on sea-level over the last glacial cycle*. Quaternary Science Reviews 29(3-4): 410-423.

Stive, M. J. F., Cowell, P. J., Nicholls, R. J. (2009). *Impacts of Global Environment Change on Beaches, Cliffs and Deltas*. In: Slaymaker, O., Spencer, T., Embleton-Hamann, C., (eds). Geomorphology and Global Environmental Change. International Association of Geomorphologists. Cambridge University Press, Ch. 7.

Sunamura, T. (1988). *Beach morphologies and their change*. Nearshore dynamics and coastal processes. H. K. Tokyo, University of Tokyo Press: 136-166.

Sutter, J. R. (1994). *Deltaic coasts.* Coastal Evolution - Late Quaternary shoreline morphodynamics. R. W. G. Carter & C. D. Woodrofee., Cambridge University Press: 87-120.

Swift, D. J. P., Phillips, S., Thorne, J. A. (1991). *Sedimentation on continental margins IV: lithofacies and depositional systems*. In Swift, D. J. P., Oertal, G. F., Tillman, R. W. & Thorne, J. A. (Eds.) Shelf sand and sandstone bodies - Geometry, facies and sequence stratigraphy. Special Publication No.14 of the International Association of Sedimentologists ed. Blackwell Scientific Publications, Oxford, 89-152.

Teixeira, S. B. (1990). *Dinâmica das Praias da Península de Setúbal (Portugal)*. MSc. Universidade de Lisboa.

Thieler, E. R., Himmelstoss, E.A., Zichichi, J.L., Ergul, A. (2009). *Digital Shoreline Analysis System (DSAS) version 4.2 — An ArcGIS extension for calculating shoreline change*. U.S. Geological Survey Open-File Report. U.S. Geological Survey. Open-File Report 2008-1278.

Tsoar, H. (1983). *Wind Tunnel Modelling of Echo Dunes and Climbing Dunes*. Developments in Sedimentology 38: 247-259.

Tsoar, H., White, B., Berman, E. (1996). *The effect of slopes on sand transport - numerical modelling*. Landscape and Urban Planning(34): 171-181.

Vis, G., Kasse, C., Vandenberghe, J. (2008). *Late Pleistocene and Holocene palaeogeography of the Lower Tagus Valley (Portugal): effects of relative sea level, valley morphology and sediment supply*. Quaternary Science Reviews 27(17–18): 1682-1709.

Vis, G., Kasse, C., Kroon, D., Jung, S.,Zuur, H., Prick, A. (2010). *Late Holocene sedimentary changes in floodplain and shelf environments of the Tagus River (Portugal)*. Proceedings of the Geologists' Association 121(2): 203-217.

Wright, L. D. & Thom, B. G. (1977). *Coastal depositional landforms: a morphodynamics approach*, Progress in Physical Geography, 1, 412-459.

Wright, L. D. (1978). *River Deltas*. Coastal Sedimentary Environments. A. Davis (ed) Springer: ch 1. 5-68.

Wright, L.D., Thom, B.G., Higgins, R.J. (1980). *Wave influences on river-mouth depositional process: Examples from Australia and Papua New Guinea*. Estuarine and Coastal Marine Science, 263-277.

Wright, L. D. Short, A. D. (1984). *Morphodynamic variability of surf zones and beaches: A synthesis*. Marine Geology 56(1–4): 93-118.

APPENDIX

Borehole data

Reports from Tecnosol-FGE S.A., Teixeira Duarte Lda. and GNR Sto. António da Caparica

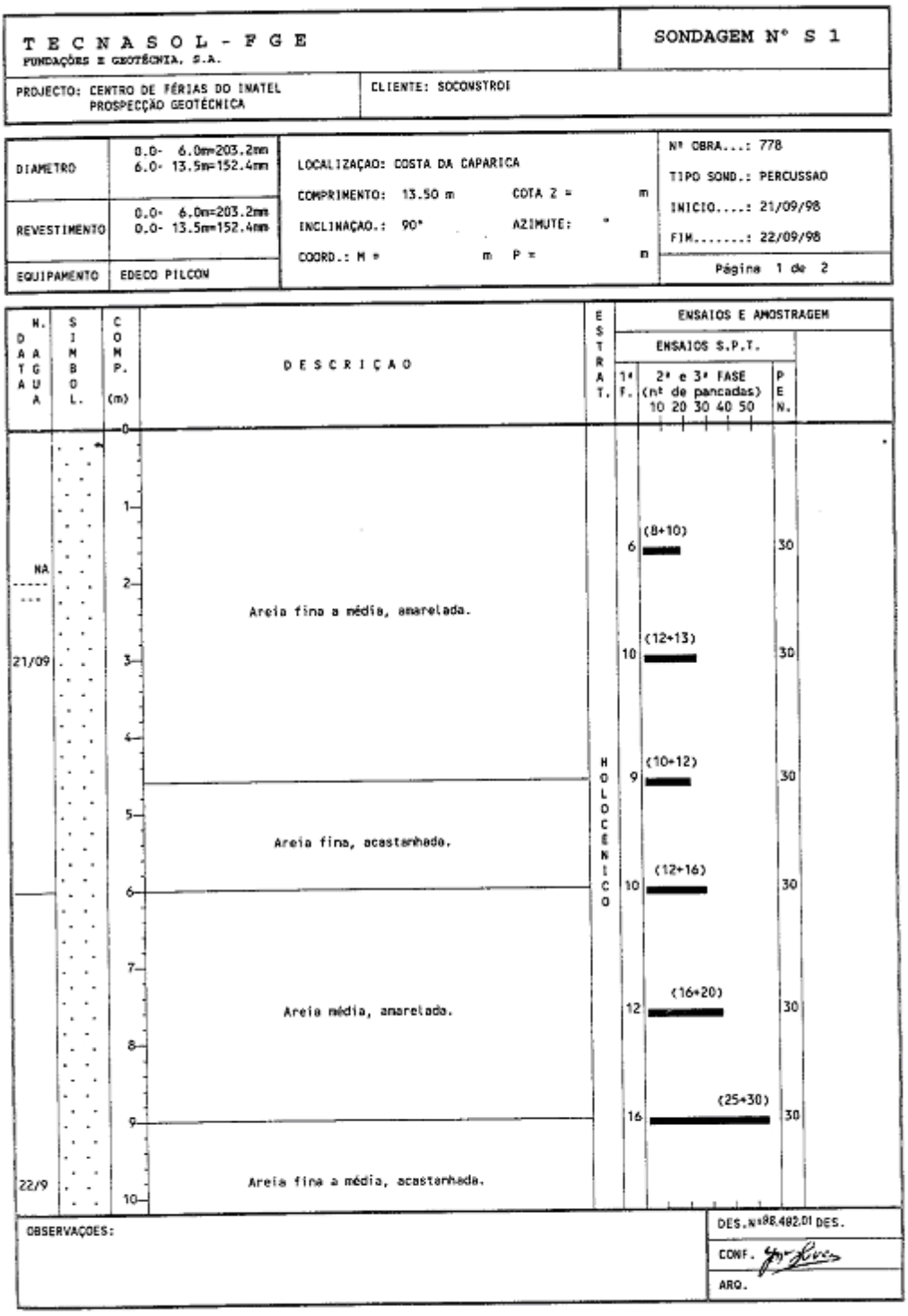

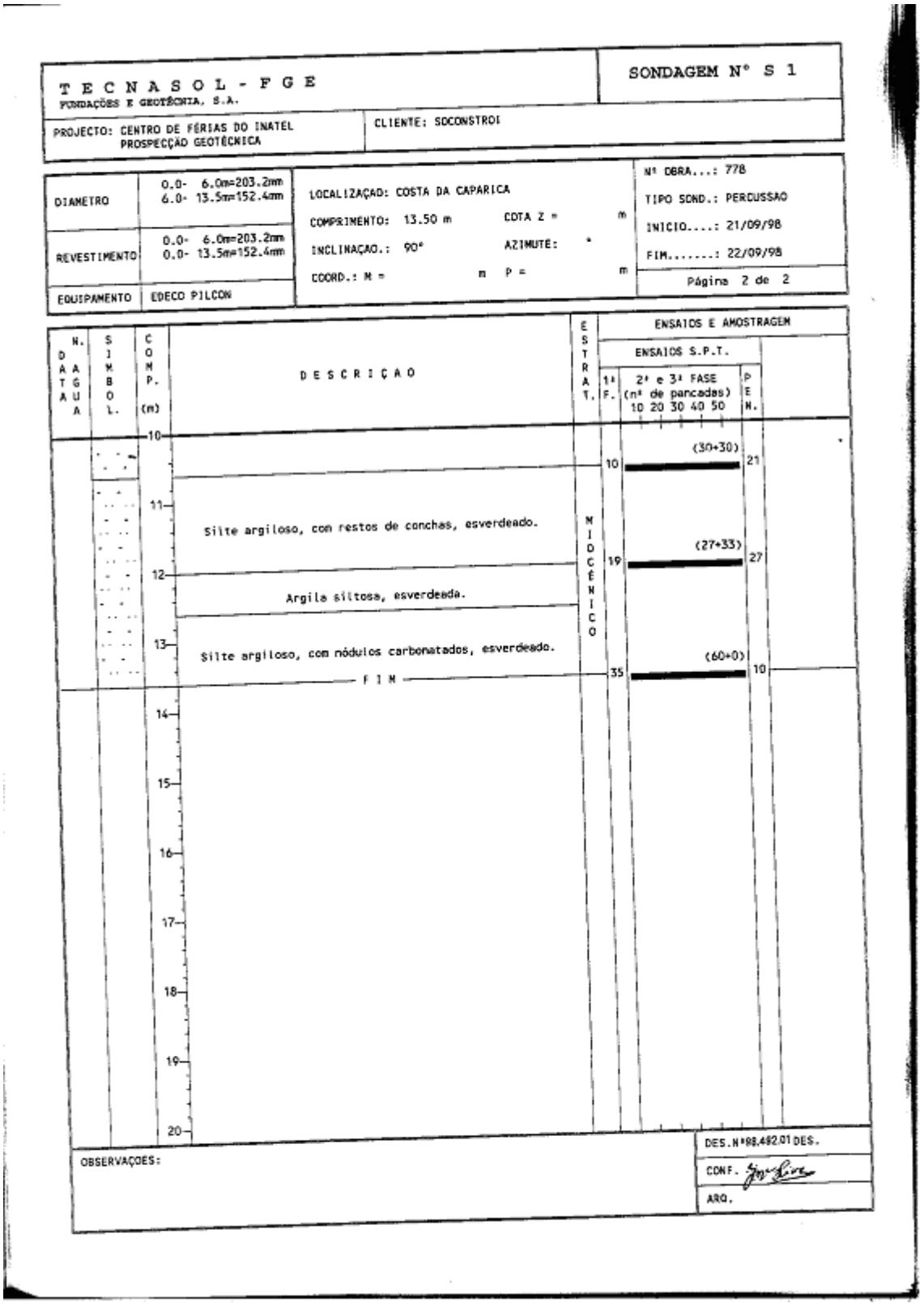

TECNASOL - FGE
FUNDAÇÕES E GEOTÉCNIA, S.A.

SONDAGEM Nº S 1

PROJECTO: CENTRO DE FÉRIAS DO INATEL
PROSPECÇÃO GEOTÉCNICA

CLIENTE: SOCONSTROI

DIAMETRO	0.0- 6.0m=203.2mm 6.0- 13.5m=152.4mm
REVESTIMENTO	0.0- 6.0m=203.2mm 0.0- 13.5m=152.4mm
EQUIPAMENTO	EDECO PILCON

LOCALIZAÇAO: COSTA DA CAPARICA
COMPRIMENTO: 13.50 m COTA Z = m
INCLINAÇAO.: 90° AZIMUTE: °
COORD.: M = m P = m

Nº OBRA...: 778
TIPO SOND.: PERCUSSAO
INICIO....: 21/09/98
FIM.....: 22/09/98
Página 2 de 2

DATA N. AGUA	SIMBOL.	COMP. (m)	DESCRIÇÃO	ESTRAT.	ENSAIOS E AMOSTRAGEM: ENSAIOS S.P.T. 1ª F.	2ª e 3ª FASE (nº de pancadas) 10 20 30 40 50	PEN.
		10			10	(30+30)	21
		11	Silte argiloso, com restos de conchas, esverdeado.	MIOCÉNICO			
		12			19	(27+33)	27
			Argila siltosa, esverdeada.				
		13	Silte argiloso, com nódulos carbonatados, esverdeado.				
			FIM		35	(60+0)	10
		14					
		15					
		16					
		17					
		18					
		19					
		20					

OBSERVAÇÕES:

DES. Nº 98.492.01 DES.
CONF.
ARQ.

TECNASOL - FGE
FUNDAÇÕES E GEOTÉCNIA, S.A.

SONDAGEM Nº S 2

PROJECTO: CENTRO DE FÉRIAS DO INATEL
PROSPECÇÃO GEOTÉCNICA

CLIENTE: SOCONSTROI

DIAMETRO	0.0- 13.5m=203.2mm
REVESTIMENTO	0.0- 13.5m=203.2mm
EQUIPAMENTO	EDECO PILCON

LOCALIZAÇAO: COSTA DA CAPARICA
COMPRIMENTO: 13.50 m COTA Z = m
INCLINAÇAO.: 90° AZIMUTE: °
COORD.: M = m P = m

Nº OBRA...: 778
TIPO SOND.: PERCUSSAO
INICIO....: 30/09/98
FIM.....: 01/10/98
Página 1 de 2

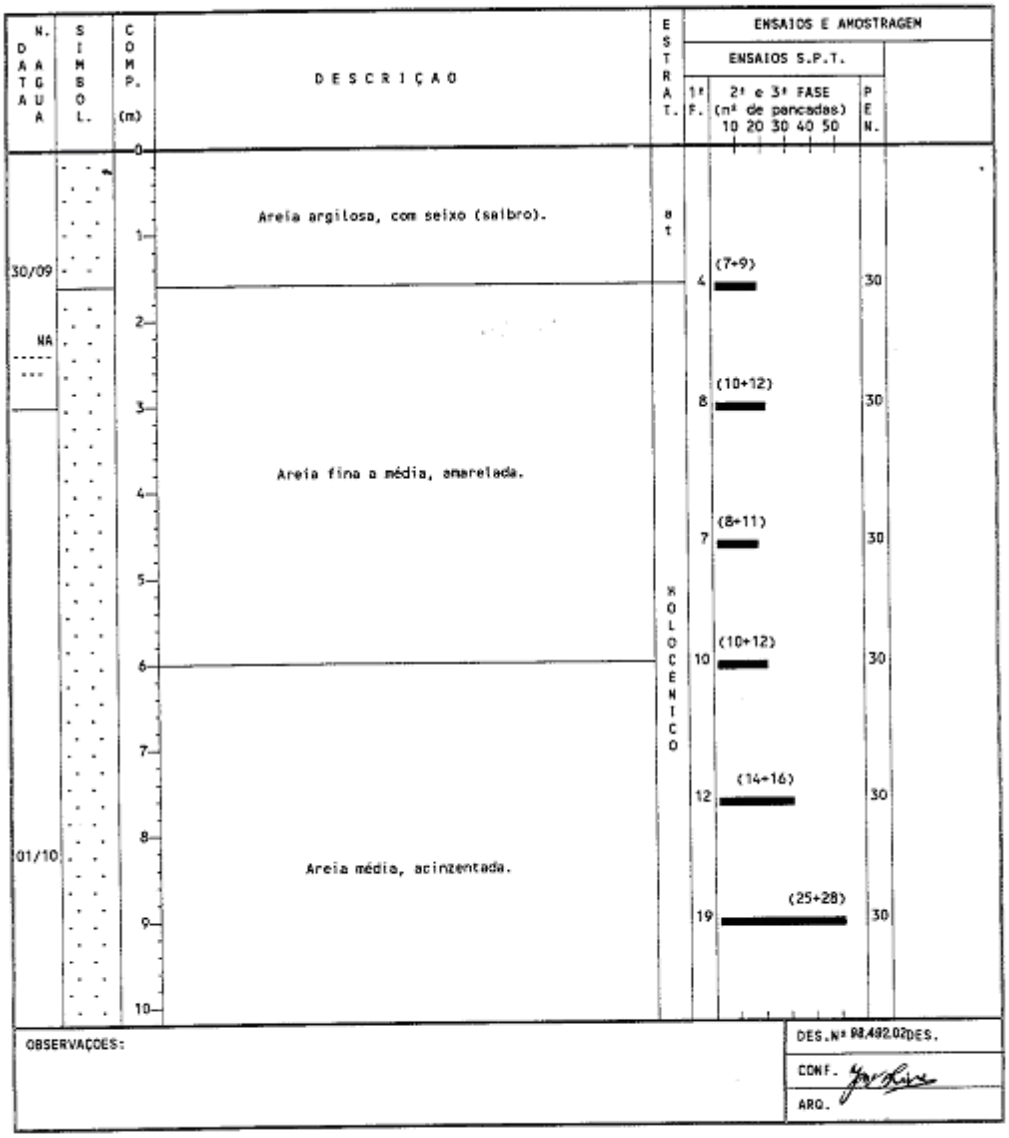

OBSERVAÇÕES:

DES.Nº 98.492.02DES.
CONF.
ARQ.

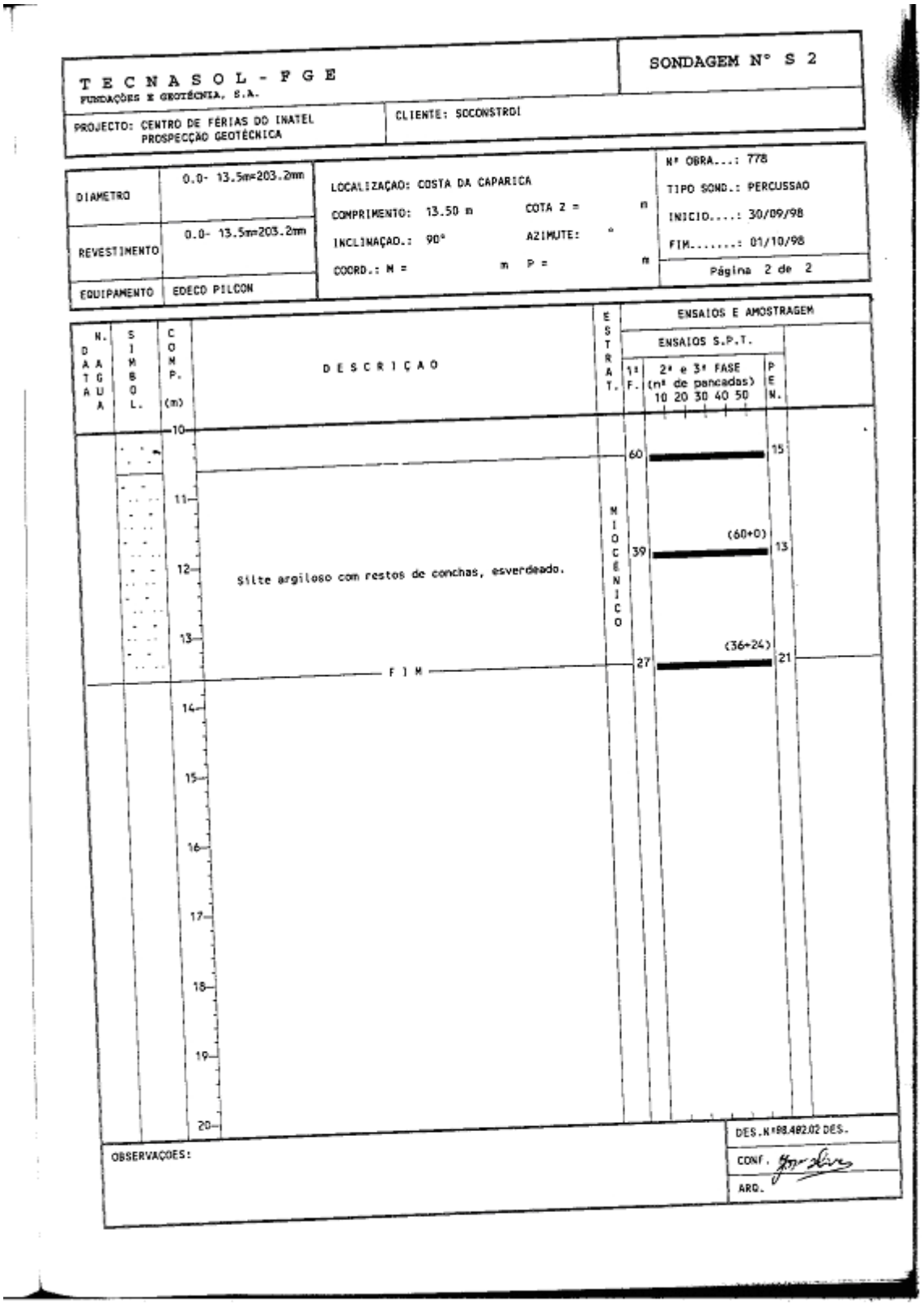

TECNASOL - FGE
FUNDAÇÕES E GEOTÉCNIA, S.A.

SONDAGEM Nº S 2

PROJECTO: CENTRO DE FÉRIAS DO INATEL
PROSPECÇÃO GEOTÉCNICA

CLIENTE: SCONSTRDI

DIAMETRO	0.0- 13.5m=203.2mm
REVESTIMENTO	0.0- 13.5m=203.2mm
EQUIPAMENTO	EDECO PILCON

LOCALIZAÇAO: COSTA DA CAPARICA
COMPRIMENTO: 13.50 m COTA Z = m
INCLINAÇAO.: 90° AZIMUTE: °
COORD.: M = m P = m

Nº OBRA...: 778
TIPO SOND.: PERCUSSAO
INICIO....: 30/09/98
FIM.....: 01/10/98
Página 2 de 2

N. DA AGUA	SIMBOL.	COMP. (m)	DESCRIÇAO	ESTRAT.	ENSAIOS E AMOSTRAGEM	
					ENSAIOS S.P.T.	
					1ª F.	2ª e 3ª FASE (nº de pancadas) 10 20 30 40 50	PEN.
		10			60		15
		11	Silte argiloso com restos de conchas, esverdeado.	MIOCENICO	39	(60+0)	13
		12					
		13	FIM		27	(36+24)	21
		14					
		15					
		16					
		17					
		18					
		19					
		20					

OBSERVAÇOES:

DES. Nº98.482.02 DES.
CONF.
ARQ.

TECNASOL - FGE
FUNDAÇÕES E GEOTÉCNIA, S.A.

SONDAGEM Nº S 3

PROJECTO: CENTRO DE FÉRIAS DO INATEL
PROSPECÇÃO GEOTÉCNICA

CLIENTE: SOCONSTROI

DIAMETRO	0.0- 9.0m=203.2mm 9.0- 13.5m=152.4mm
REVESTIMENTO	0.0- 9.0m=203.2mm 0.0- 10.5m=152.4mm
EQUIPAMENTO	EDECO PILCON

LOCALIZAÇAO: COSTA DA CAPARICA
COMPRIMENTO: 13.50 m COTA Z = m
INCLINAÇAO.: 90° AZIMUTE: °
COORD.: M = m P = m

Nº OBRA...: 778
TIPO SOND.: PERCUSSAO
INICIO....: 11/09/98
FIM.....: 14/09/98
Página 1 de 2

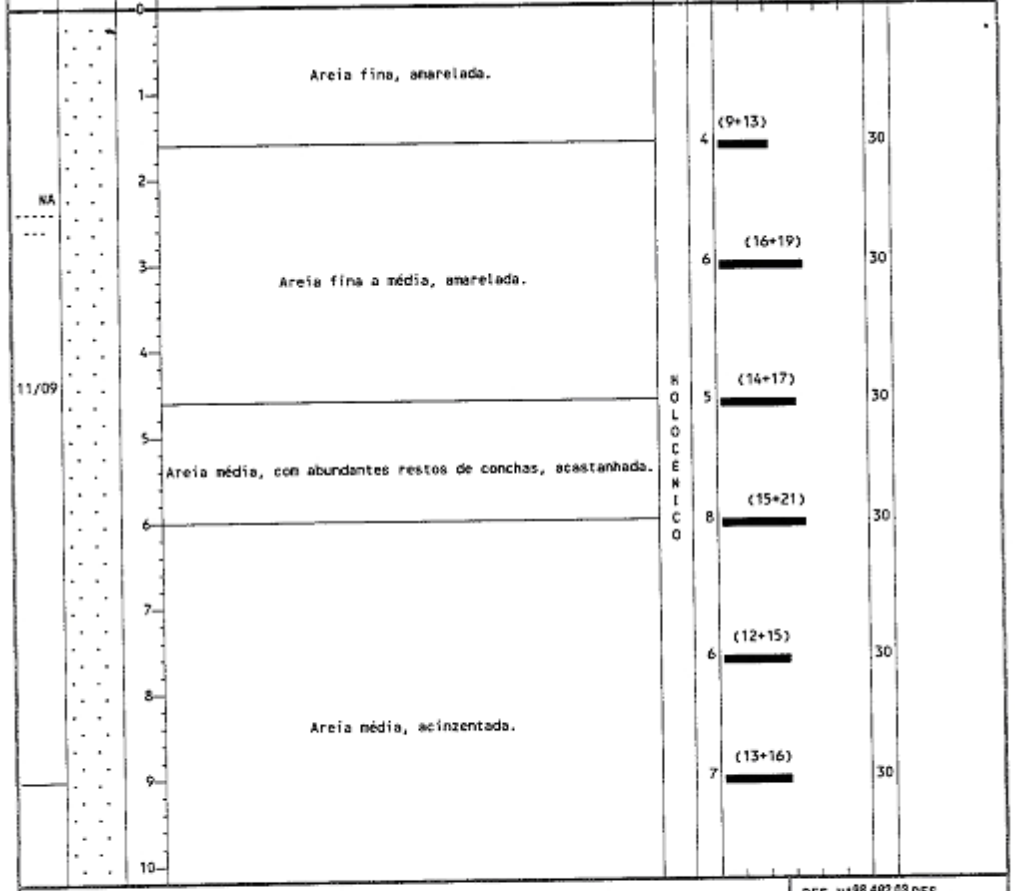

OBSERVAÇÕES:

DES. M+98.402.03 DES.
CONF.
ARQ.

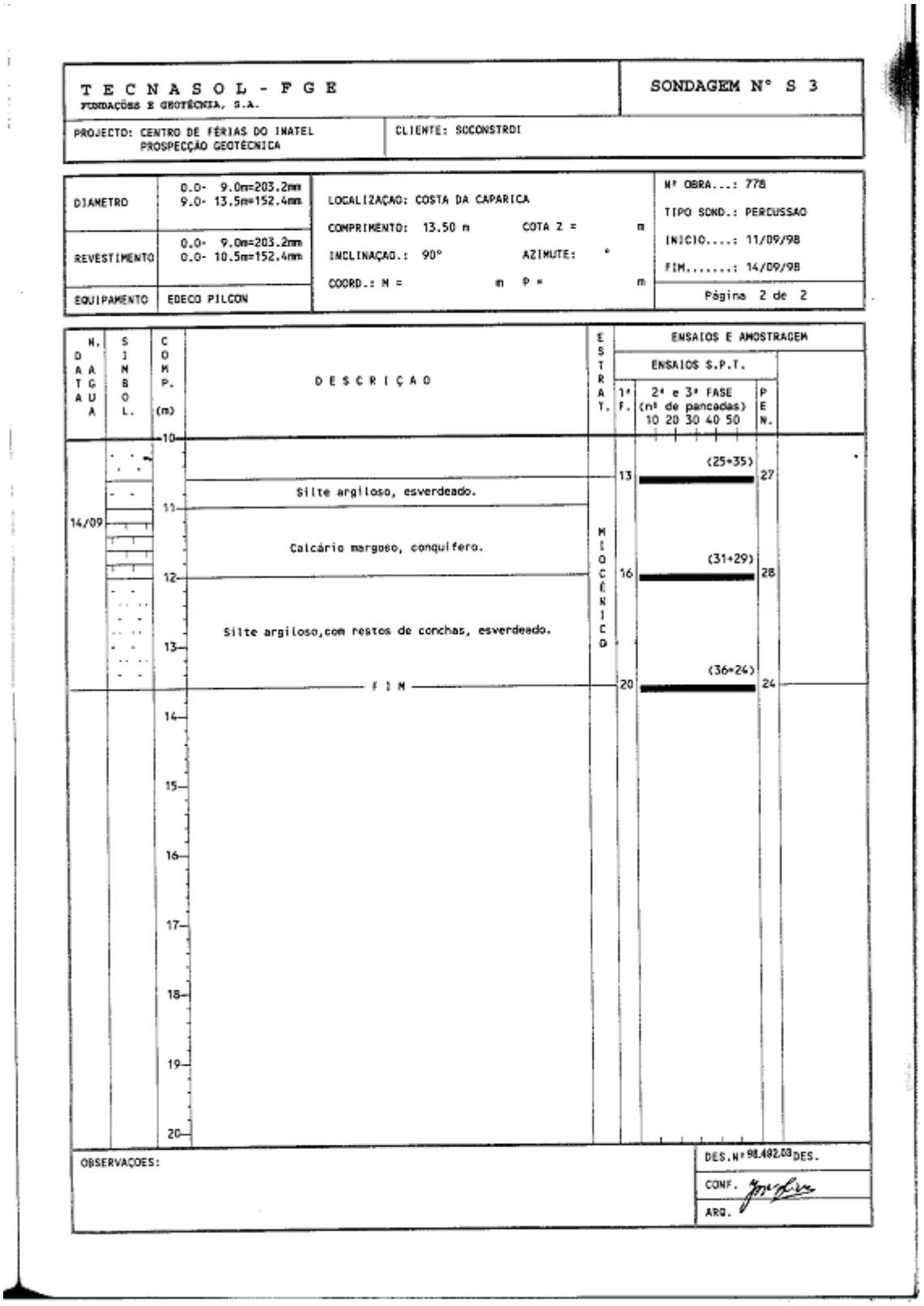

TECNASOL - FGE
FUNDAÇÕES E GEOTÉCNIA, S.A.

SONDAGEM Nº S 4

PROJECTO: CENTRO DE FÉRIAS DO INATEL
PROSPECÇÃO GEOTÉCNICA

CLIENTE: SOCONSTROI

DIAMETRO	0.0- 7.5m=203.0mm 7.5- 13.5m=152.0mm	LOCALIZAÇÃO: COSTA DA CAPARICA	Nº OBRA...: 778
REVESTIMENTO	0.0- 7.5m=203.0mm 0.0- 13.5m=152.0mm	COMPRIMENTO: 13.50 m COTA Z = m INCLINAÇÃO.: 90° AZIMUTE: °	TIPO SOND.: PERCUSSÃO INICIO....: 17/09/98
EQUIPAMENTO	EDECO PILCON	COORD.: M = m P = m	FIM.....: 18/09/98 Página 1 de 2

DATA NA AGUA	SIMBOL.	COMP. (m)	DESCRIÇÃO	ESTRAT.	ENSAIOS E AMOSTRAGEM ENSAIOS S.P.T. 1ª F.	2ª e 3ª FASE (nº de pancadas) 10 20 30 40 50	PEN.
		0					
		1	Areia fina a média, amarelada. Areia fina, amarelada.		6	(12+17)	30
NA		2					
		3	Areia fina a média, amarelada.		7	(14+19)	30
17/09		4			8	(16+22)	30
		5		HOLOCENICO			
		6			8	(15+20)	30
		7	Areia média, acastanhada.		7	(10+12)	30
		8					
		9			16	(20+25)	30
		10					

OBSERVAÇÕES: Sondagem realizada no interior do cinema a uma cota 1.5 m inferior à cota do exterior.

DES.Nº 98.492.04 DES.
CONF.
ARQ.

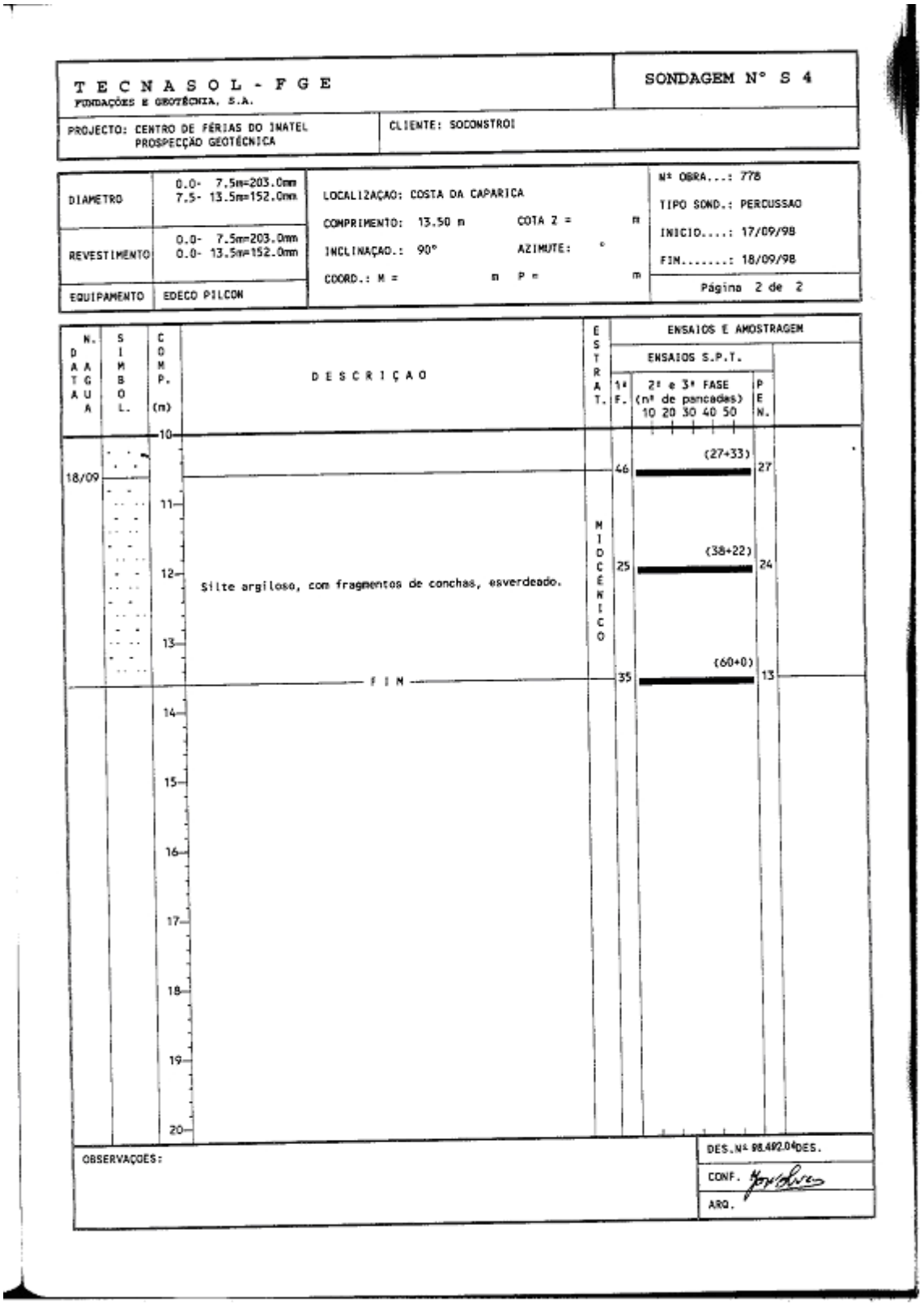

TECNASOL - FGE
FUNDAÇÕES E GEOTÉCNIA, S.A.

SONDAGEM Nº S 4

PROJECTO: CENTRO DE FÉRIAS DO INATEL
PROSPECÇÃO GEOTÉCNICA

CLIENTE: SOCONSTROI

DIAMETRO	0.0- 7.5m=203.0mm 7.5- 13.5m=152.0mm	LOCALIZAÇAO: COSTA DA CAPARICA	Nº OBRA...: 778
REVESTIMENTO	0.0- 7.5m=203.0mm 0.0- 13.5m=152.0mm	COMPRIMENTO: 13.50 m COTA Z = m	TIPO SOND.: PERCUSSAO
EQUIPAMENTO	EDECO PILCON	INCLINAÇAO.: 90° AZIMUTE: °	INICIO....: 17/09/98
		COORD.: M = m P = m	FIM.....: 18/09/98
			Página 2 de 2

DATA	SIMBOL.	COMP. (m)	DESCRIÇAO	ESTRAT.	ENSAIOS E AMOSTRAGEM	
					ENSAIOS S.P.T.	
					1ª F.	2ª e 3ª FASE (nº de pancadas) 10 20 30 40 50
18/09		10			46	(27+33) 27
		11		MIDCENICO		
		12	Silte argiloso, com fragmentos de conchas, esverdeado.		25	(38+22) 24
		13			35	(60+0) 13
			FIM			
		14				
		15				
		16				
		17				
		18				
		19				
		20				

OBSERVAÇÕES:

DES.Nº 98.492.04 DES.
CONF.
ARQ.

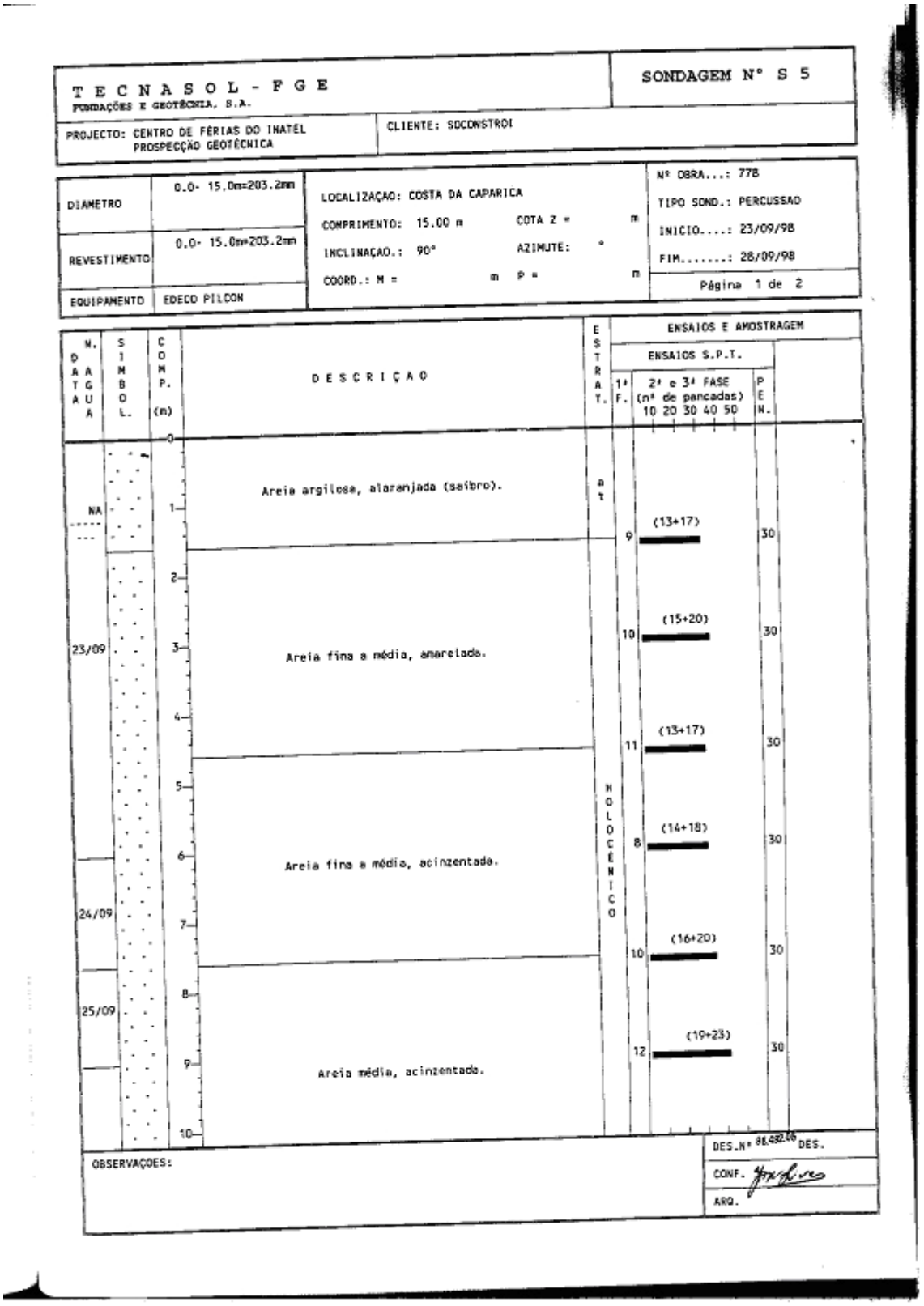

TECNASOL - FGE
FUNDAÇÕES E GEOTÉCNIA, S.A.

SONDAGEM Nº S 5

PROJECTO: CENTRO DE FÉRIAS DO INATEL
PROSPECÇÃO GEOTÉCNICA

CLIENTE: SOCONSTROI

DIAMETRO	0.0- 15.0m=203.2mm
REVESTIMENTO	0.0- 15.0m=203.2mm
EQUIPAMENTO	EDECO PILCON

LOCALIZAÇAO: COSTA DA CAPARICA
COMPRIMENTO: 15.00 m COTA Z = m
INCLINAÇAO.: 90° AZIMUTE: °
COORD.: M = m P = m

Nº OBRA...: 778
TIPO SOND.: PERCUSSAO
INICIO....: 23/09/98
FIM.....: 28/09/98
Página 1 de 2

DATA NA AGUA	SIMBOL.	COMP. (m)	DESCRIÇÃO	ESTRAT.	ENSAIOS E AMOSTRAGEM: ENSAIOS S.P.T. 1ª F.	2ª e 3ª FASE (nº de pancadas) 10 20 30 40 50	PEN.
NA		0					
		1	Areia argilosa, alaranjada (saibro).	At	9	(13+17)	30
23/09		2	Areia fina a média, amarelada.		10	(15+20)	30
		3					
		4			11	(13+17)	30
		5	Areia fina a média, acinzentada.	HOLOCÉNICO	8	(14+18)	30
24/09		6					
		7			10	(16+20)	30
25/09		8	Areia média, acinzentada.		12	(19+23)	30
		9					
		10					

OBSERVAÇÕES:

DES.Nº 86.492.06 DES.
CONF.
ARQ.

TECNASOL - FGE
FUNDAÇÕES E GEOTÉCNIA, S.A.

SONDAGEM Nº S 5

PROJECTO: CENTRO DE FÉRIAS DO INATEL
PROSPECÇÃO GEOTÉCNICA

CLIENTE: SOCONSTROI

DIAMETRO	0.0- 15.0m=203.2mm
REVESTIMENTO	0.0- 15.0m=203.2mm
EQUIPAMENTO	EDECO PILCON

LOCALIZAÇAO: COSTA DA CAPARICA
COMPRIMENTO: 15.00 m COTA Z = m
INCLINAÇAO.: 90° AZIMUTE: °
COORD.: M = m P = m

Nº OBRA...: 778
TIPO SOND.: PERCUSSAO
INICIO....: 23/09/98
FIM.....: 28/09/98
Página 2 de 2

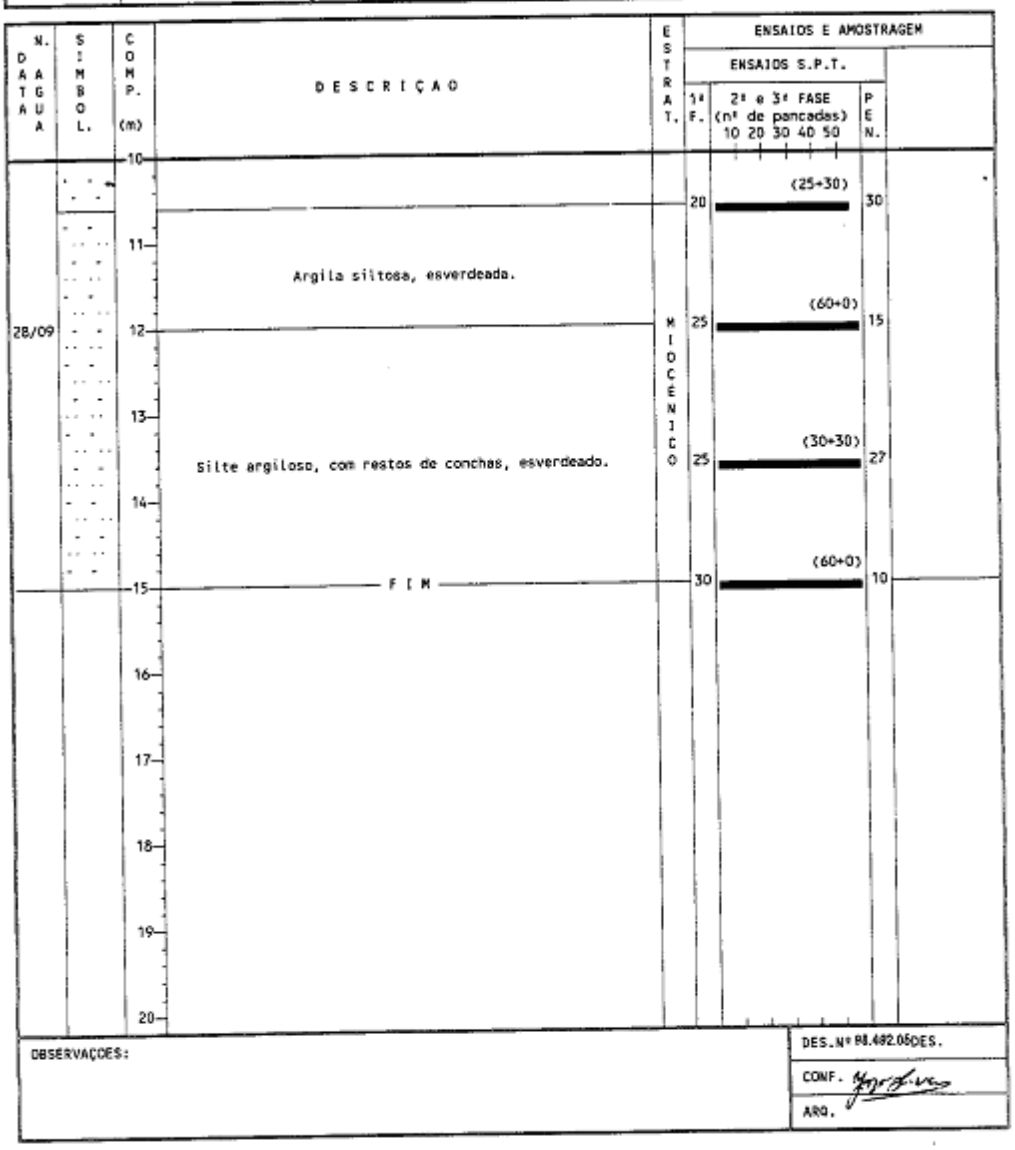

OBSERVAÇÕES:

DES.Nº 98.492.05DES.
CONF.
ARQ.

T E C N A S O L - F G E
FUNDAÇÕES E GEOTÉCNIA, S.A.

SONDAGEM Nº S 6

PROJECTO: CENTRO DE FÉRIAS DO INATEL
PROSPECÇÃO GEOTÉCNICA

CLIENTE: SOCONSTRDI

DIAMETRO	0.0- 7.5m=203.2mm 7.5- 13.5m=152.4mm	LOCALIZAÇÃO: COSTA DA CAPARICA	Nº OBRA...: 778
REVESTIMENTO	0.0- 7.5m=203.2mm 0.0- 13.5m=152.4mm	COMPRIMENTO: 13.50 m COTA Z = m	TIPO SOND.: PERCUSSAO
EQUIPAMENTO	EDECO PILCON	INCLINAÇÃO.: 90° AZIMUTE: °	INICIO....: 15/09/98
		COORD.: M = m P = m	FIM.....: 16/09/98
			Página 1 de 2

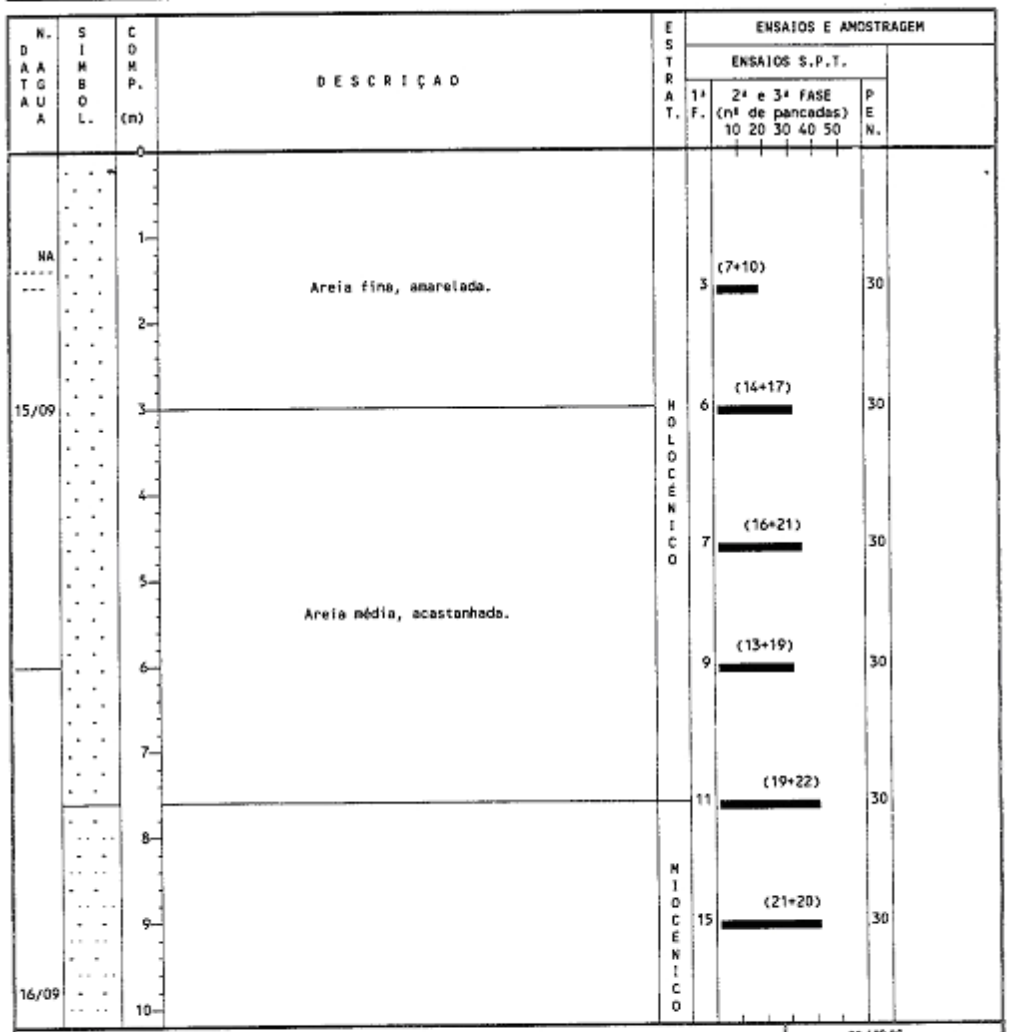

OBSERVAÇÕES: Sondagem realizada no interior do cinema, a uma cota 1,5 m inferior à cota do exterior.

DES. Nº88.482.06 DES.
CONF.
ARQ.

TECNASOL - FGE
FUNDAÇÕES E GEOTÉCNIA, S.A.

SONDAGEM Nº S 6

PROJECTO: CENTRO DE FÉRIAS DO INATEL
PROSPECÇÃO GEOTÉCNICA

CLIENTE: SOCONSTROI

DIAMETRO	0.0- 7.5m=203.2mm 7.5- 13.5m=152.4mm	LOCALIZAÇAO: COSTA DA CAPARICA	Nº OBRA...: 778
REVESTIMENTO	0.0- 7.5m=203.2mm 0.0- 13.5m=152.4mm	COMPRIMENTO: 13.50 m COTA Z = m	TIPO SOND.: PERCUSSAO
EQUIPAMENTO	EDECO PILCON	INCLINAÇAO.: 90° AZIMUTE: °	INICIO....: 15/09/98
		COORD.: M = m P = m	FIM.....: 16/09/98
			Página 2 de 2

NÍVEL DE ÁGUA	SIMBOL.	COMP. (m)	DESCRIÇÃO	ESTRAT.	ENSAIOS E AMOSTRAGEM	
					ENSAIOS S.P.T.	
					1ª F.	2ª e 3ª FASE (nº de pancadas) 10 20 30 40 50
		10	Silte argiloso, esverdeado, com restos de conchas e passagens carbonatadas esbranquiçadas.		20	(32+28) 27
		11				
		12			24	(35+25) 23
		13				
			FIM		34	(60+0) 10
		14				
		15				
		16				
		17				
		18				
		19				
		20				

OBSERVAÇÕES:

DES. Nº98.402.06 DES.
CONF.
ARQ.

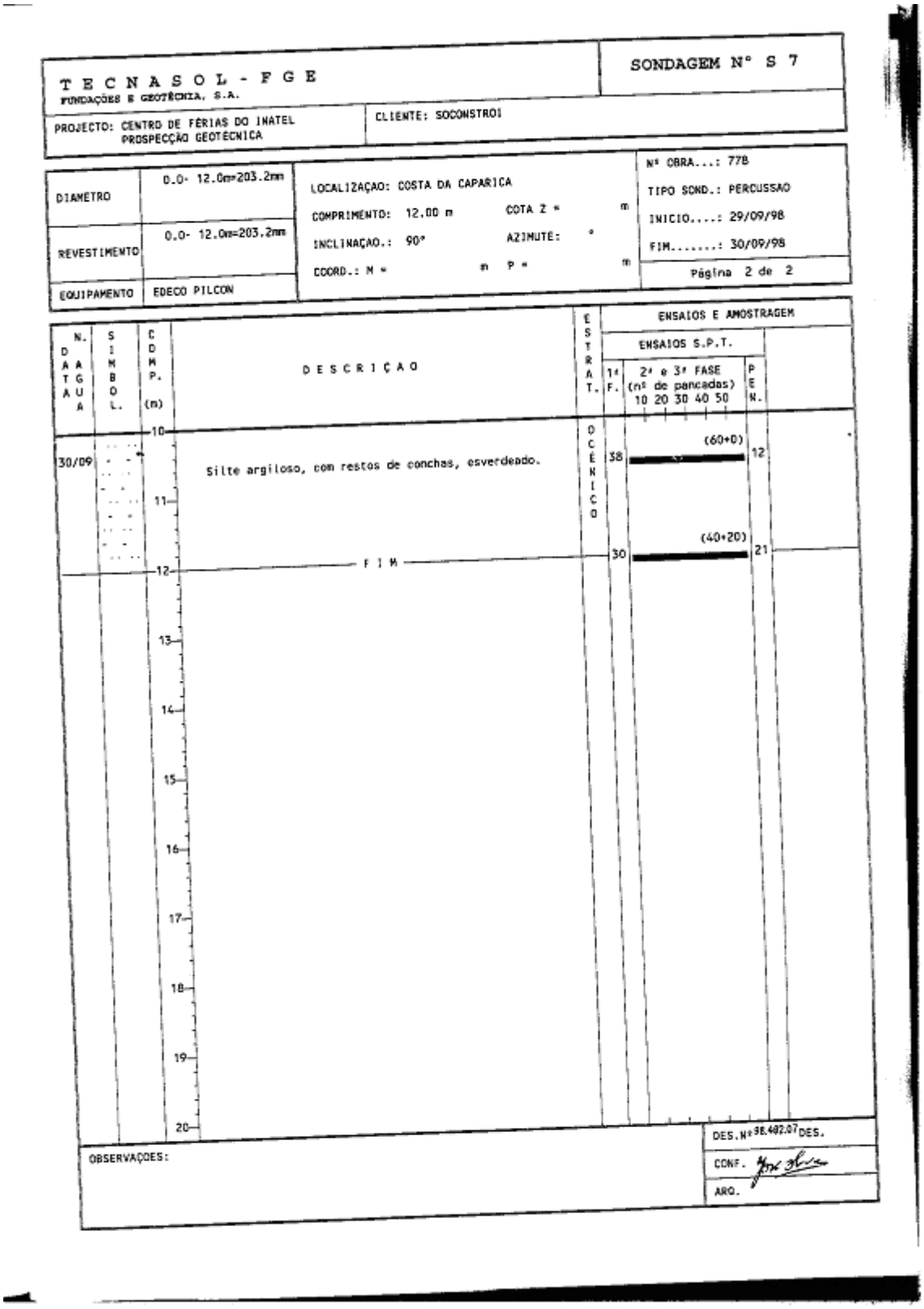

TECNASOL - FGE
FUNDAÇÕES E GEOTÉCNIA, S.A.

SONDAGEM Nº S 7

PROJECTO: CENTRO DE FÉRIAS DO INATEL
PROSPECÇÃO GEOTÉCNICA

CLIENTE: SOCONSTROI

DIAMETRO	0.0- 12.0m=203.2mm	LOCALIZAÇAO: COSTA DA CAPARICA	Nº OBRA...: 778
REVESTIMENTO	0.0- 12.0m=203.2mm	COMPRIMENTO: 12.00 m COTA Z = m	TIPO SOND.: PERCUSSAO
EQUIPAMENTO	EDECO PILCON	INCLINAÇAO.: 90° AZIMUTE: °	INICIO....: 29/09/98
		COORD.: M = m P = m	FIM.....: 30/09/98
			Página 2 de 2

DATA N. AGUA	SIMBOL.	COMP. (m)	DESCRIÇAO	ESTRAT.	ENSAIOS E AMOSTRAGEM — ENSAIOS S.P.T. 1ª F.	2ª e 3ª FASE (nº de pancadas) 10 20 30 40 50	PEN.
30/09		10	Silte argiloso, com restos de conchas, esverdeado.	OCÉNICO	38	(60+0)	12
		11					
		12	FIM		30	(40+20)	21
		13					
		14					
		15					
		16					
		17					
		18					
		19					
		20					

OBSERVAÇÕES:

DES.Nº 98.402.07 DES.
CONF.
ARQ.

TECNASOL - FGE
FUNDAÇÕES E GEOTÉCNIA, S.A.

SONDAGEM Nº S 7

PROJECTO: CENTRO DE FÉRIAS DO INATEL
PROSPECÇÃO GEOTÉCNICA

CLIENTE: SOCONSTROI

DIAMETRO	0.0- 12.0m=203.2mm	LOCALIZAÇÃO: COSTA DA CAPARICA	Nº OBRA...: 778
REVESTIMENTO	0.0- 12.0m=203.2mm	COMPRIMENTO: 12.00 m COTA Z = m	TIPO SOND.: PERCUSSÃO
EQUIPAMENTO	EDECO PILCON	INCLINAÇÃO.: 90° AZIMUTE: °	INICIO....: 29/09/98
		COORD.: M = m P = m	FIM.....: 30/09/98
			Página 1 de 2

DATA AGUA	SIMBOL.	COMP. (m)	DESCRIÇÃO	ESTRAT.	ENSAIOS E AMOSTRAGEM: ENSAIOS S.P.T. 1ª f.	2ª e 3ª FASE (nº de pancadas) 10 20 30 40 50	PEN.
		0					
		1	Areia argilosa, alaranjada (saibro).	at	7	(8+12)	30
NA		2					
		3	Areia fina a média, amarelada.		11	(13+15)	30
29/09		4		HOLOCÉNICO	7	(10+13)	30
		5					
		6			10	(13+14)	30
		7	Areia média, acastanhada.				
		8			12	(15+18)	30
		9			30	(60+0)	11
		10		N1			

OBSERVAÇÕES:

DES.Nº 98.482.07 DES.
CONF.
ARQ.

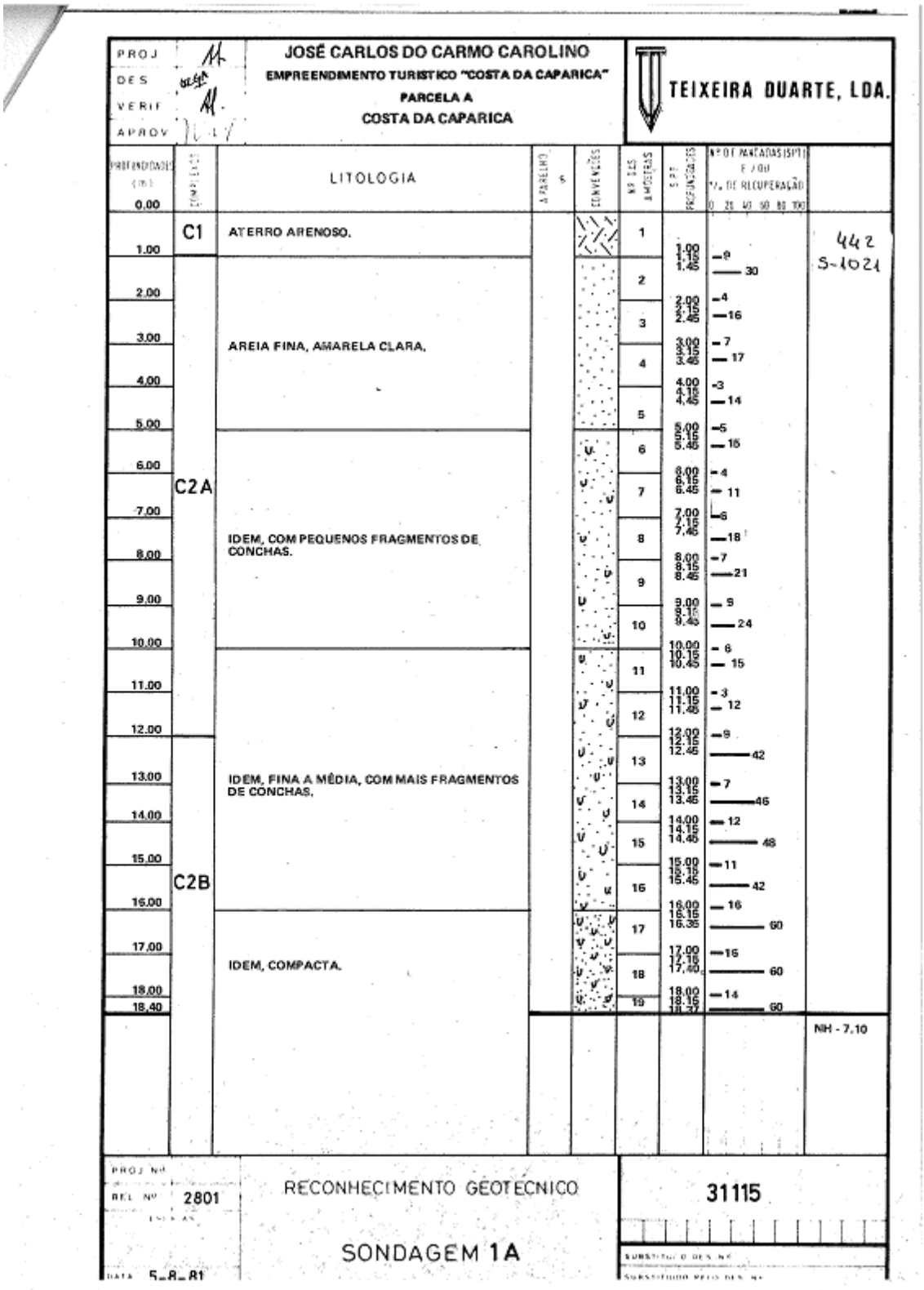

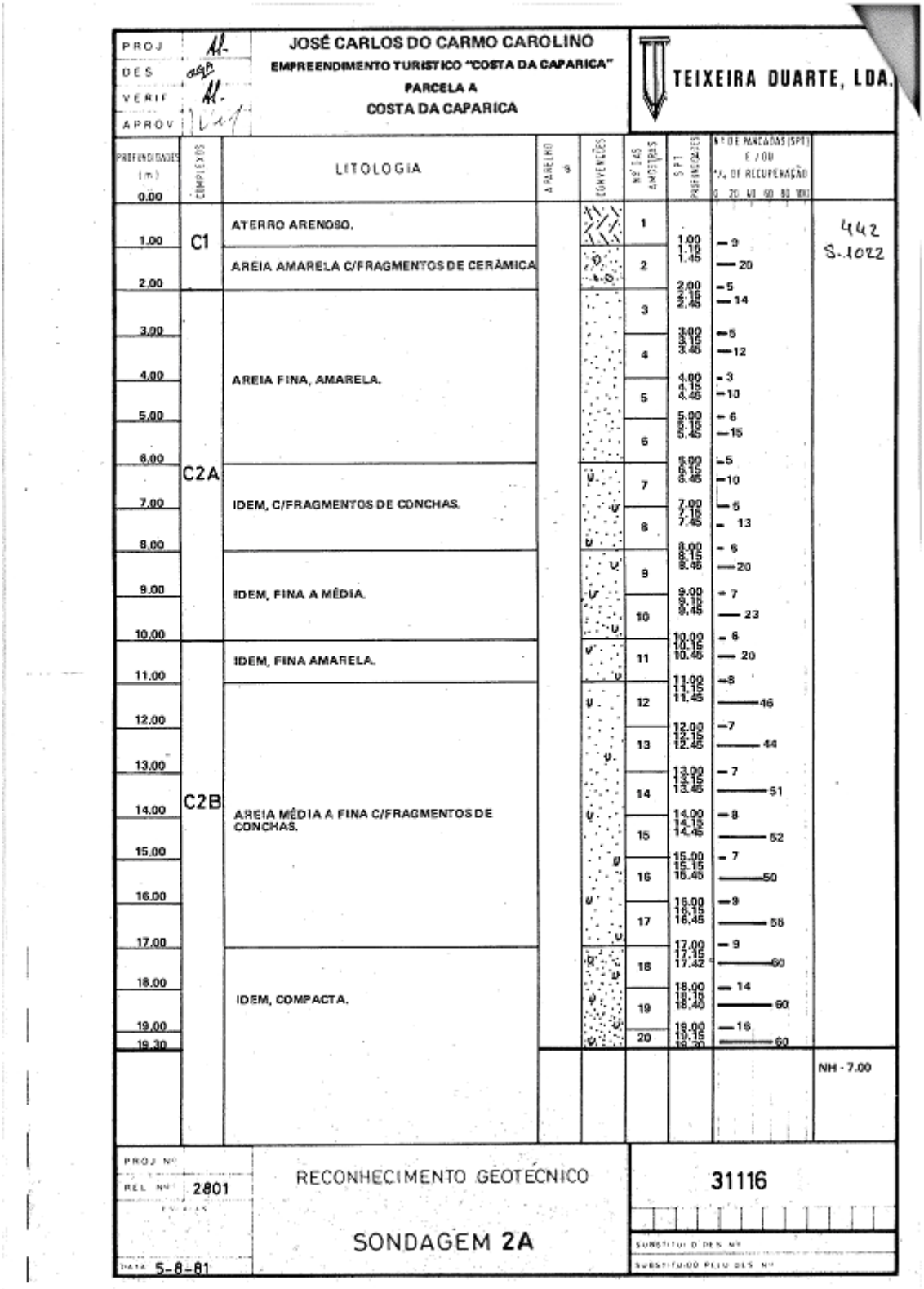

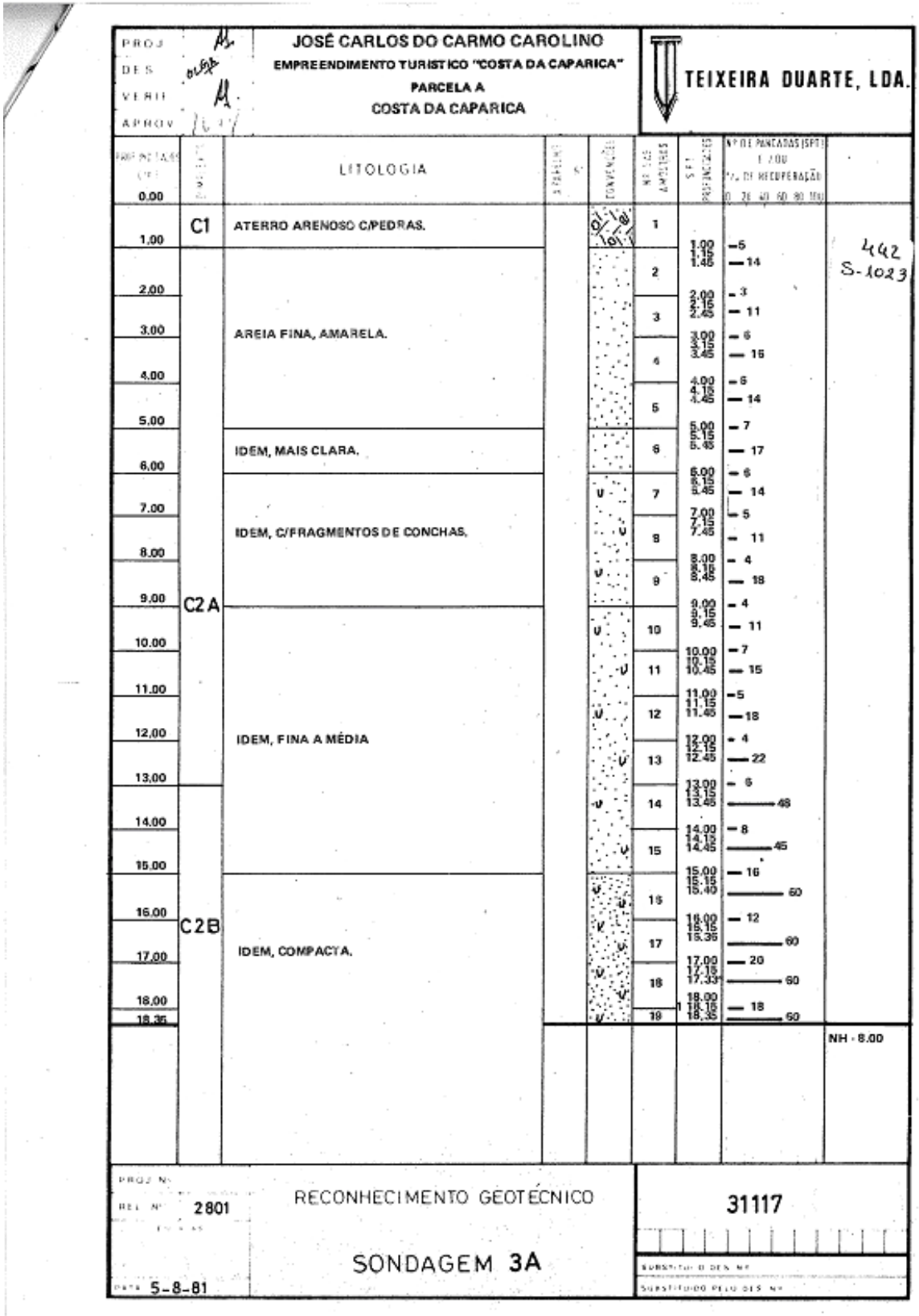

LEGENDA

C1 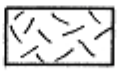 ATERRO ARENOSO POR VEZES COM FRAGMENTOS DE CERÂMICA E PEDRAS.

C2A 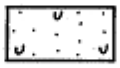 AREIAS FINAS A MÉDIAS POR VEZES COM FRAGMENTOS DE CONCHAS, MEDIANAMENTE COMPACTAS (10 < SPT < 25).

C2B 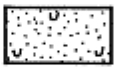 AREIAS FINAS A MÉDIAS POR VEZES COM FRAGMENTOS DE CONCHAS, COMPACTAS A MUITO COMPACTAS (SPT > 40).

N.F. NÍVEL FREÁTICO.

INDICE	ALTERAÇÃO	DATA	RUBRICA

PROJ.		JOSÉ CARLOS DO CARMO CAROLINO	TEIXEIRA DUARTE, LDA.
DES.	MARTINS	EMPREENDIMENTO TURISTICO "COSTA DA CAPARICA"	
VERIF.		PARCELA A	
APROV.		COSTA DA CAPARICA	
PROJ. Nº		RECONHECIMENTO GEOTÉCNICO	31118
REL. Nº	2801	PERFIL GEOLÓGICO INTERPRETATIVO	
ESCALAS	1/200	A – A'	
DATA:	5-8-81		SUBSTITUI O DES. Nº
			SUBSTITUIDO PELO DES. Nº

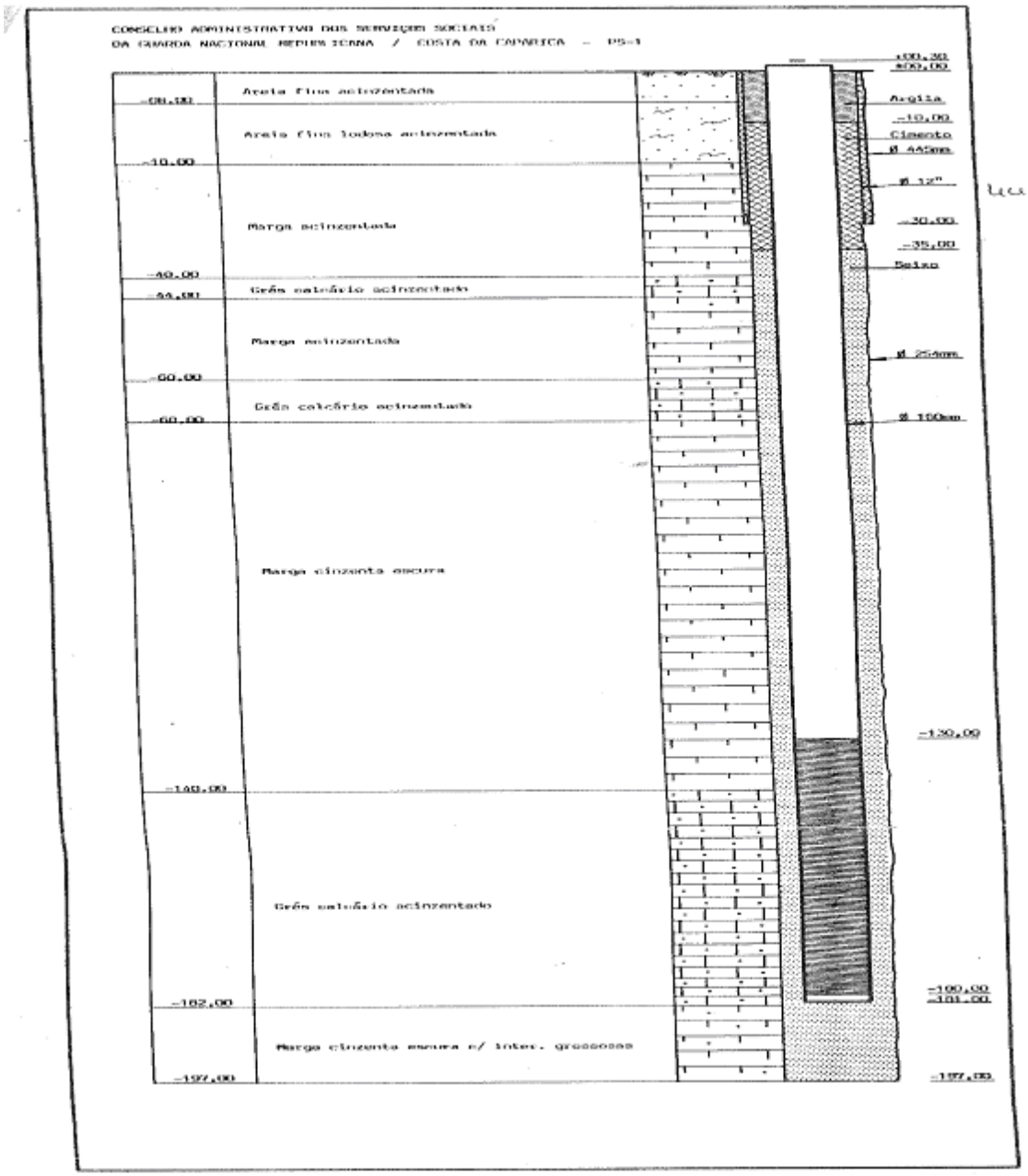

© GNR Sto. António da Caparica

APPENDIX

Wave data

Data from Sines buoy Costa et al. (2001) and 57 year hindcast data (Dodet et al., 2010)

Frequency of occurrences for each interval of T_m and H_{sig}

Trend	T_m (s)|H_{sig}(m)	<0.5	1	2	3	4	5	6	7	8	9	10
SW (180°-260°)	4-6	0.000	0.246	0.152	0.007	0.000	0.000	0.000	0.000	0.000	0.000	0.000
	6-8	0.000	0.478	0.804	0.507	0.159	0.000	0.000	0.000	0.000	0.000	0.000
	8-10	0.000	0.152	0.311	0.413	0.326	0.072	0.000	0.000	0.000	0.000	0.000
	10-12	0.014	0.080	0.065	0.014	0.014	0.000	0.000	0.000	0.000	0.000	0.000
	12-14	0.000	0.014	0.014	0.000	0.000	0.000	0.000	0.000	0.000	0.000	0.000
	14-16	0.000	0.000	0.000	0.000	0.000	0.000	0.000	0.000	0.000	0.000	0.000
	16-18	0.000	0.000	0.000	0.000	0.000	0.000	0.000	0.000	0.000	0.000	0.000
W (260°-280°)	4-6	0.000	0.072	0.029	0.000	0.000	0.000	0.000	0.000	0.000	0.000	0.000
	6-8	0.000	0.572	0.854	0.224	0.029	0.000	0.000	0.000	0.000	0.000	0.000
	8-10	0.000	0.768	0.688	0.702	0.282	0.065	0.014	0.000	0.000	0.000	0.000
	10-12	0.000	0.130	0.340	0.377	0.232	0.116	0.029	0.007	0.000	0.000	0.000
	12-14	0.000	0.000	0.036	0.036	0.022	0.014	0.007	0.000	0.000	0.000	0.000
	14-16	0.000	0.000	0.000	0.000	0.000	0.000	0.000	0.000	0.000	0.000	0.000
	16-18	0.000	0.000	0.000	0.000	0.000	0.000	0.000	0.000	0.000	0.000	0.000
NW (280°-360°)	4-6	0.000	1.644	1.340	0.000	0.000	0.000	0.000	0.000	0.000	0.000	0.000
	6-8	0.036	9.739	14.206	3.360	0.145	0.014	0.000	0.000	0.000	0.000	0.000
	8-10	0.109	8.399	13.236	7.313	1.644	0.492	0.087	0.007	0.000	0.000	0.000
	10-12	0.000	1.361	6.864	6.430	3.939	1.426	0.384	0.174	0.007	0.000	0.000
	12-14	0.000	0.109	0.739	2.281	1.484	0.869	0.333	0.152	0.116	0.022	0.000
	14-16	0.000	0.007	0.087	0.232	0.130	0.130	0.130	0.174	0.065	0.007	0.014
	16-18	0.000	0.000	0.000	0.007	0.014	0.000	0.007	0.007	0.014	0.029	0.000

Frequency of occurrences for each interval of T_p and H_{sig}

Trend	Tp(s)|Hsig(m)	<1	1	2	3	4	5	6	7	8	9	10
SW (180°-260°)	0-2	0.000	0.000	0.000	0.000	0.000	0.000	0.000	0.000	0.000	0.000	0.000
	2-4	0.000	0.000	0.000	0.000	0.000	0.000	0.000	0.000	0.000	0.000	0.000
	4-6	0.000	0.001	0.030	0.030	0.017	0.008	0.004	0.001	0.000	0.000	0.000
	6-8	0.000	0.046	1.046	1.066	0.585	0.266	0.129	0.032	0.009	0.003	0.001
	8-10	0.000	0.364	8.216	8.375	4.597	2.094	1.013	0.250	0.068	0.023	0.011
	10-12	0.000	0.454	10.232	10.431	5.726	2.608	1.261	0.312	0.085	0.028	0.014
	12-14	0.000	0.384	8.664	8.832	4.848	2.208	1.068	0.264	0.072	0.024	0.012
	14-16	0.000	0.164	3.705	3.776	2.073	0.944	0.457	0.113	0.031	0.010	0.005
	16-18	0.000	0.034	0.762	0.777	0.426	0.194	0.094	0.023	0.006	0.002	0.001
	18-20	0.000	0.007	0.164	0.168	0.092	0.042	0.020	0.005	0.001	0.000	0.000
	20-22	0.000	0.001	0.030	0.030	0.017	0.008	0.004	0.001	0.000	0.000	0.000
W (260°-280°)	0-2	0.000	0.000	0.000	0.000	0.000	0.000	0.000	0.000	0.000	0.000	0.000
	2-4	0.000	0.000	0.000	0.000	0.000	0.000	0.000	0.000	0.000	0.000	0.000
	4-6	0.000	0.000	0.000	0.000	0.000	0.000	0.000	0.000	0.000	0.000	0.000
	6-8	0.000	0.029	0.281	0.183	0.114	0.054	0.025	0.012	0.005	0.002	0.000
	8-10	0.000	0.408	3.952	2.578	1.600	0.760	0.349	0.169	0.075	0.021	0.003
	10-12	0.000	0.847	8.207	5.353	3.323	1.578	0.725	0.351	0.156	0.045	0.006
	12-14	0.000	1.347	13.045	8.508	5.282	2.508	1.152	0.558	0.248	0.071	0.009
	14-16	0.000	1.122	10.864	7.085	4.399	2.089	0.959	0.465	0.207	0.059	0.007
	16-18	0.000	0.288	2.786	1.817	1.128	0.536	0.246	0.119	0.053	0.015	0.002
	18-20	0.000	0.066	0.637	0.416	0.258	0.122	0.056	0.027	0.012	0.003	0.000
	20-22	0.000	0.009	0.086	0.056	0.035	0.017	0.008	0.004	0.002	0.000	0.000
NW (280°-360°)	0-2	0.000	0.000	0.000	0.000	0.000	0.000	0.000	0.000	0.000	0.000	0.000
	2-4	0.000	0.000	0.000	0.000	0.000	0.000	0.000	0.000	0.000	0.000	0.000
	4-6	0.000	0.004	0.017	0.006	0.002	0.001	0.000	0.000	0.000	0.000	0.000
	6-8	0.000	0.135	0.636	0.240	0.082	0.030	0.011	0.004	0.001	0.000	0.000
	8-10	0.000	1.940	9.162	3.455	1.186	0.439	0.155	0.052	0.018	0.005	0.002
	10-12	0.000	3.060	14.453	5.450	1.871	0.692	0.245	0.082	0.029	0.008	0.002
	12-14	0.000	3.281	15.497	5.843	2.006	0.742	0.263	0.088	0.031	0.009	0.003
	14-16	0.000	2.460	11.618	4.381	1.504	0.557	0.197	0.066	0.023	0.007	0.002
	16-18	0.000	0.715	3.379	1.274	0.438	0.162	0.057	0.019	0.007	0.002	0.001
	18-20	0.000	0.197	0.929	0.350	0.120	0.044	0.016	0.005	0.002	0.001	0.000
	20-22	0.000	0.027	0.128	0.048	0.017	0.006	0.002	0.001	0.000	0.000	0.000

Ratio between f_p and P for different intervals of T_p and H_{sig}

Trend	Tp(s)|Hsig (m)	<1	1	2	3	4	5	6	7	8	9	10	11	12
SW (180°-260°)	0-2	0.000	0.000	0.000	0.000	0.000	0.000	0.000	0.000	0.000	0.000	0.000	0.000	0.000
	2-4	0.000	1.680	4.486	10.586	20.818	34.290	54.533	74.855	99.208	164.262	0.000	0.000	0.000
	4-6	0.000	1.238	3.305	7.799	15.337	25.263	40.177	55.149	73.091	121.019	0.000	0.000	0.000
	6-8	0.000	0.952	2.543	6.001	11.801	19.437	30.912	42.432	56.237	93.113	0.000	0.000	0.000
	8-10	0.000	0.753	2.012	4.747	9.335	15.377	24.454	33.568	44.488	73.661	0.000	0.000	0.000
	10-12	0.000	0.611	1.630	3.847	7.566	12.462	19.819	27.205	36.056	59.698	0.000	0.000	0.000
	12-14	0.000	0.516	1.379	3.254	6.400	10.541	16.764	23.011	30.498	50.496	0.000	0.000	0.000
	14-16	0.000	0.449	1.198	2.827	5.559	9.157	14.563	19.990	26.493	43.865	0.000	0.000	0.000
	16-18	0.000	0.384	1.025	2.418	4.755	7.833	12.457	17.099	22.662	37.522	0.000	0.000	0.000
	18-20	0.000	0.000	0.000	0.000	0.000	0.000	0.000	0.000	0.000	0.000	0.000	0.000	0.000
	20-22	0.000	0.000	0.000	0.000	0.000	0.000	0.000	0.000	0.000	0.000	0.000	0.000	0.000
W (260°-280°)	0-2	0.000	0.000	0.000	0.000	0.000	0.000	0.000	0.000	0.000	0.000	0.000	0.000	0.000
	2-4	0.000	0.000	0.000	0.000	0.000	0.000	0.000	0.000	0.000	0.000	0.000	0.000	0.000
	4-6	0.000	1.625	4.787	11.848	22.215	36.738	57.164	77.718	107.978	149.638	0.000	0.000	0.000
	6-8	0.000	1.226	3.613	8.942	16.766	27.727	43.142	58.655	81.492	112.934	0.000	0.000	0.000
	8-10	0.000	1.107	3.261	8.071	15.133	25.027	38.941	52.943	73.557	101.937	0.000	0.000	0.000
	10-12	0.000	0.784	2.309	5.716	10.717	17.722	27.576	37.491	52.088	72.185	0.000	0.000	0.000
	12-14	0.000	0.669	1.971	4.879	9.148	15.128	23.539	32.004	44.464	61.620	0.000	0.000	0.000
	14-16	0.000	0.584	1.721	4.258	7.984	13.203	20.544	27.931	38.807	53.779	0.000	0.000	0.000
	16-18	0.000	0.509	1.498	3.708	6.953	11.499	17.892	24.325	33.796	46.835	0.000	0.000	0.000
	18-20	0.000	0.447	1.318	3.261	6.114	10.111	15.732	21.389	29.717	41.183	0.000	0.000	0.000
	20-22	0.000	0.000	0.000	0.000	0.000	0.000	0.000	0.000	0.000	0.000	0.000	0.000	0.000
NW (280°-360°)	0-2	0.000	0.000	0.000	0.000	0.000	0.000	0.000	0.000	0.000	0.000	0.000	0.000	0.000
	2-4	0.184	1.524	4.923	12.989	25.195	41.735	62.406	87.593	119.550	158.333	200.814	250.520	354.830
	4-6	0.129	1.065	3.443	9.084	17.619	29.186	43.642	61.255	83.603	110.725	140.432	175.192	248.137
	6-8	0.093	0.768	2.481	6.545	12.696	21.030	31.446	44.137	60.240	79.782	101.188	126.234	178.795
	8-10	0.074	0.617	1.994	5.260	10.204	16.902	25.274	35.474	48.416	64.122	81.326	101.456	143.700
	10-12	0.060	0.497	1.605	4.235	8.215	13.607	20.347	28.559	38.978	51.624	65.474	81.680	115.690
	12-14	0.051	0.421	1.362	3.593	6.970	11.546	17.265	24.233	33.073	43.803	55.555	69.306	98.164
	14-16	0.044	0.367	1.187	3.131	6.074	10.061	15.044	21.115	28.819	38.168	48.408	60.390	85.535
	16-18	0.039	0.322	1.040	2.745	5.324	8.818	13.186	18.508	25.260	33.455	42.431	52.934	74.974
	18-20	0.035	0.290	0.937	2.473	4.796	7.945	11.880	16.675	22.758	30.141	38.228	47.691	67.548
	20-22	0.032	0.262	0.847	2.234	4.332	7.176	10.731	15.062	20.557	27.225	34.530	43.077	61.013